# Synthesis of functional chalcogenide materials for memory/sensing devices and their integration into artificial sensory systems

OPEN ACCESS
IMMT | IOP Publishing
International Journal of Extreme Manufacturing
Int. J. Extrem. Manuf. **8** (2026) 022003 (41pp)
https://doi.org/10.1088/2631-7990/ae1db9

**Topical Review**

# Synthesis of functional chalcogenide materials for memory/sensing devices and their integration into artificial sensory systems

**Pengfei Liu[1,§], Jae Won Heo[1,2,3,§], Hyeonmin Bong[4,5,§], Jinsik Choe[4], Huiyoung Lee[4,5], Won-Kyu Lee[6], Myung-Gil Kim[1,2,3], Donghee Son[1,3,7,8], Joohoon Kang[9], Taeyong Eom[10,*], Sungjin Park[4,*] and In Soo Kim[1,2,3,11,*]**

[1] Nanophotonics Research Center, Korea Institute of Science and Technology, Seoul 02792, Republic of Korea
[2] School of Advanced Materials Science and Engineering, Sungkyunkwan University (SKKU), Suwon 16419, Republic of Korea
[3] KIST-SKKU Carbon-Neutral Research Center, Sungkyunkwan University (SKKU), Suwon 16419, Republic of Korea
[4] Icheon Branch, Korea Institute of Ceramic Engineering and Technology, Icheon 17303, Republic of Korea
[5] Department of Physics, Yonsei University, Seoul 03722, Republic of Korea
[6] Department of Materials Science and Engineering, Hongik University, Seoul 04066, Republic of Korea
[7] Department of Electrical and Computer Engineering, Sungkyunkwan University (SKKU), Suwon 16419, Republic of Korea
[8] Center for Neuroscience Imaging Research, Institute for Basic Science (IBS), Sungkyunkwan University (SKKU), Suwon 16419, Republic of Korea
[9] Department of Chemical and Biomolecular Engineering, Yonsei University, Seoul 03722, Republic of Korea
[10] Department of Semiconductor System Engineering, Sejong University, Seoul 05006, Republic of Korea
[11] Center for Nanoscale Materials, Argonne National Laboratory, Lemont, IL 60439, United States of America

E-mail: eomt@sejong.ac.kr, sj1107.park@kicet.re.kr and isk@anl.gov

Received 25 April 2025, revised 27 June 2025
Accepted for publication 10 November 2025
Published 2 December 2025

**Abstract**

With distinctive phase-change and switching properties, chalcogenide materials have emerged as critical components in various cutting-edge technologies. This review attempts to provide an overview of chalcogenide materials, from their fundamental properties to their diverse

§ These authors contributed equally to this work and should be considered co-first-author.
* Authors to whom any correspondence should be addressed.

 

applications with focus on memory and sensing technologies, which are indispensable components in human-like electronic artificial sensory systems. After reviewing the synthesis and application of chalcogenide materials with respect to dimensionality, we focus on the key advances in (1) memory devices, including phase-change memory (PCM), ovonic threshold switching (OTS) selectors, and selector-only memory (SOM), and (2) sensing devices, including optical sensors, gas sensors, and neuromorphic sensors. Emphasis will be given on how chalcogenide materials can be integrated into next-generation systems, such as wearable platforms, artificial intelligence, and neuromorphic/quantum computing systems, to meet the growing demands for high-performance memory and multi-functional sensing. We also provide an overview of emerging research trends as well as a comprehensive perspective on the current status of research on chalcogenides. Finally, we attempt to provide insights into how chalcogenides can continue to drive technological breakthroughs in both memory and sensing applications while shaping the future landscape of intelligent systems, smart sensing platforms, and sustainable technology development.

Keywords: functional chalcogenides, materials synthesis, device integration, artificial sensory system, phase-change memory, sensing modalities

## 1. Introduction

### *1.1. Overview of chalcogenide materials*

Chalcogenide materials are known for their intrinsic versatility and functionality, making them attractive across a wide range of applications. Compared to oxide- or carbon-based materials, chalcogenides offer distinct advantages, such as lower phonon energies, higher polarizability, and superior optical nonlinearities, which are critical for applications in infrared photonics, memory, and sensing. Unlike oxides, which often require high processing temperatures and exhibit wide bandgaps, many chalcogenides are processable at low temperatures and provide tunable bandgaps spanning from the visible to the infrared. In contrast to carbon-based materials that may suffer from stability or integration issues, chalcogenides offer well-established compatibility with existing semiconductor processes. Moreover, reversible phase transitions, multi-level resistance states, and high sensitivity to external stimuli of chalcogenide materials enable multi-functionality in a single material platform, making chalcogenides particularly appealing for emerging applications in memory, sensing, and neuromorphic computing.

Chalcogenide materials are compounds formed by at least one chalcogen element—sulfur, selenium, or tellurium—combined with electropositive elements, such as metals[1]. These materials are known for their diverse and remarkable physical and chemical properties, including tunable electrical/optical properties[2], high refractive indices[3], and low phonon energies[4]. Furthermore, chalcogenides exhibit unique atomic structure and bonding characteristics, allowing for significant flexibility in manipulating their electrical and optical behavior.

Among a wide range of chalcogenide materials, germanium-antimony-tellurium (GST) alloys, a widely studied class of phase-change materials, have received much attention owing to their ability to switch between discrete states of electrical resistance[5]. This switching behavior renders them ideal for non-volatile devices like phase-change memory (PCM)[6]. On the other hand, chalcogenide glasses (ChGs) exhibit high transparency in the infrared region, and therefore have found use predominantly in the field of infrared optics and sensing components for applications in thermal imaging[7], environmental monitoring[8], and infrared spectroscopy[9], where low loss and high transmission are crucial[10].

Apart from electronic/optical applications, chalcogenides are also considered as appealing candidates for thermoelectrics[11] and nanophotonics[12] as they exhibit tunable bandgaps which can be adjusted based on their composition[2]. By adjusting their composition, the electronic properties of chalcogenides can be optimized to achieve efficient charge transport while minimizing heat conduction, which is essential for high-performance thermoelectric devices[2]. Moreover, their tunable bandgaps allow for improved absorption and/or bandwidth of the solar spectrum, which leads to maximization of photon-to-electron conversion, and ultimately the efficiency of solar cells[1].

The inherent atomic flexibility and diverse structural modification options of chalcogenide materials enable significant advancements in applications such as quantum computing, artificial intelligence, and advanced sensor systems[12–15].

### *1.2. Chalcogenides for next-generation memory and sensing systems*

The modern era of electronics is characterized by a relentless pursuit of higher performance, miniaturization, and lower power consumption. Traditional memory technologies, such as dynamic random-access memory (DRAM) and flash memory, are now facing fundamental scaling limitations, creating issues associated with data retention, reliability, and power dissipation[5]. Chalcogenide materials, with their unique phase-change behavior, offer a promising solution to these challenges. Their ability to transition between

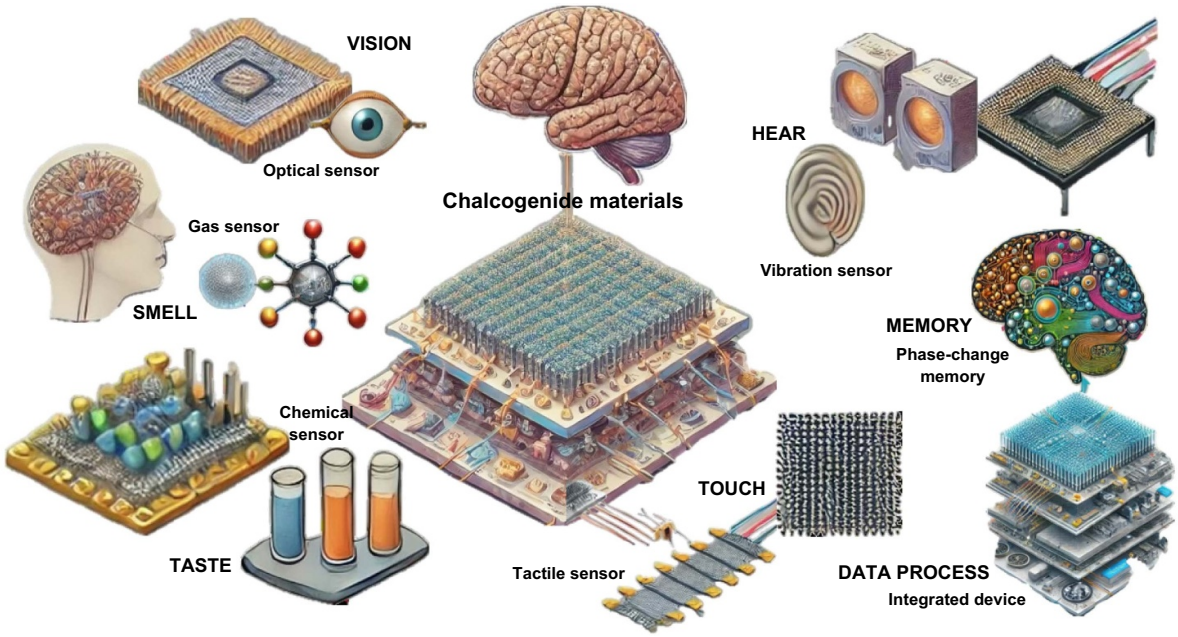


**Figure 1.** An overview of human-like electronic artificial sensory system based on chalcogenide materials. Parts of elements in this figure were generated using OpenAI's generative AI tool (DALL·E) based on author-provided descriptions.

amorphous and crystalline phases with corresponding changes in electrical resistance makes them an appealing class of materials for emerging non-volatile memory devices, namely, PCM[5]. Compared to DRAM and flash memory, PCM offers non-volatility, fast switching speed, and high endurance, which makes it a strong candidate for addressing key limitations of conventional memory technologies, such as the volatility of DRAM and slow write/erase speeds of flash memory. In addition, PCM supports multi-level data storage, all of which are essential for mimicking the rapid, high-throughput information processing of sensory systems. These capabilities enable the development of next-generation electronic sensory platforms that can efficiently capture, store, and interpret large volumes of complex data in real-time.

The integration of memory and sensing devices into artificial sensory systems is also an essential technology for the development of platforms designed to mimic human perception and cognition. In these systems, memory devices are vital not just in the sense of storing information, but also for enabling adaptive learning and response to stimuli—analogous to how human brains rely on memories for the interpretation and response to sensory input. As stated earlier, chalcogenide-based memory technologies, such as PCM, provide the speed, efficiency, and multi-level storage needed to enable these human-like capabilities, where real-time processing of sensory data is critical. On the sensing side, chalcogenides are becoming increasingly important for creating artificial sensory organs mimicking those of the mankind, such as neuromorphic sensors, which aim to replicate the way the human nervous system processes sensory information. Among various traits, their sensitivity to environmental stimuli, such as temperature, light, and chemical exposure, makes them ideal for developing sensing elements (e.g., optical, gas, chemical, vibration, tactile, etc.). These sensors can be engineered to serve as artificial sensory organs (e.g., eye, nose, tongue, ear, skin, etc.), which can relay information to brain-inspired computing systems (Figure 1). For instance, chalcogenides in optical sensors can detect subtle changes in light, making them key components in vision-like systems. In gas sensing, they respond to changes in the chemical environment, allowing for real-time environmental monitoring, much like a human's sense of smell. Along with the artificial sensory systems, the ability to seamlessly integrate memory and sensing functions is also crucial in the development of autonomous systems and the Internet of Things (IoT). To this end, chalcogenide materials offer the unique ability to merge both functionalities in a single platform, providing a pathway to create multifunctional, adaptive, and energy-efficient sensory systems that mimic the human sensory experience[14]. This is an essential feature for creating autonomous robots, wearable health monitors, and smart devices that can perceive, process, and react to their environment in a manner akin to human cognition and sensory processing[16–18].

In this review, we will attempt to provide a comprehensive and focused discussion of chalcogenide materials and devices, highlighting their roles in device integration to achieve intelligent system solutions. Unlike previous reviews that have primarily focused on structure and synthesis techniques[2,19,20] or specific applications such as neuromorphic computing[14,21,22], this review sets itself apart by exploring how chalcogenide materials are integrated into functional devices, particularly for memory and sensing technologies, tracing the progression from their fundamental structure/dimensionality to diverse fields of applications.

We start by familiarizing the readers with the fundamentals of chalcogenides, such as structure, fabrication, and general applications. We then move onto introducing their applications in memory and sensing. On the memory front, we concentrate on advancements in PCM, ovonic threshold switching (OTS) selectors, and selector-only memory (SOM), highlighting how these technologies leverage the unique properties of chalcogenides. For sensing applications, we emphasize optical sensors, gas sensors, and neuromorphic sensors, illustrating their potential in artificial sensory systems. Based on these technologies, we aim to underscore the underexplored opportunities for chalcogenides in enabling human-like electronic artificial sensory systems. Moving forward, we attempt to provide insights into how chalcogenides can continue to drive technological breakthroughs in both memory and sensing applications, as well as contribute to the future landscape of intelligent systems, smart sensing platforms, and sustainable technology development.

## 2. Materials: chalcogenides

The development of functional chalcogenide materials has evolved through several key milestones, as summarized in Figure 2. The foundational discovery of reversible electrical switching in glassy chalcogenides was first reported in 1968[23], followed by the introduction of OTS concept in 1970[24]. In 1987, the high-speed phase change behavior of Ge-Sb-Te alloys was reported[25], enabling breakthroughs in phase-change data storage. The exploration of 2D transition metal dichalcogenides (TMDs) in 2005 marked a transition toward device miniaturization and device scaling[26]. In 2007, compositional design principles were established to systematically tune phase-change behavior[27]. By 2012, GST-based devices were shown to emulate synaptic plasticity, demonstrating their applicability in neuromorphic computing[28]. In 2019, OTS devices were proposed for use as standalone memory elements, expanding their utility beyond conventional selector roles[29]. The implementation of atomic layer deposition (ALD) in 2020 enabled scalable fabrication of OTS devices with improved uniformity and control[30]. In 2022, Ge-doped Se opto-memristors were introduced, offering advanced neuromorphic functionalities, such as learning and inhibition[31]. Most recently, in 2023, $NbTe_4$ was identified as a phase-change material for the first time, which exhibited fast crystallization and high thermal stability, expanding the library of 2D chalcogenide materials for the development of PCM[32]. Together, these developments reflect a dynamic progress in chalcogenide research, highlighting their expanding potential in emerging memory and sensing technologies.

### 2.1. Basics of chalcogenide materials

Chalcogenide materials are composed of compounds that include at least one chalcogen element. While oxygen is technically a chalcogen, compounds that contain only oxygen as the anion are typically classified as oxides rather than chalcogenides[1]. Hence, we will focus our discussions on sulfides, selenides, and tellurides throughout the review. As stated earlier, chalcogenide materials have garnered significant attention from researchers across various fields owing to their unique optical and electronic properties, which include, but not limited to, memory[5], sensing[15,33], optoelectronics[34], photonics[35], infrared/nonlinear optics[36–39], and thermoelectrics[40].

Chalcogenides can be classified into binary, ternary, and quaternary (or higher-order) compounds, depending on their elemental composition. They can be further classified into subgroups, such as ChGs, which are typically amorphous, and crystalline metal dichalcogenides, which feature crystalline 2D layered structure, often involving transition metals (e.g., molybdenum, tungsten, etc.), hence given the name transition metal dichalcogenides (TMDs). As a result of variations in the classification criteria, an overlap can exist between these categories.

The crystal structure of chalcogenides varies widely depending on the composition, and therefore, is a key factor determining their intrinsic properties (Figure 3). For example, an archetypal phase-change material $Ge_2Sb_2Te_5$ (GST-225) exhibits low electrical/thermal conductivity and low optical reflectivity in its amorphous state. Upon heating, the material undergoes reversible phase transitions to face-centered cubic (fcc) (Figure 3(b)), trigonal (t1) (Figure 3(c)), and hexagonal close packed (hcp) (Figure 3(d)) phases, with corresponding increases in electrical/thermal conductivity and optical reflectivity. This behavior makes GST-225 an ideal material for applications in switching devices such as PCM. Another important example is layered TMDs, such as $MoS_2$ and $WS_2$. Unlike the bulk TMDs exhibiting an indirect bandgap, monolayer TMDs transition into direct bandgap systems. Such modification in the bandgap results from quantum confinement and the absence of interlayer coupling in monolayers, which makes TMDs highly promising for applications in semiconductor devices and optoelectronics. The chalcogenide family also exhibits a huge structural diversity, including fcc for crystallized GST-225 (Figure 3(b)), tetragonal for $CuInSe_2$ (Figure 3(h)), hexagonal for layered $MoS_2/WS_2$ (Figures 3(i) and (j)), orthorhombic for SnSe (Figure 3(k)), and monoclinic for GaTe (Figure 3(l)). Their unique crystal symmetries support discrete electronic, optical, and thermal behaviors, making them highly adaptable across diverse technological fields, and therefore highlight the broad versatility, which allows for chalcogenides to be tailored for various applications, from memory devices and sensing technologies to energy storage and catalysis.

### 2.2. Composition of chalcogenide materials

Binary chalcogenides represent the simplest form, consisting of only one chalcogen element combined with another element, typically a metal. A well-known example is ZnSe, an infrared-transparent material, which is commonly used

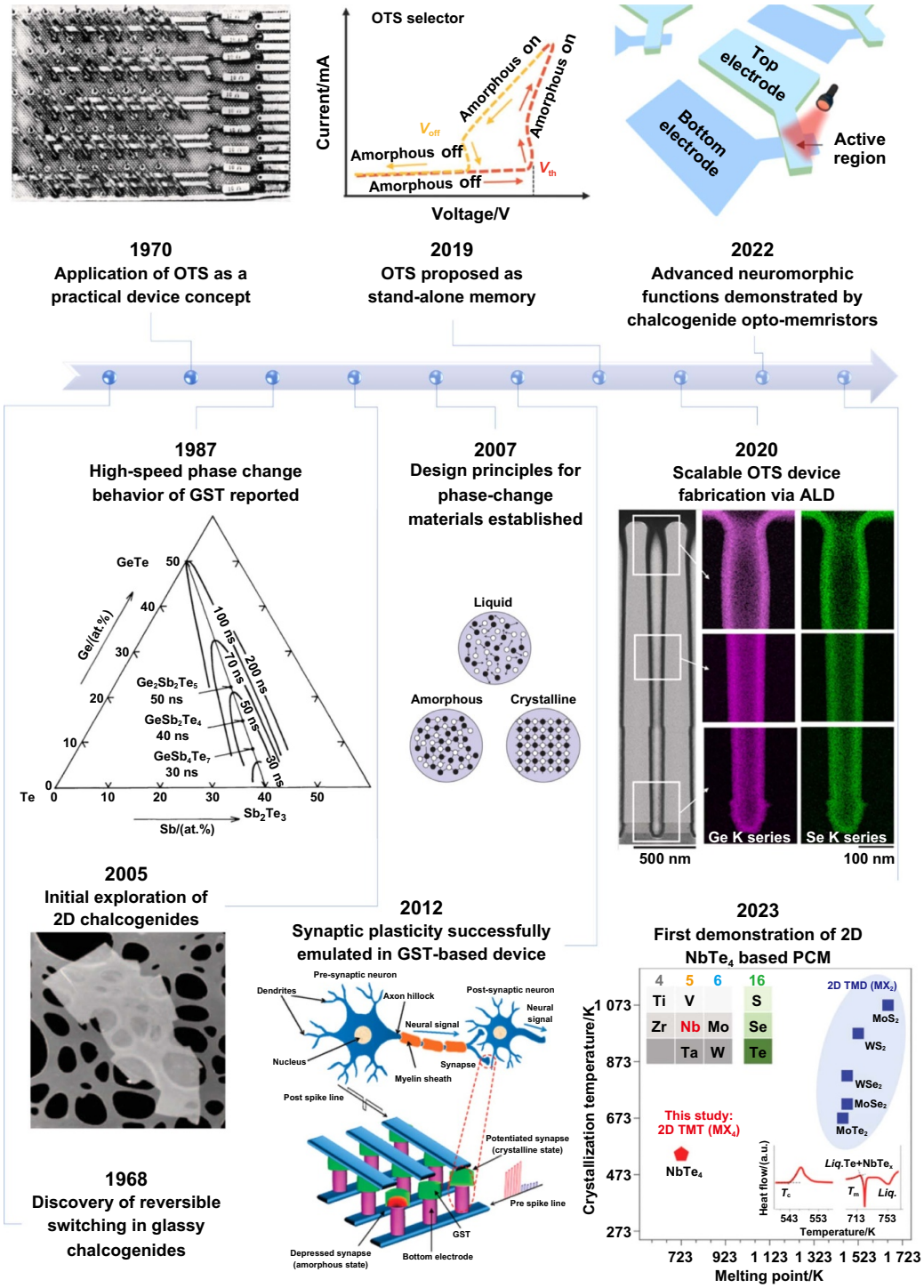


**Figure 2.** Historical timeline of key milestones in the development of functional chalcogenide materials. Image of a 5 × 5 OTS isolated OMS array (1970). Reprinted from[24], Copyright (1970), with permission from Elsevier. Threshold crystallizing laser pulse durations for GST films (1987). Reproduced from[25]. Copyright (c) 1987 The Japan Society of Applied Physics. All rights reserved. 2D $MoS_2$ crystal visualized by scanning electron microscopy (2005). Reproduced with permission from[26]. Copyright (2005) National Academy of Sciences, U.S.A. Change of refractive index and absorption coefficient with stoichiometry (2007). Adapted from[27], with permission from Springer Nature. Interconnection scheme of PCM synapses to reach ultrahigh density and compactness of brain (2012). Reprinted (adapted) with permission from[28]. Copyright (Year) American Chemical Society. *V-I* curve of an OTS device (2019). ALD made OTS device (2020). Reprinted (adapted) with permission from[30]. Copyright (2020) American Chemical Society. Sketch of synaptic plasticity and reinforcement learning emulation (2022). Reproduced from[31]. CC BY 4.0. Comparison of crystallization and melting temperature of various 2D materials (2023). Reproduced from[32]. CC BY 4.0.

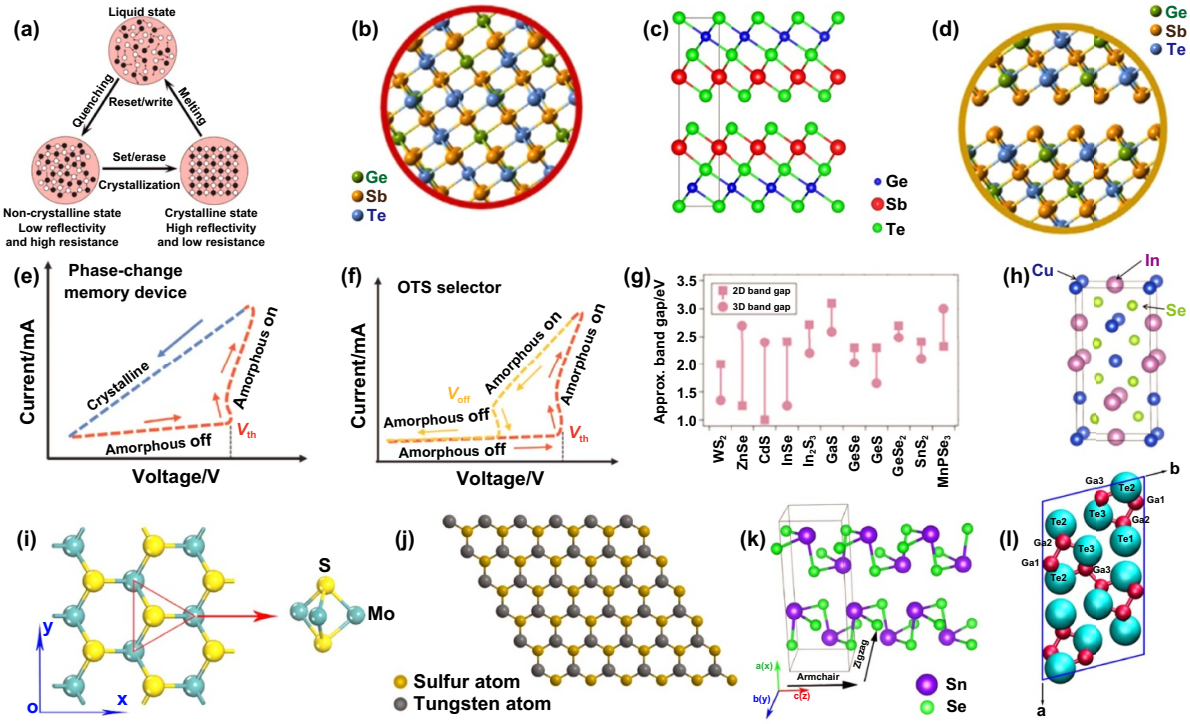


**Figure 3.** Crystal structure of chalcogenide materials. (a) Reversible phase-change process of GST-225. GST-225 exhibiting.[41] John Wiley & Sons.© 2024 Wiley-VCH GmbH. (b) face centered cubic. Reproduced from[42]. CC BY 4.0. (c) trigonal. Reprinted from[43], with the permission of AIP Publishing. And (d) hexagonal structures. Reproduced from[42]. CC BY 4.0. (e) Phase change process in a memory device. (f) Switching behavior in an OTS selector. (e) and (f) Adapted from[29], with permission from Springer Nature. (g) Range of bandgaps observed in various chalcogenide based materials. Reprinted (adapted) with permission from[2]. Copyright (2020) American Chemical Society. (h) Tetragonal structure of $CuInSe_2$. Reproduced from[44]. The Author(s). CC BY 4.0. Hexagonal structures of (i) $MoS_2$ with top and side view. Reproduced from[45]. CC BY 4.0. And (j) $WS_2$ with top view. Reproduced from[46]. CC BY 4.0. (k) Orthorhombic structure of SnSe. Reprinted figure with permission from[47], Copyright (2017) by the American Physical Society. (l) Monoclinic structure of GaTe. Reprinted figure with permission from[48], Copyright (2015) by the American Physical Society.

in optical devices[49]. On the other hand, metalloid chalcogenides, such as $As_2S_3$, are generally integrated into nonlinear optics. Third-harmonic generation measurement of $As_2S_3$ shows a third-order optical susceptibility $\chi^{(3)}$ of $5.6 \times 10^{-19}$ $m^2 \cdot V^{-2}$ at the fundamental-light wavelength of 2.1 μm, which is more than 300 times higher than that of a silica glass[50]. Notably, binary TMDs (e.g., $MoS_2$, $WS_2$, etc.), traditionally known as lubricants, have found new applications in optoelectronics, catalysis, and spintronics, among others, when present in 2D layered structures[51].

Ternary chalcogenides incorporate two different metals (or a metal and a metalloid) combined with a chalcogen. $CuInS_2$ is an example of ternary chalcogenide compounds, which offers promising solutions for thin-film optoelectronics (e.g., photodetectors, solar cells) across various structural configurations[52]. Another widely studied ternary chalcogenide is GST, which is almost exclusively used in PCM devices based on its phase transition characteristics. Utilizing the changes in infrared emissivity upon phase transition, GST has also shown promise for applications in adaptive radiative cooling, demonstrating its versatility[53].

Quaternary and higher-order chalcogenides consist of three or more elements combined with a chalcogen[54,55]. For instance, copper zinc tin sulfide (CZTS) is a commonly used quaternary chalcogenide compound, which is widely used as a charge transport material in thin film solar cells[56]. More complex multi-chalcogen compounds, such as zinc sulfide-selenide, have also been explored for applications in optoelectronic devices, laser diodes, and hard coatings designed to operate in the infrared spectral region[57]. Nevertheless, these devices fall outside the scope of this review, and therefore, the readers are directed to the relevant literature for further details on this topic[2,55,58,59].

### 2.3. *Dimensionality of chalcogenide materials*

The versatility of chalcogenide materials emerges not only from their composition but also their ability to adopt various structural dimensionalities ranging from 0D to 3D, which influences their optical, electronic, and mechanical properties. Consequently, the dimensionalities of chalcogenide materials can be tailored to meet the specific requirements depending on the nature of intended applications[60,61]. However, synthesizing chalcogenide materials with a particular dimensionality involves specialized synthesis methods, each with its own set of benefits and challenges (Figure 4).

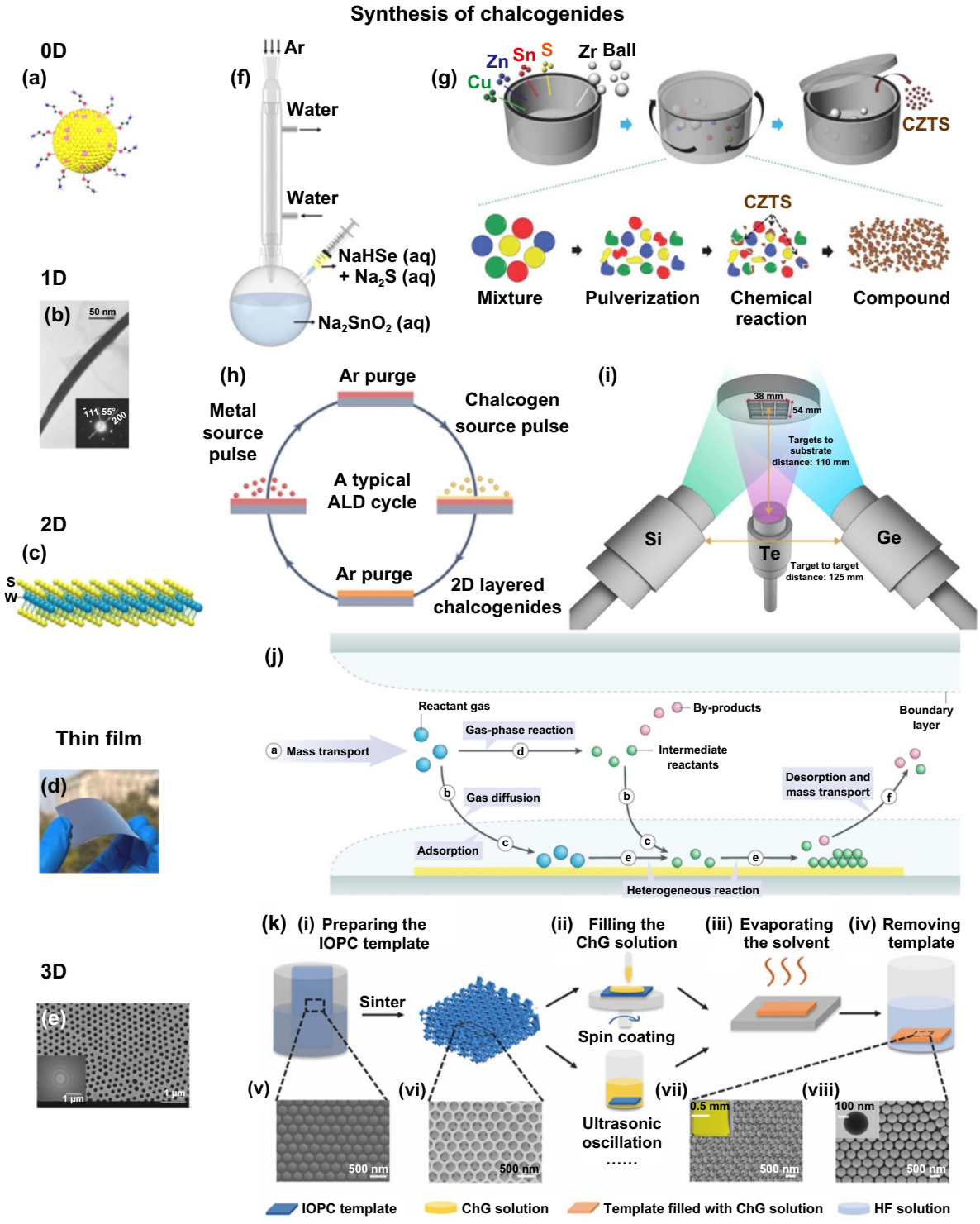


**Figure 4.** Schematic illustration of dimensionalities found in the chalcogenide materials system and common synthetic methods of chalcogenide materials. (a) 0D transition metal dichalcogenide. Reprinted (adapted) with permission from[62]. Copyright (2023) American Chemical Society. (b) 1D PbSe crystal.[63] John Wiley & Sons.© 2002 WILEY-VCH Verlag GmbH & Co. KGaA, Weinheim. (c) 2D $WS_2$ crystal. Reprinted (adapted) with permission from[2]. Copyright (2020) American Chemical Society. (d) $Sb_2S_3$ thin film. Reprinted (adapted) with permission from[64]. Copyright (2023) American Chemical Society. (e) 3D $As_{30}S_{70}$ chalcogenide glass. "Reprinted from[65], Copyright (2013), with permission from Elsevier. (f) Solution synthesis. Reprinted (adapted) with permission from[11]. Copyright (2021) American Chemical Society. (g) Mechanochemistry method. Adapted from[58] with permission from the Royal Society of Chemistry. (h) Atomic layer deposition. Adapted from[66], with permission from Springer Nature. (i) Magnetron sputtering. Reproduced from[67]. CC BY 4.0. (j) Chemical vapor deposition. Adapted from[68], with permission from Springer Nature. (k) Template-based method. Reproduced from[69]. CC BY 4.0. (As the synthesis methods for different dimensionalities often overlap, they are not presented in one-to-one correspondence.).

0D chalcogenide materials (i.e., quantum dots, nanoparticles) are confined in all three spatial dimensions, giving rise to quantum confinement effects. Their size-tunable optical and electronic properties make them highly suitable for use in optoelectronic devices[70] as well as fluorescent markers[71], while their large surface-to-volume ratio allows for application in sensing devices[72]. One common synthesis method for 0D chalcogenides is hydrothermal/solvothermal process, where precursors are dissolved in water or an organic solvent and then heated in a sealed autoclave. This method allows for control of particle size and morphology while operating at relatively low temperatures. However, the requirement for high-pressure equipment limits the scalability of this method. $MoS_2$ quantum dots, widely studied for their optoelectronic properties, are often synthesized using this technique[73,74]. The hot-injection method is another approach, where a precursor solution is rapidly injected into a hot solvent containing another precursor. This method provides precise control over nanoparticle size and composition, making it ideal for the production of quantum dots. Nevertheless, its application in industrial production has been largely limited as it produces rather small quantities of the material. CdSe quantum dots, widely used in displays and optoelectronics, are often synthesized using this technique[73]. Researchers have also explored the possibility of synthesizing crystalline chalcogenides under ambient conditions (e.g., the reaction of bis(cyclopentadienyl) tungsten dihydride with sulfur at room temperature and ambient pressure)[75]. With $WS_2$ nanodots being an exemplary material for energy applications, this technique offers lower energy consumption and avoids the need for high-temperature processes[75]. However, poor material uniformity and crystallinity are seen as major drawbacks associated with this method. Mechanochemistry, which involves grinding or milling precursors together, can also produce 0D chalcogenide materials in an energy-efficient and solvent-free manner. However, this method often falls short in providing control over particle size and morphology, in addition to the possibility of introducing impurities associated with the grinding process[76].

1D chalcogenide materials such as nanowires, nanotubes, and nanorods are characterized by their high surface-area-to-volume ratio, making them ideal candidates for sensing devices[72]. These structures can also accommodate facilitated charge transport, making them useful in optoelectronics[77,78]. Similar to 0D chalcogenide materials, hydrothermal/solvothermal process is commonly used for 1D materials, which offers delicate control over length and morphology. However, maintaining high pressure and temperature required for synthesis poses practical challenges, particularly for large-scale production, as discussed previously. $SnS_2$ nanowires for applications in optoelectronic devices (e.g., photoelectrodes, solar cells, and photodetectors) are often produced using this method. Mechanochemistry can also be employed to produce 1D materials, such as $MoS_2$ nanorods. However, as with its use in 0D materials, mechanochemistry for 1D chalcogenides offers limited control over morphology and can result in contamination from grinding media, which can influence the purity of the final material[76].

2D chalcogenide materials, such as $MoS_2$ and $WS_2$, are particularly attractive for applications in field-effect transistors (FETs)[75], gas sensors[72], catalysts[79], and photoelectrodes as they possess high surface area as well as unique surface chemistry[80]. Chemical vapor deposition (CVD) is a widely used technique for the synthesis of 2D materials, which involves high temperature chemical reaction and/or decomposition of precursors on the substrate[81]. While this method offers excellent thickness uniformity and scalability, various issues remain for commercialization: (1) the cost prohibitive precursors associated with the difficulties in their development, and (2) imperfections in stoichiometry for complex systems owing to incorporation of impurities from the gas phase reactions[82]. To this end, atomic layer deposition (ALD), a deposition technique based on the sequential introduction of metal-organic precursors to achieve self-limiting gas-phase surface chemical reactions, can be helpful. In strict terms, ALD is considered as a subgroup of CVD, although ALD mainly utilizes surface chemistry instead of precursor decomposition. A complete cycle of self-limiting surface reactions results in the growth of a single atomic layer, and thus atomic-scale thickness control can be achieved under ideal conditions. Moreover, ALD offers excellent conformality even on the most complex geometries, which makes it particularly appealing for synthesizing 2D materials. Thus far, materials such as $MoS_2$, $WS_2$, $SnS_2$, etc. have been deposited by ALD[20]. Recently, atomic layer etching (ALE), a reverse process of ALD, has attracted much attention as a highly controlled, layer-by-layer etching method to synthesize 2D chalcogenides, such as $WSe_2$[83]. Mechanical exfoliation is a simple yet effective method for producing high-quality monolayers, primarily for laboratory-scale research, which involves peeling thin layers from bulk crystals using adhesive tape. On the other hand, liquid-phase exfoliation involves dispersing bulk chalcogenides in a solvent, which is then exfoliated into 2D layers by sonication or other mechanical forces[84]. More recently, electrochemical exfoliation based on the intercalation of ions into the layers of bulk chalcogenides to weaken the interlayer forces to generate 2D layers has become popular in producing high-quality solution processible 2D TMDs[80,85]. Finally, molecular beam epitaxy (MBE) is another technique which allows for precise epitaxial growth of 2D materials. However, it is not a scalable approach when it comes to industrial production, making it suitable primarily for academic and small-scale experiments[66].

3D chalcogenide materials encompass porous structures, nanophotonic structures, and inverse opal structures, all of which have important applications in energy storage[86], photonics[87], catalysis[88], and sensing devices[89]. The high surface area is advantageous in energy storage and catalysis, while the ordered structure provides improved light management in optoelectronics. Template-based methods, including electrochemical deposition, sol-gel, and self-assembly, have been frequently used to fabricate 3D chalcogenide materials.

These methods offer excellent control over pore size and architecture, making them suitable for producing complex 3D structures. However, the removal of the template may introduce defects or impurities within the material, and the scalability of self-assembly remains a challenge.

Thin film chalcogenide materials are crucial in many applications owing to their thicknesses, being suitable to exploit reliable/reversible phase change as well as to manipulate light-matter interactions in the visible/near-infrared range. GST thin films, for example, have been widely used in Blu-ray discs, phase-change memory, and other optoelectronic devices. For thin-film synthesis, physical vapor deposition (PVD) techniques, such as magnetron sputtering and thermal evaporation, are commonly used. PVD offers good control over film thickness and uniformity, and despite its reliance on high-vacuum systems with significant maintenance costs, it remains the preferred deposition method for GST thin films. CVD, on the other hand, provides better control over film composition and conformality, though it comes with higher precursor and equipment maintenance costs. $MoS_2$ thin films, used in flexible electronics, are commonly produced using CVD. Finally, ALD offers atomic-level control over film thickness, which is also critical for producing ultra-thin conformal layers required in complex structured memory devices. However, one of the main limitations of the ALD process is its slow deposition rates and high operational costs. $SnS_2$ films, used in advanced memory architectures, are often synthesized using this method[19]. MBE can also be used to fabricate thin films, providing precise control over thickness as well as composition. However, owing to the high equipment costs and low throughput, this method is better suited for fundamental research rather than industrial-scale production. Nanophotonic $MoS_2$ structures, which are used in optoelectronic devices, are often synthesized using MBE[66]. As thin films are predominantly used for memory and sensing applications, these are best aligned with the focus of this review. Therefore, we will attempt to provide a more detailed insight into the devices technologically relevant to human-like artificial sensory systems.

It is important to emphasize that the choice of synthesis method has a direct impact on the resulting material properties, and consequently, device performance[90]. In thin films, for instance, ALD offers precise thickness and conformality, critical for ensuring uniform and stable switching behavior in memory devices[20]. CVD, on the other hand, enables the synthesis of large-area films with high crystallinity, making it well-suited for applications in transistors and photodetectors[91]. In contrast, solution-based or mechanochemical methods offer low-cost processing routes, but may lead to higher defect densities, potentially compromising electrical conductivity, optical uniformity, or thermal stability[92]. Therefore, aligning the synthesis strategy with the specific functional requirements of the intended device is essential for optimizing performance[93].

### *2.4. Applications of chalcogenide materials*

Phase-change chalcogenide materials, particularly GST-based alloys, exhibit reversible transitions between amorphous and crystalline states, enabling their use in non-volatile memory devices. In phase-change random-access memory (PCRAM), electrical switching of GST allows for high-speed, low-power, and multi-level data storage[41], with alternatives like scandium-doped antimony tellurides expanding performance characteristics[5]. OTS devices, typically using ChGs based on selenides and tellurides, transition from high to low resistance at threshold voltage, making them essential as selectors in resistive memory crossbar arrays[29,54]. Chalcogenide materials can also exhibit dual functionalities, integrating phase-change, electrical switching, and sensing properties. For example, doped GST can serve both as memory and OTS device, enabling the creation of dual-functional selector-only memory.[94] Materials like AgInSeTe (memory and light sensitivity)[94], GaSe (bandgap tunability and nonlinear optics)[9], and $SnSe_{1-x}S_x$ (high thermoelectric efficiency and semiconducting properties)[11] demonstrate the versatility of chalcogenides for multifunctional applications in neuromorphic, photonic, and energy-harvesting devices.

Beyond their roles in data storage and memory, chalcogenide materials exhibit remarkable versatility, enabling their use across a wide range of device platforms. In Figure 5, representative applications of chalcogenides are illustrated with more comprehensive details provided in Table 1. In optoelectronics, chalcogenides are integral to the development of devices for optical communication, holographic 3D imaging, and next-generation wearable electronics due to their unique interaction with light. Their high sensitivity to environmental changes also makes them ideal candidates for gas and light sensors, as well as chemical detection, enabling real-time monitoring and analysis in industrial and environmental settings. In the energy sector, chalcogenides contribute to the advancement of solid-state batteries, solar cells, and thermoelectric devices, where their ability to efficiently convert energy forms is crucial for improving device performance. Additionally, their piezoelectric properties open avenues for applications in energy harvesting and mechanical sensing. Chalcogenides are also increasingly investigated for catalysis, particularly in processes such as water splitting and environmental remediation, where their catalytic properties can be fine-tuned for specific reactions. In the medical and biotechnology fields, these materials are being explored for biodegradable electronics and nanomedicine, offering new possibilities for therapeutic delivery and diagnostics. Moreover, chalcogenides are attracting significant attention in emerging areas like quantum information science, where their unique electronic and optical characteristics are being leveraged for developing quantum devices and systems. This broad range of applications, beyond traditional memory and sensing roles, underscores the exceptional adaptability of chalcogenides and their potential to drive innovation across multiple disciplines, ensuring their continued relevance

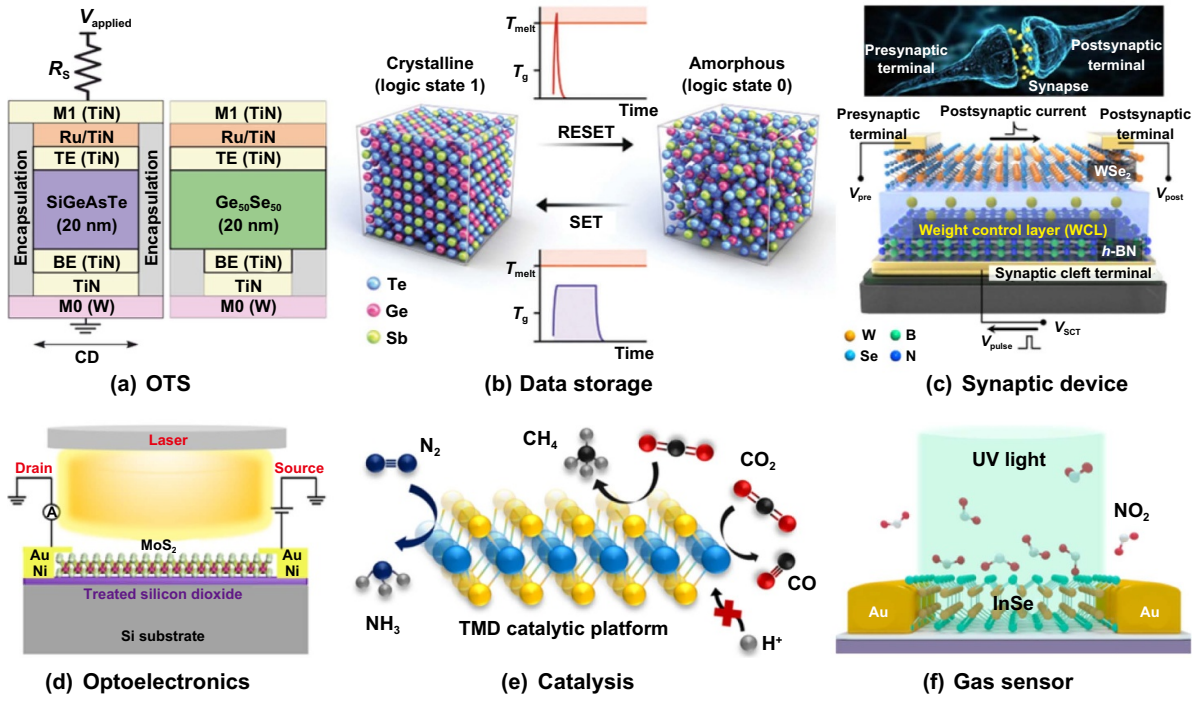


**Figure 5.** Representative applications of functional chalcogenide materials. (a) Schematic of OTS selector devices.[95] John Wiley & Sons.© 2023 Wiley-VCH GmbH. (b) Principle of phase-change memory. Adapted from[20] with permission from the Royal Society of Chemistry. (c) Functional/structural/architectural comparison of a biological synapse with a synthetic synaptic device. Reproduced from[96]. CC BY 4.0. (d) Schematic view of a $MoS_2$ photodetector illuminated by a monochromatic laser beam. Reprinted (adapted) with permission from[97]. Copyright (2023) American Chemical Society. (e) Schematic of the TMD catalytic platform. Reproduced with permission from[98]. Copyright © 2021 The Authors. Published by American Chemical Society. This publication is licensed under CC BY-NC-ND 4.0. (f) $NO_2$ gas sensor based on few-layered InSe. Reprinted (adapted) with permission from[99]. Copyright (2020) American Chemical Society.

in future technological advancements. A table outlining various applications based on previous reports utilizing chalcogenides is provided in Table 1.

In the following section, we will provide an in-depth discussion on key applications of chalcogenides, focusing on two major areas: (1) memory devices, including phase-change memory (PCM), ovonic threshold switching (OTS) selectors, and selector-only memory (SOM); and (2) sensing devices, including optical sensors, gas sensors, and neuromorphic sensors.

## 3. Device and integration

### *3.1. Phase change memory (PCM)*

*3.1.1. Device characteristics.* PCM is a non-volatile memory technology that leverages the reversible phase change of chalcogenide materials between amorphous (high resistance) and crystalline (low resistance) states. This bistable property allows PCM to store data as binary information. The two primary operations in PCM are the SET and RESET processes, corresponding to writing binary '1' and '0', respectively[23]. The SET operation involves heating the chalcogenide material above its crystallization temperature (typically around 423 K to 573 K) using a relatively long, low-amplitude electrical pulse (50 to 200 ns), allowing the material to crystallize into a low-resistance state. The RESET operation is more energy-intensive, which requires melting of the chalcogenide material with a short, high-amplitude pulse (10 to 50 ns) and rapid quenching to revert it back to the high-resistance amorphous state. This pulse is typically sharp and rectangular with a short trailing edge to maximize heating efficiency, reduce thermal budget, and enable rapid cooling.

While PCM offers high endurance (up to $10^{12}$ cycles)[138,139], fast switching speeds, and good data retention at high temperatures, it faces challenges such as high programming currents and power consumption, particularly during the RESET operation. This can cause thermal disturbances in adjacent cells, an issue which becomes more pronounced as device dimensions continue to scale. Additionally, the relatively slow crystallization speed can limit SET speed and endurance. To mitigate these challenges, recent research has concentrated on tailoring material properties and refining device architectures to enhance switching speed, reduce power consumption, and improve scalability. However, because PCM relies on heat-driven phase transitions, there are inherent limitations in improving its performance. As a result, selector-only memory devices, which operate based on threshold voltage shifts without involving phase transitions, have been proposed as a potential successor to PCM. Table 2 provides

**Table 1.** Composition, dimensionality, and characteristics of chalcogenide-based materials categorized into their respective applications.

| Application category | Subcategory | Materials (e.g.) | Dimensi-onality | Characteristics of chalcogenide enabling applications | References |
|---|---|---|---|---|---|
| Data storage | Blu-ray discs | GST | Thin film | Reversible optical phase change with distinct reflectivity contrast | [100,101] |
| | PCRAM | GST | Thin film | Fast, reversible electrical switching between amorphous and crystalline phases | [20,102,103] |
| | Magneto-optical storage | EuSe, EuTe | Thin film | Strong magneto-optical response in chalcogenide thin films | [104] |
| Memory and computing | OTS | GeSe | Thin film | Sharp threshold switching due to electronic excitation in disordered structure | [30,94,105] |
| | Memristors | GST | Thin film | Multi-level resistance states for analog information storage | [12,106] |
| | Artificial synapses/neuromorphic | $MoS_2$, $MoTe_2$ | 2D/Thin film | Layered structure enabling gradual conductance modulation | [21,107] |
| | Spintronics | $Fe_3GeTe_2$ | 2D | Intrinsic ferromagnetism in 2D layered chalcogenides | [108,109] |
| Optoelectronics | Optical communication/photonics | $As_2S_3$, $As_2Se_3$ | 3D | High refractive index and wide IR transparency | [3,110] |
| | Phase-change displays | GST, GeTe | Thin film | Optical property tuning via phase transition | [111,112] |
| | Holographic and 3D imaging | GST, ITO-GST | Thin film | High phase modulation depth from refractive index changes | [7,113] |
| | Wearable and flexible electronics | ZnSe, $MoS_2$, $WS_2$ | 2D/Thin film | Mechanical flexibility and strain-tolerant electronic properties | [112,114] |
| Sensing and detection | 2D gas sensors | InSe, $MoS_2$, $WS_2$, $SnS_2$ | 2D | Surface-sensitive electronic states for gas adsorption | [99,115] |
| | 2D light sensors | $Si_2Te_3$, $MoS_2$, $WS_2$ | 2D | Strong light-matter interaction with tunable bandgap | [116–118] |
| | Chemical sensing | $AgIAs_2S_3$, CuAgAsSe | 2D | Compositional versatility enabling high selectivity | [15,33,119] |
| Energy and power | Solid-state Li-ion batteries | $Li_{10}GeP_2S_{12}$ (LGPS) | 3D | High ionic conductivity in chalcogenide-based superionic conductors | [120,121] |
| | Solar cells | $Cu(In,Ga)Se_2$, CdTe | 0D/1D/Thin film | Direct bandgap and high absorption coefficient | [34,74,122] |
| | High-temperature thermoelectrics | $MoS_2$, PbSe, SnS | 3D | Low thermal conductivity and high Seebeck coefficient | [45,123,124] |
| | Flexible and stretchable thermoelectrics | $Cu_2Se$, $Ag_2S$ | Thin film | High ZT under strain due to phonon scattering control | [125,126] |
| | Piezoelectric devices | $BaZrS_3$, $CaZrS_3$ | 0D/3D | Distortion-induced dipole generation in perovskite-like structures | [127] |
| | Cryogenic applications | $Ta_2NiSe_5$/GaSe, $TiS_2$ | 0D/3D | Layered structure with low thermal conductivity at cryogenic temperatures | [9,128] |

(Continued.)

**Table 1.** (Continued.)

| Application category | Subcategory | Materials (e.g.) | Dimensi-onality | Characteristics of chalcogenide enabling applications | References |
|---|---|---|---|---|---|
| Catalysis applications | Catalysis for energy conversion | $Co_9S_8$, $WS_2$ | 0D/3D | Catalytically active sites with tunable electronic structure | [118,129,130] |
| | Environmental remediation | $Cu_2InSnS_4$ | 0D/2D/3D | Visible-light-responsive photocatalytic activity | [59,79] |
| Medical and biotechnology | Biodegradable applications | CdSe, Se, ZnS | 0D | Biocompatibility and controlled degradation in physiological environments | [131] |
| | Nanomedicine | CdSe, Se, ZnS | 0D | Size-tunable fluorescence and surface functionalizability | [131,132] |
| Metamaterials /plasmonics /nanophotonics | Metamaterials | GST | 3D | Large, reversible refractive index modulation | [5,94] |
| | Surface plasmon resonance (SPR) | $MoS_2$, $WS_2$ | 2D | Enhanced light-matter coupling at surface plasmon resonance frequencies | [133,134] |
| | Photonic crystals | $As_2Se_3$, As-Se-Te, Sb-Se | 1D/3D | Periodic dielectric structure supporting photonic bandgaps | [78,135] |
| Emerging technology | Quantum information science and technology | $MoS_2$, $WS_2$, ZnS | 0D | Strong quantum confinement and spin-orbit coupling | [136,137] |

**Table 2.** Key performance parameters of selected PCM devices.

| Device | Set latency/ns | Reset Current/μA | Endurance/cycles | Retention/yr | References |
|---|---|---|---|---|---|
| μTrench PCM (0.18 μm CMOS) | 100 | 600 | $10^{11}$ | 300 @ 358 K | [140] |
| AgInSbTe (AIST) PCM | 0.25 | N/A | N/A | N/A | [141] |
| CVD GST confined PCM | N/A | 260 | $10^{8}$ | N/A | [142] |
| ALD GST confined PCM | 80 | N/A | $2 \times 10^{12}$ | N/A | [139] |

key performance parameters of selected PCM devices based on previous reports.

Chalcogenide-based memory can also be utilized in optical-based applications. Unlike electrically driven PCM, chalcogenide optical memory leverages the material's ability to reversibly switch between amorphous (high resistance) and crystalline (low resistance) states when exposed to light or heat[143,144]. In chalcogenide-based optical memory, laser pulses induce phase transitions that write data by switching the material between amorphous and crystalline states. The intensity and duration of the laser determine whether the material transitions into an amorphous or crystalline state. For reading operations, a low-power laser measures the reflectivity difference between the two states: the high reflectivity crystalline state and the low reflectivity amorphous state. This is a non-volatile memory technology, enabling powerless data retention. Moreover, the amorphous and crystalline states are stable over time, making them suitable for long-term data storage. The switch between the two states occurs within nanoseconds, allowing for high-speed data storage applications. Based on its scalability, fast switching speeds, and multi-level storage capability, chalcogenide-based optical memory is gaining attention for advanced technologies, such as neuromorphic and quantum computing.

*3.1.2. Device structure and integration.* PCM devices have evolved from the mushroom structure to the confined structure and finally to the crossbar array to improve performance, scalability, and bit density. The mushroom structure was known for ease of fabrication and ability to produce high-quality thin films, both essential for reliable operation. However, it required high current densities, which led to electrode degradation from electromigration and significant thermal effects. These issues became increasingly problematic with continued device scaling, resulting in thermal crosstalk and reduced endurance. To overcome these limitations, the confined structure was developed, confining the phase-change material within a narrow, insulated opening. This design reduced the active volume, lowered power consumption, and improved thermal isolation, effectively mitigating the issues of the mushroom design. As the demand for higher memory densities continued to grow, the crossbar array structure emerged, forming memory cells at the intersections of perpendicular word lines and bit lines. This architecture significantly reduced the area required for each cell and enabled the stacking of multiple memory layers in 3D configuration.

The mushroom structure, also known as the T-shape structure, is one of the earliest and most traditional designs for PCM devices[145] (Figure 6(a)). It features a chalcogenide phase-change material layer sandwiched between a small bottom electrode and a larger top electrode. The name 'mushroom' originates from the shape of the heated region in the phase-change material, which resembles a mushroom cap in cross-section (Figure 6(b)). The main advantage of this structure is its ease of fabrication, allowing for the deposition of high-quality thin films that are essential for reliable PCM operation. However, the mushroom structure requires high current densities, which can accelerate degradation of the bottom electrode through electromigration and/or temperature gradients, ultimately reducing device endurance. Only about 2% of the generated heat contributes to PCM operation, while the remaining 98% is lost as thermal dissipation. The dissipation of excess heat leads to thermal crosstalk between adjacent cells, undermining the overall performance and reliability of the device[146]. With continued scaling of PCM devices, managing thermal effects becomes increasingly challenging as programming induced heat more readily impacts neighboring cells, intensifying thermal crosstalk[142].

The shape of the bottom electrode in a mushroom-structured PCM cell has a significant influence on the device's electrical and thermal performance, scalability, and reliability. Circular electrodes have been traditionally employed for their ability to provide uniform current distribution and localized heating within the chalcogenide layer. This symmetrical design ensures consistent phase transitions, enhancing the reliability of both SET and RESET operations. However, as memory arrays continue to scale, circular electrodes may cause increased thermal crosstalk between adjacent cells, potentially compromising data integrity and limiting the achievable packing density.

μ-Trench electrodes offer improved current confinement by channeling the electrical and thermal energy into narrower regions[140,148] (Figures 6(c) and (d)). This enhanced confinement reduces power consumption and minimizes thermal interference with neighboring cells, making μ-trench designs better suited for high-density memory applications (Figure 6(e)). Additionally, μ-trench structures promote more efficient heat dissipation, thereby improving the endurance and longevity of PCM devices. To this end, Pellizzer et al. reported that PCM cells featuring μ-trench electrode structures, fabricated using a 90 nm node process, required a reset current approximately 57% lower than that of mushroom structured cells at the same node[148].

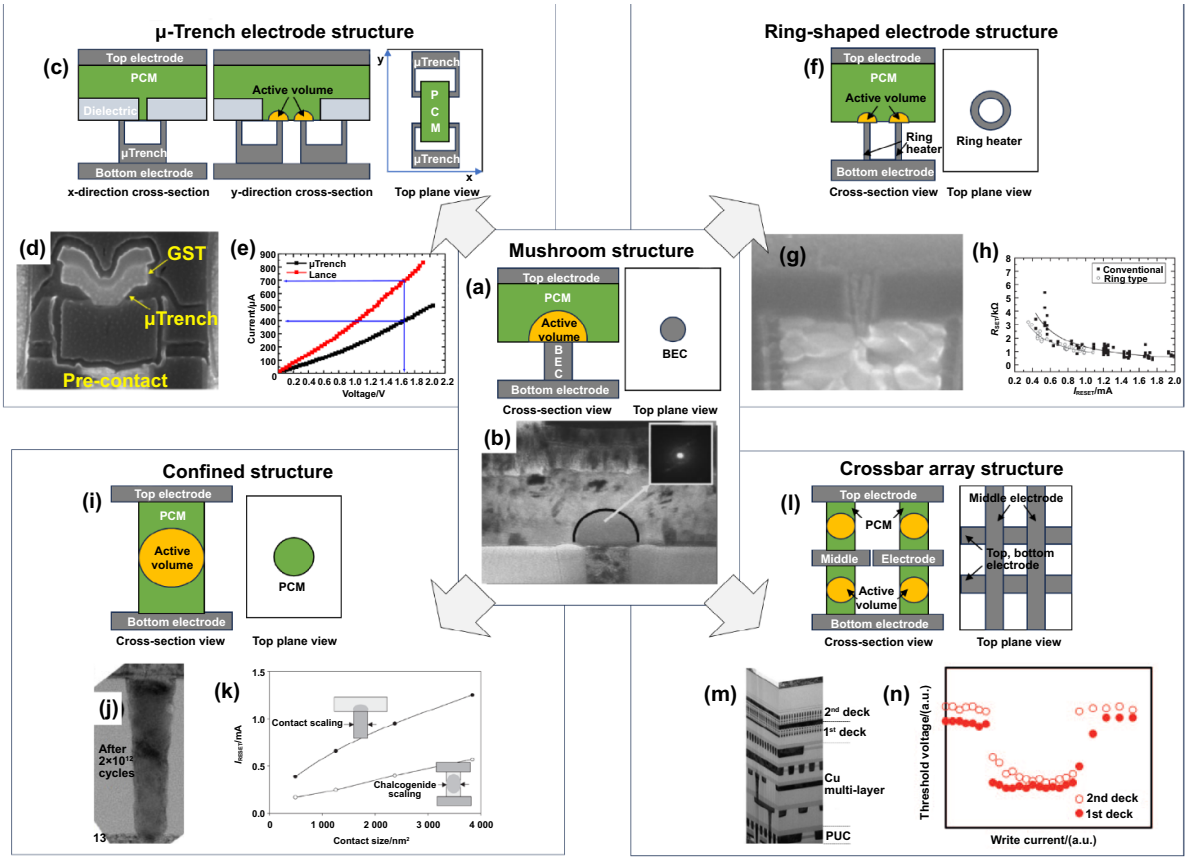


**Figure 6.** Cross-sectional images and device performance of various structured PCM. (a) and (b) Mushroom structure, which shows (a) schematic illustration and (b) TEM image. (a) and (b) Reproduced from[147]. Copyright (c) 2006 The Japan Society of Applied Physics. All rights reserved. (c)–(e) Schematic illustration, TEM image, and *I-V* characteristics of μ-Trench electrode structured cell. © (2006) IEEE. Reprinted, with permission, from[148]. (f)–(h) Schematic illustration, SEM image, and reliability data of ring-shaped electrode. Reproduced from[147]. Copyright (c) 2006 The Japan Society of Applied Physics. All rights reserved. (i) and (j) Schematic illustration and TEM image of confined structure. © (2016) IEEE. Reprinted, with permission, from[139]. (k) Comparison of reset current between mushroom and confined structures. Reproduced from[149]. [insert partner copyright line]. All rights reserved. Copyright (c) 2005 The Japan Society of Applied Physics. (l)–(n) Schematic illustration, TEM image, and *I-V* characteristics of a two-deck crossbar array structure. © (2018) IEEE. Reprinted, with permission, from[150].

Ring-shaped electrodes offer an alternative geometry that further provides enhanced current confinement while maintaining a high degree of symmetry[147,151,152] (Figures 6(f)–(h)). The ring shape enhances the uniformity of the electric field around the chalcogenide material, promoting more consistent phase changes and reducing variability in device-switching behavior. This geometry also allows for a more efficient use of space within the memory array, potentially increasing the overall storage density.

The confined structure, also known as the vertical pillar or pore structure, evolved from the mushroom design to improve scalability and thermal management[139,142,149,153,154]. In this structure, the phase-change material is confined within a narrow cylindrical or pore-shaped opening surrounded by an insulating material such as $SiO_2$ (Figures 6(i) and (j)). This confined space ensures that current flows vertically through a well-defined volume of chalcogenide material, reducing the active volume, lowering power consumption, and improving thermal isolation. Simulation results comparing the performance of the confined structure with the mushroom structure have demonstrated that, with identical contact sizes, the confined structure can reduce the reset current by over 50%[149]. Furthermore, thermal interference between neighboring cells spaced 100 nm apart is reduced by 573 K[142] (Figure 6(l)), highlighting the advantage of this structure for high-density memory applications.

ALD[139] or CVD[142] are commonly used for depositing chalcogenide materials in confined structures owing to their excellent step coverage, which ensures uniform/conformal deposition even along the sidewalls of narrow and deep trenches. The integration process starts with etching deep trenches or pores into an insulating layer to create confined spaces, followed by depositing a bottom electrode. The chalcogenide material is then deposited using ALD or CVD to achieve uniform coverage. Subsequent planarization processes, such as chemical mechanical planarization (CMP), may be used to create a flat surface for the deposition of a top electrode. This process minimizes the active volume of

the chalcogenide material, reducing power consumption and enhancing thermal isolation. While confined structures theoretically offer superior performance, in practice, thin films produced by ALD or CVD tend to experience greater degradation during integration. In contrast, crossbar array structures can leverage higher-quality thin films fabricated by PVD[150], providing performance advantages in actual devices.

The crossbar array structure is a commonly adopted configuration to achieve high-density integration in PCM devices. In this architecture, memory cells are formed at the intersections of perpendicular word lines and bit lines, with each intersection representing a memory cell composed of a chalcogenide layer and a selector device, such as an OTS (Figure 6(l)). This structure minimizes the footprint of each memory cell, allowing densities comparable to those of DRAM and flash memory. Furthermore, it supports multiple layers of memory cells in a three-dimensional stack, as demonstrated in technologies like 3D XPoint[155] (Figures 6(m) and (n)). The main challenge of the crossbar array structure is suppressing sneak currents, unintended currents flowing through unselected cells, which can degrade read and write performance. As selector devices at each memory cell intersection are designed to suppress sneak currents, reducing power consumption and increasing reliability, effective selector devices are crucial for controlling these currents and ensuring precise access to memory cells.

*3.1.3. Chalcogenide materials for PCM.* Chalcogenide materials in PCM devices have continuously evolved to enhance performance and reliability. GST remains the standard material, but it requires high RESET power and has lower thermal stability. To address these limitations, materials such as GeSb and GeTe were explored offering faster switching speeds and lower power consumption. Nevertheless, these materials suffer from reduced data retention owing to their tendency for rapid crystallization. To further enhance the performance of these materials, doped GST variants such as N-doped, C-doped, and Sn-doped GST have been developed. These modifications improve thermal stability and reduce RESET power, enhancing data retention and device endurance.

As discussed earlier, GST exhibits reliable phase-change characteristics, making it suitable for both planar and 3D device structures[25,156]. Its unique crystal structure and bonding nature enable rapid crystallization and excellent scalability for high-density applications (Figure 7(a)). Notably, GST maintains a prearranged atomic network in its amorphous phase, which closely resembles the crystalline phase at the local level, requiring only minimal bond rearrangements for crystallization, ultimately enabling rapid phase transitions[157] (Figure 7(a)). However, GST requires relatively high power during the RESET process, which involves melting of the material to re-establish the amorphous state. Additionally, its limited thermal stability can compromise data retention, particularly under high-temperature environments.

Although Ge-Sb-Te systems beyond conventional GST show distinct phase-transition behaviors depending on composition, they can offer complementary properties to GST (Figure 7(c)). GeSb alloys, such as $GeSb_4$, have simpler structures with the absence of tellurium from the material system, resulting in faster switching speeds and lower power consumption compared to GST. However, GeSb's fast crystallization kinetics compromises data retention, as the material crystallizes more readily at elevated temperatures[162]. GeTe, known for its high-speed switching and relatively lower power consumption compared to GST[163], also features a simple phase-change mechanism, which makes it attractive for high-performance memory applications. However, GeTe's rapid crystallization tendency similarly leads to reduced data retention and phase separation issues compared to GST.

AgInSbTe (AIST), which replaces Ge with Ag and In in Ge-Sb-Te compounds, was originally used in optical data storage and later explored for PCM due to its fast switching and high resistivity contrast between phases[141,159]. In AIST, six Sb atoms form an octahedral arrangement with three long bonds and three short bonds, creating a distorted structure. Phase transition occurs utilizing a bond-interchange mechanism, where short and long bonds simply swap during crystallization, yielding a low energy barrier and exceptionally fast phase transitions (Figure 7(d)). However, AIST suffers from poor thermal stability, especially at elevated temperatures, leading to potential data loss.

Extensive efforts have been devoted to doping diverse elements into Ge-Sb-Te systems to tailor their properties for PCM applications. Dopant atoms can substitute Ge, Sb, or Te, or occupy interstitial sites or vacancies, altering material's structural and electrical properties[160] (Figure 7(e)). N-doped GST improves the thermal stability and endurance by stabilizing the amorphous phase and reducing grain growth in the crystalline phase, which helps maintain consistent resistance and prevents resistance drift (Figure 7(f)). It also reduces the required RESET current, making the material more energy-efficient (Figure 7(g))[161]. However, nitrogen doping can retard the overall switching speed, making it less ideal for high-speed memory applications. Much like nitrogen doping, C-doped GST further enhances device endurance and thermal stability, while also reducing RESET current, thus lowering overall power consumption during the operation of PCM[164]. However, achieving uniform carbon incorporation into GST during deposition poses fabrication challenges. Sn-doped GST stabilizes both the amorphous and crystalline phases, improving data retention and reducing resistance drift to enhance long-term reliability[165]. However, similar to nitrogen doping, Sn-doped GST may exhibit slower switching speeds compared to undoped GST due to its enhanced phase stability.

While sputtering is well-suited for flat and large-area PCM applications, advanced device structures, such as confined PCM cells and high-density 3D architectures require more conformal deposition methods, including CVD and ALD. Common CVD precursors include $GeH_4$, $SbCl_3$, and $TeCl_4$. Metal-organic CVD (MOCVD) utilizing alkyl-based chemistry is particularly effective as it offers fast growth rates, precise control over film composition, and excellent gap-filling capabilities, ideal for confined PCM devices. Frequently used

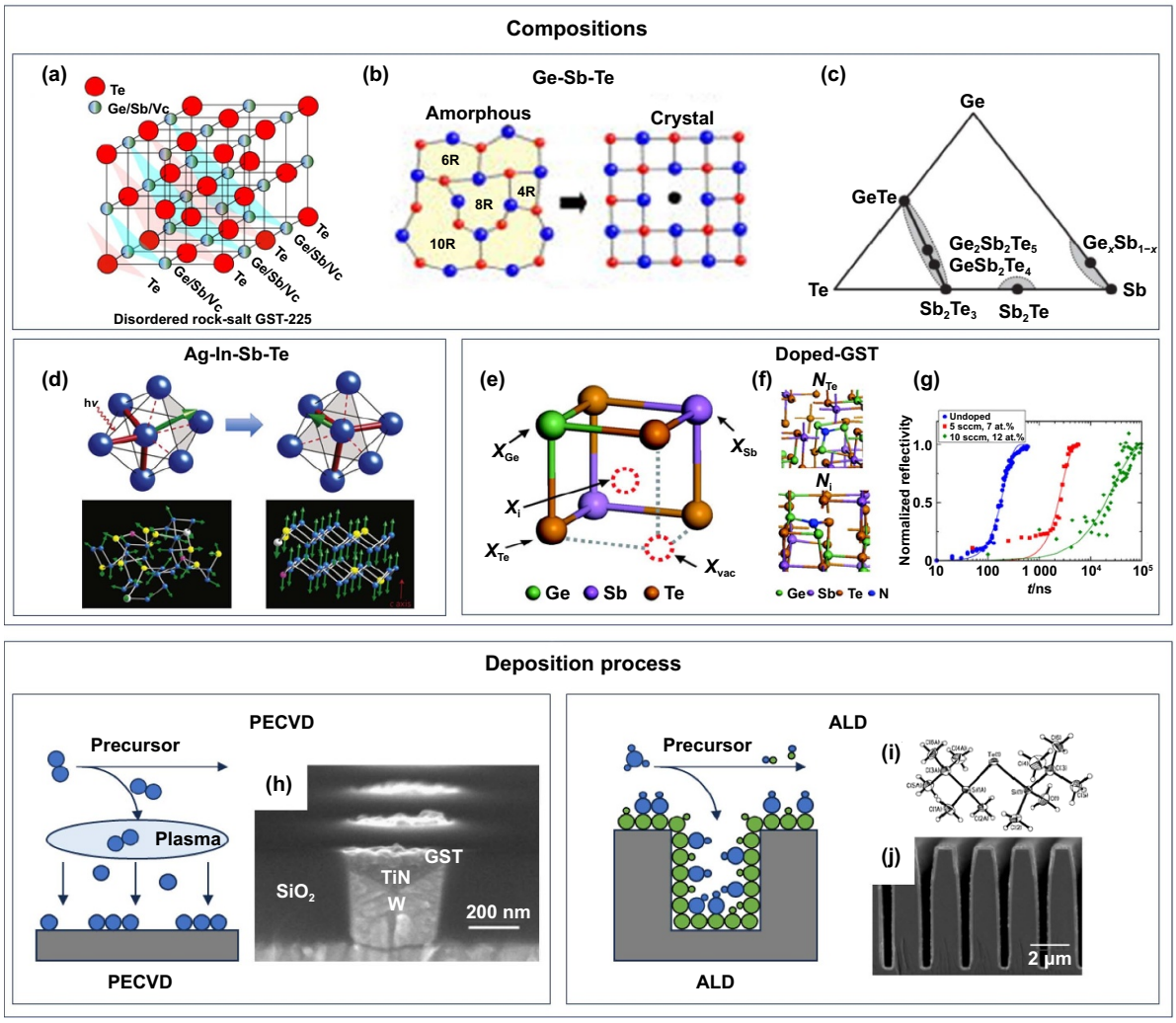


**Figure 7.** Composition engineering and deposition strategies for chalcogenide materials in phase-change memory applications. (a) Crystal structure of GST. Reproduced from[158]. CC BY 4.0. (b) Switching mechanism of GST. Reprinted from[157], with the permission of AIP Publishing. (c) Ternary phase diagram of the Ge-Sb-Te system phase change materials. Adapted from[156], with permission from Springer Nature. (d) Switching mechanism of AgInSbTe material. Adapted from[159], with permission from Springer Nature. (e) Representative doping sites of $Ge_2Sb_2Te_5$. (f) Local structure of N-GST. (e) and (f) Reprinted from[160], with the permission of AIP Publishing. (g) Crystallization time of N-GST material. Reprinted from[161], with the permission of AIP Publishing. (h) PECVD deposition result of the GST layer. Reproduced from[102]. [insert partner copyright line]. All rights reserved. © 2007 ECS—The Electrochemical Society. (i) and (j) Silyl-Te precursor and thermal ALD deposition result of GST layer. Reprinted (adapted) with permission from[103]. Copyright (2009) American Chemical Society.

precursors include $Ge(i\text{-}Bu)_4$, $Ge(allyl)_4$, and $Ge(NMe_2)_4$ for Ge sources that provide high vapor pressure, which facilitates the deposition process, especially when used in conjunction with Sb precursors such as $(i\text{-}Pr)_3Sb$ and $(Me_2N)_3Sb$. For Te, $(i\text{-}Pr)_2Te$ is preferred owing to its relatively high vapor pressure and ease of activation under plasma or thermal conditions in reducing gas environment. In CVD processes, the combinations of $Ge(i\text{-}Bu)_4$, $(i\text{-}Pr)_3Sb$, and $(i\text{-}Pr)_2Te$ have been extensively studied for their ability to balance growth rates and control film stoichiometry[102,166]. By controlling the cycling of each precursor, film composition can be finely tuned. For instance, increasing the number of Ge cycles leads to an increase in both Ge and Te content, while Sb content remains stable. Achieving the desired GST composition requires careful control of the Te feeding time, as Te tends to incorporate preferentially into the Ge layers over Sb layers. Plasma-enhanced CVD (PECVD) has been developed to lower the deposition temperatures while maintaining film quality. Plasma activation allows for the deposition of smooth, conformal films at temperatures below 573 K. In PECVD, hydrogen gas serves as a reducing agent to help break the bonds in metal-organic precursors and enhance step coverage.

In recent years, there has been growing interest in ALD for GST film deposition owing to its superior step coverage and precise thickness control. However, developing a compatible set of precursors remains challenging as Ge, Sb,

and Te precursors differ in chemical reactivity. In ALD processes, $Ge(NMe_2)_4$ and $Ge(N(SiMe_3)_2)_4$ are commonly used for Ge, while $(Me_2N)_3Sb$ and $((Me_3Si)_2N)_3Sb$ are selected for Sb. For Te, $(i\text{-}Pr)_2Te$, which can be reduced by $H_2$ plasma at high temperatures (above 573 K), is often employed[167]. However, differences in bond strengths between Ge-C, Sb-C, and Te-C complicate optimization of deposition conditions, leading to issues such as unwanted impurities (Si, C, and N) in the films. To address these issues, several research groups have developed ALD processes for GST films using silyl-based Te precursors, such as $(Me_3Si)_2Te$, which exhibit higher reactivity[103,168–172] (Figure 7(i)). These precursors enable the formation of GeTe and $Sb_2Te_3$ compounds through ligand exchange reactions at relatively low temperatures (as low as 363 K), eliminating the need for additional reducing gases (e.g., hydrogen). This results in improved film coverage and smoothness with lower impurity concentration (Figure 7(j)). Furthermore, researchers have demonstrated that GST films can be grown at even lower temperatures (around 333 K) using $GeCl_2$(dioxane), $Ge(OMe)_4$, and $Ge(OEt)_4$ for Ge; $SbCl_3$ and $Sb(OEt)_3$ for Sb; and $(Me_3Si)_2Te$, $(Et_3Si)_2Te$, and $(t\text{-}BuMe_2Si)_2Te$ for Te. Here, ligand exchange reactions, including $Ge(OMe)_4 + 2(Me_3Si)_2Te \rightarrow GeTe_2 + 4Me_3SiOMe$ and $2\,Sb(OEt)_3 + 3(Me_3Si)_2Te \rightarrow Sb_2Te_3 + 6Me_3SiOme$, facilitate the formation of GeTe and $Sb_2Te_3$ layers. The deposition of GST films through these low-temperature ALD reactions helps prevent crystallization during growth, enabling the formation of smooth, amorphous films with low impurity content. The amorphous nature of these films is crucial for preventing grain formation, which can negatively impact device performance by increasing surface roughness and film instability.

*3.1.4. Chalcogenide materials for optical memory.* Chalcogenide-based optical memory also holds promise in the field of quantum information science. As an emerging technology, chalcogenide-based quantum optical memory leverages the unique properties of chalcogenide materials with the principles of quantum computing and quantum optics. Chalcogenide materials such as GST-225 offer great potential for quantum information storage and processing due to their ability to reversibly switch between amorphous and crystalline states. Quantum optical memory is a technology that stores information encoded in quantum states, typically the quantum states of light, such as photons, which enables applications in quantum communication, quantum computing, and quantum encryption through processes of quantum state storage and retrieval. Moreover, chalcogenides exhibit transparency in the infrared spectrum, making them ideal candidates for quantum communication systems utilizing infrared photons[173,174]. In chalcogenide-based quantum optical memory, photons carrying quantum information can be stored within the materials system. Here, the phase transitions in chalcogenides can be controlled by optical or electrical pulses, enabling precise storage and manipulation of photon states. The ability to interact and control single-photon states makes chalcogenides highly suitable for quantum information processing. Notably, foundational research on quantum information has already explored chalcogenide materials, such as GST, underscoring their potential in this field. Recent studies have demonstrated the potential of chalcogenide materials as promising platforms for quantum optical storage. For example, reversible phase switching in GST-based nanostructures has been shown to modulate the coherence and phase of single photons, enabling programmable quantum photonic circuits[175]. Additionally, femtosecond laser excitation has been used to induce ultrafast phase transitions in Ge-Sb-Te systems, allowing subnanosecond optical switching suitable for quantum logic operations[176]. In another example, chalcogenide photonic crystal cavities have been utilized to trap and manipulate infrared photons with minimal loss, showing potential for quantum memory nodes integrated in on-chip systems[177]. These findings collectively demonstrate that chalcogenides are not only capable of storing quantum information via phase modulation but also offer low-loss optical properties and fast switching, which are essential for practical quantum information processing. Therefore, continued exploration of chalcogenide-based quantum optical memory could lead to novel architectures for quantum networks and integrated quantum photonic circuits.

As illustrated in Figures 8(a)–(c)[178], an experimental study was conducted on non-volatile chalcogenide phase-change metaswitches. In this work, the authors proposed a metaswitch platform using GST phase-change material, which controlled optical signals at the nanoscale. Operating across the near-infrared to mid-infrared spectrum, this platform offers thinner and faster operation compared to conventional optical switches. The study exploits GST's phase transitions to tune the optical properties of the metamaterial, significantly modulating signal transmission and reflectivity. The phase transitions induced by laser pulses shift the resonant frequency of the metamaterial, producing drastic changes in optical characteristics. The results demonstrated high contrast signal control over a broad range of wavelengths, providing applications in nanoscale optical switching, memory, and spatial light modulation devices based on chalcogenides. Furthermore, chalcogenide phase-change metamaterials can reversibly switch in response to diverse stimuli (i.e., electrical, thermal, optical), offering promising prospects for next-generation high-speed and multi-level switching devices.

To achieve rapid data processing and encryption, the development of high-speed, non-volatile, multi-level, rewritable memory devices operating in the THz frequency range has been pursued. To this end, a terahertz (THz) multi-level non-volatile optically rewritable encryption memory based on GST-225 was reported (Figures 8(e)–(n))[179]. By exploiting the phase-change behavior of GST to create multiple intermediate states, large areas of amorphous structures were created. By controlling the crystalline state of GST via laser pulses, a wide range of phase-change states were generated, enabling the storage of multi-level information. This THz memory device demonstrated fast operation with a response time of 4 ns, high reproducibility, and long-term stability. The device

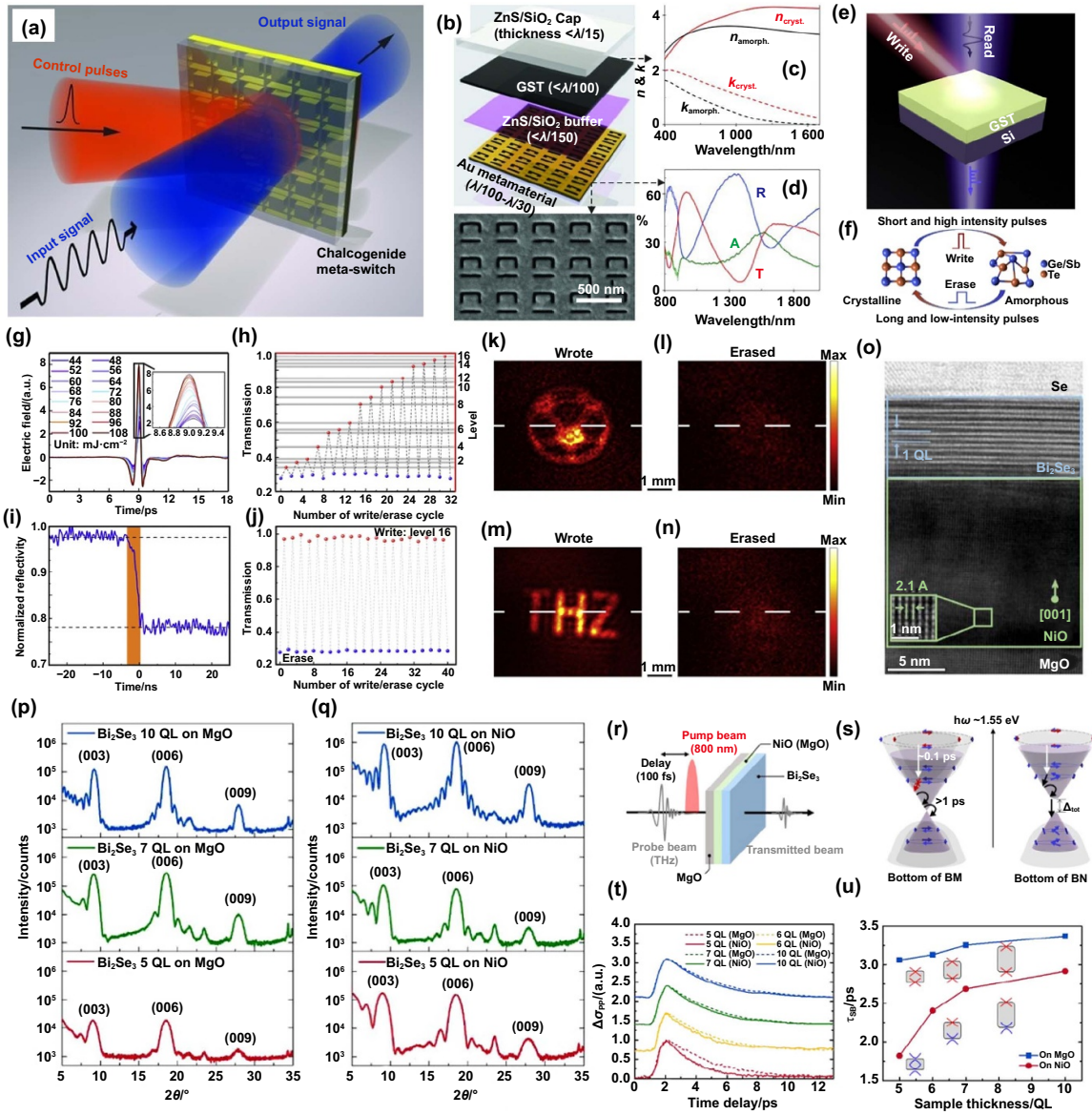


**Figure 8.** Operating principles and dynamics of chalcogenide materials for optical memory applications. (a) Schematic diagram of chalcogenide hybrid metamaterial switches experiment. (b) Multilayer structure of chalcogenide hybrid metamaterial switches. (c) Ellipsometrically measured visible/near-infrared index of refraction $n$ and extinction coefficient $k$ of the GST layer in its amorphous and crystalline states. (d) Reflection, transmission, and absorption spectra of a near-IR resonant metamaterial prior to application of the buffer, GST, and capping layers. (a)–(d)[178] John Wiley & Sons. Copyright © 2013 WILEY-VCH Verlag GmbH & Co. KGaA, Weinheim. Operation principle of a GST-based optical multi-level encryption memory cell. (e) Control pulses with various powers are used to switch the GST from crystalline to intermediate and amorphous states, as a write channel. Information is stored in the phase states of GST, which exhibit varied THz transmission. (f) By applying short and high-intensity pulses, GST can be transited from crystalline to amorphous state, whereas by using long and low-intensity pulses, GST can be switched back. Totally different bonding structures between amorphous-GST and crystalline-GST lead to striking optical contrasts in the two states. (g) Measured time-domain THz signals through the memory cell at sixteen pump energies. A magnified view of the signals is shown in the inset. (h) Sixteen storage levels and corresponding THz transmissions. (i) The writing speed of 4 ns is measured by a pump-probe system. (j) Repeatability of the switching between level '16' and erased status. High-density information storage of designed memory cells has been experimentally verified by using a near-field scanning terahertz microscopy system. (k) The writing and (l) erasing results of basketball. (m) The writing and (n) erasing results of 'THz'. (e)–(n) Reprinted (adapted) with permission from[179]. Copyright (2022) American Chemical Society. (o) Cross-sectional image of Se(5 nm)/$Bi_2Se_3$(7 nm)/NiO(15 nm)/MgO structure using HR-TEM. A c-axis-oriented $Bi_2Se_3$ 7 QL (∼7 nm) grew well on NiO (001). Each layer of $Bi_2Se_3$ has Van der Waals gaps, represented as the dark image. XRD (θ-2θ scan) result of the $Bi_2Se_3$ (001) family grown on (p) MgO and (q) NiO substrates with different crystallinity according to substrate. The films grown on NiO have a better c-axis orientation than those grown on MgO, which can be inferred by the clarity of the fringes. (r) Illustration of OPTP measurement with pump beam (800 nm) and probe beam (THz). (s) Schematic decay process in the band structure of $Bi_2Se_3$ (5 QL) on MgO and NiO. Δtot is defined as Δexchange + Δhybrid. (t) Change in transmitted THz signal intensity is converted to optical conductivity on the fs time scale by thin-film approximation. Exponential decay process through the surface band of film on NiO (solid line) is faster compared with the film on MgO (dashed line). (u) Recombination time of BN is reduced drastically in the thin film, indicating that surface band gap is induced (red straight line and blue parabolic line represent Dirac band and hybridized band, respectively). (o)–(u)[180] John Wiley & Sons. © 2023 Wiley-VCH GmbH.

was able to store hexadecimal code information in 16 discrete levels with robust performance over multiple write-erase cycles. Furthermore, optical printing and encryption memory functions were implemented successfully. These findings have contributed significantly to high-speed data storage and encryption in THz communication and next-generation computing systems, while also laying the groundwork for device fabrication without the need for optical lithography.

Earlier efforts using chalcogenide materials faced challenges in enhancing device performance due to limitations in device patterning. To address this issue, researchers have developed new materials and patterning-free fabrication techniques for chalcogenide thin films. To this end, Zhen Hu and co-workers[181] demonstrated a method for high spatial resolution (∼0.6 μm) laser-induced oxidation of $Sb_2S_3$ to alter the refractive index. This approach provides precise, multi-level control of the refractive index, facilitating the fabrication of integrated photonic devices, such as color printing patterns, metasurfaces, and Fresnel zone plates. The resulting metasurfaces effectively manipulate infrared light, while Fresnel zone plates demonstrated effective beam focusing capabilities. By utilizing the phase-change properties of $Sb_2S_3$, these devices offer reconfigurable optical functionalities expanding their applicability as active photonic components, such as optical communication, sensing, and imaging. Moreover, the simplified fabrication process is compatible with commercial manufacturing technologies, representing a significant progress toward the development of chalcogenide-based photonic structures for advanced optical systems.

In pursuit of enhanced quantum optical performance, efforts have also been made to develop synthetic procedures for high-quality single-crystal chalcogenide thin films. To this end, a method employing MBE-based self-ordering technique was reported to achieve single-crystallinity in chalcogenide-based materials. Recently, researchers investigated the interaction of $Bi_2Se_3$, a topological insulator, with antiferromagnetic NiO (Figures 8(o)–(u))[180]. Topological insulators, characterized by insulating interiors but conductive surface states, hold promise for quantum devices due to their spin-polarized Dirac cones formed by strong spin-orbit coupling (SOC). The study revealed that when $Bi_2Se_3$ is grown on NiO, exchange interactions induced by the antiferromagnetic layer suppress the surface states of $Bi_2Se_3$. In thinner films, surface state hybridization is further accelerated, leading to bandgap opening and altered topological properties. Using THz spectroscopy, Hall measurements, and density functional theory (DFT) calculations, the researchers confirmed surface state hybridization and its impact on electronic properties. These findings deepen our understanding of how magnetic interactions affect topological insulators and pave the way for new device architectures that exploit surface state control, with potential applications in spintronics and quantum technologies. Furthermore, the synthetic strategies developed for these materials are applicable not only to chalcogenides but also to a broader class of quantum materials.

Advances in spin-charge conversion (SCC) and THz emission have also been made using bismuth-antimony ($Bi_{1-x}Sb_x$) alloy thin films[182]. The ability to convert spin into charge is crucial in spintronics, and $Bi_{1-x}Sb_x$ alloy films exhibited significantly stronger THz emission compared to conventional materials such as Bi-Se and Bi-Te alloys. By varying the Sb concentration, researchers systematically analyzed SCC efficiency using THz spectroscopy and identified the origins of enhanced THz emission. The $Bi_{1-x}Sb_x$ alloy films exhibited much stronger spintronic THz emission than both platinum (Pt) and $Bi_2Se_3$, with exceptionally high SCC efficiency. Specifically, the topological surface states (TSS) of the material were found to play a significant role in enhancing SCC. The findings highlight the potential of $Bi_{1-x}Sb_x$ alloys to maximize SCC efficiency in topological insulator states, offering valuable insights for developing high-performance spintronic devices and THz emitters.

Recent efforts have also focused on utilizing TMDs to improve the properties of single-crystal-based materials. Yanyu Jia and co-workers explored metallization-induced superconductivity on 2D chalcogenide surfaces[183]. The authors introduced palladium (Pd) metallization to monolayers and bilayers of various chalcogenides, such as $WTe_2$ and $MoTe_2$, to create novel superconducting materials. Conducted at a relatively low temperature (around 473 K), the non-diffusive metallization process transformed TMDs into new compounds, such as $Pd_7WTe_2$ and $Pd_xMoTe_2$, which exhibited superconductivity at extremely low temperatures. For example, $Pd_7WTe_2$ showed a superconducting transition temperature ($T_c$) of approximately 0.45 K, with bilayer $WTe_2$ exhibiting a higher $T_c$ than the monolayer analogue when combined with Pd. This report provides a promising approach to introducing superconductivity in a wide range of 2D materials, with significant potential to advance topological quantum computing (where superconductivity is essential) as well as for experimental exploration of exotic quantum states, such as non-Abelian anyons and Majorana zero modes. Despite these efforts, achieving high-quality single-crystal chalcogenide materials remains a significant challenge for realizing practical quantum optical memory. In addition to material development, further progress is needed in device integration with quantum computing and communication platforms, as well as in manipulating light-matter interactions to fully harness the potential of these materials for next-generation quantum technologies.

### *3.2. Ovonic threshold switching selector*

*3.2.1. Device characteristics.* OTS selectors are critical components in various non-volatile memory technologies, including PCM, resistive random-access memory (ReRAM), and other emerging memory devices. They regulate electrical current flowing through memory cells, preventing sneak currents in high-density crossbar array architectures, particularly in 3D stacked architectures (e.g., 3D XPoint), as illustrated in Figure 9(a). To increase the density of these two-terminal devices, they must exhibit highly nonlinear current-voltage (*I-V*) characteristic. Compared to the initially explored rectifier selectors, the threshold switching selectors offer higher nonlinearity, and thus have recently garnered significant attention.

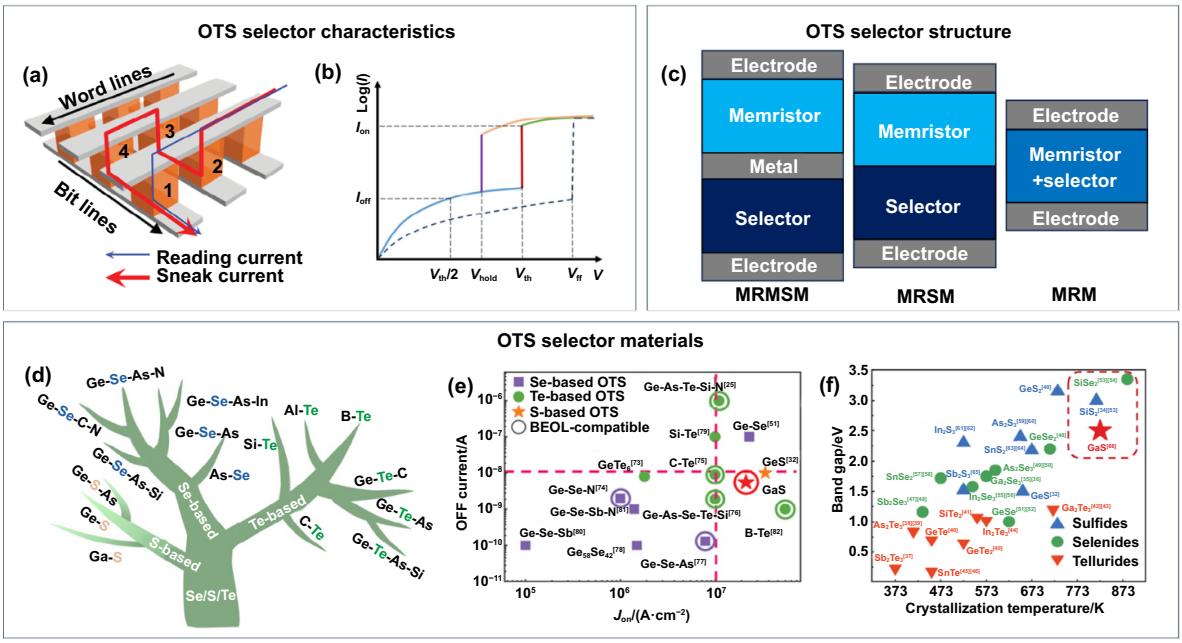


**Figure 9.** Key characteristics, architectures, and material systems of chalcogenide-based ovonic threshold switch (OTS) devices. (a) Concept of sneak current in crossbar.[184] John Wiley & Sons. © 2014 WILEY-VCH Verlag GmbH & Co. KGaA, Weinheim. (b) Operation scheme of OTS selectors. (c) Three types of crossbar array structures. (d) Schematic classification of OTS materials. (b)–(d) Reproduced from[185]. CC BY 4.0. (e) and (f) Comparation of OTS materials (e) on and off state current level, (f) band gap and crystallization temperature. (e) and (f)[186] John Wiley & Sons. © 2022 Wiley-VCH GmbH.

This enhanced nonlinearity makes threshold switching selectors particularly suitable for high-density memory applications, as it helps reduce leakage currents and improve overall device performance[184]. OTS selectors exhibit a highly nonlinear *I-V* behavior, maintaining a high-resistance 'off' state until the applied voltage reaches a specific threshold voltage ($V_{th}$). Upon reaching $V_{th}$, the OTS abruptly switches to a low-resistance 'on' state, allowing current to flow through the device, thereby enabling selective access to individual memory cells (Figure 9(b)). Activation of the selector involves a 'first fire' voltage ($V_{ff}$), which initiates switching, followed by a $V_{th}$ to sustain 'on' state, and reverts to the 'off' state once the voltage drops below the hold voltage ($V_{hold}$). The relationship between these voltages is $V_{ff} > V_{th} > V_{hold}$. Key electrical parameters for OTS devices include the 'on' state current, 'off' state leakage current, on/off ratio, endurance, thermal stability, threshold voltage/field, and switching speed.

For high-density 3D memory applications, the OTS device must satisfy several performance requirements, which are inherently linked to the material properties[29]. First, to effectively drive the connected memory cell, the OTS device must sustain a high current density, often exceeding 10 MA·cm$^{-2}$ for 3D PCM applications. This necessitates the use of materials with strong covalent bonds to prevent bond-breakage and recrystallization during operation. Second, to achieve high storage capacities, 'off' state leakage currents must be suppressed below $10^{-8}$ A, and device selectivity should reach or exceed $10^4$. To meet these requirements, materials with large mobility gaps and high activation barriers are essential. Table 3 summarizes mobility gaps and activation barriers of select candidates for OTS selector materials. Furthermore, the endurance of OTS devices must also exceed $10^8$ cycles to surpass memory unit lifetimes of typically $\sim 10^6$ cycles. Consequently, high thermal stability is crucial to prevent crystallization and phase separation during operation. Compatibility with advanced logic technologies and lower power consumption also requires OTS devices to have low $V_{th}$. However, a delicate balance exists between $V_{th}$ and leakage current, as excessively low $V_{th}$ may create conflict with the need for low leakage currents. The switching speed of OTS devices must be within 100 ns, to match the speed of memory units. To fulfil these requirements, OTS devices should operate through electron-dominated switching mechanism, while avoiding diffusion of materials such as Ag or Cu, which can degrade device performance.

*3.2.2. Device structure and integration.* In traditional rectifier selectors, the rectification characteristics of the metal-semiconductor interface, such as those found in Schottky diodes, are often utilized. In these structures, a metal layer is incorporated occasionally between the selector layer and the memristor layer to facilitate desired electrical characteristics. Noble metals with high work functions have been extensively explored for this purpose, but implementing such structures in vertical 3D configurations presents fabrication challenges, particularly with respect to optimizing the etching process. As a result, structures that do not require intermediate metal layers

**Table 3.** Mobility gap ($E_\mu$) and activation barrier ($E_a$) of OTS candidate materials.

| Materials | $E_\mu$/eV | $E_a$/eV | References |
|---|---|---|---|
| As-Te | ∼0.8 | ∼0.4 | [187] |
| Ga-Se | ∼1.76 | ∼0.66 | [188] |
| Ge-S | ∼1.52 | ∼0.38 | [189] |
| Ge-Se | ∼1.2–1.4 | ∼0.95 | [23,190] |
| Sb-Te | ∼0.6–0.9 | ∼0.3–0.4 | [191] |
| Si-S-Te | ∼1.14–1.27 | ∼0.45–0.60 | [192] |
| Si-Sn-S | ∼1.08–1.19 | ∼0.59–0.61 | [192] |
| Si-Ge-S | ∼1.26 | ∼0.56 | [192] |
| Ge-P-S | ∼1.05–1.14 | ∼0.58–0.60 | [192] |
| Ge-Sn-S | ∼1.12 | ∼0.54 | [192] |
| Si-P-S | ∼1.05 | ∼0.46 | [192] |

are favored. Moreover, there is a strong preference for designs in which the selector element and the memristor element are integrated into a single structure, simplifying fabrication and improving device scalability (Figure 9(c)).

OTS selectors typically feature a thin layer of chalcogenide material sandwiched between two metal electrodes, commonly TiN or W, in direct contact with the memory element. Unlike rectifier selectors, OTS selectors do not require an intermediate metal layer, as their non-linear *I-V* characteristics arise from the bulk properties of the chalcogenide material itself. This configuration ensures a uniform electric field across the chalcogenide layer, which is crucial for consistent switching behavior and reliable performance. The quality of interface between the chalcogenide material and the electrodes plays a critical role in determining the switching characteristics of the OTS device. A smooth, well-defined interface minimizes leakage currents and ensures the device maintains a high-resistance state until the threshold voltage is reached, preserving memory array integrity and preventing sneak current induced data corruption. The deposition of chalcogenide films for OTS devices is a key step that directly influences the electrical properties and switching behavior. Physical vapor deposition methods, such as sputtering, allow for precise control over film thickness and composition, which is essential for uniform switching characteristics across the wafer. ALD, on the other hand, provides excellent conformality and thickness control over complex 3D structures at the atomic level, making it particularly suitable for OTS layers in densely packed memory arrays. Following the bottom electrode deposition, the chalcogenide film is deposited using sputtering or ALD. Photolithography is then employed to pattern the device structure, followed by etching to remove excess material and define the active areas of the OTS devices. Once patterned and etched, an encapsulation layer, typically made of dielectric materials such as $Si_3N_4$, is deposited to protect the chalcogenide film from environmental exposure and potential damage during subsequent processing steps. In advanced memory architectures, such as 3D crossbar arrays, multiple layers of OTS selectors and memory cells are stacked vertically to increase storage density. Such architecture demands precise alignment and uniform deposition across all layers to ensure reliable operation[150]. CMP is commonly used to create a flat surface after each layer is deposited, which is essential for sequential stacking of additional layers and maintaining device integrity. While PCM materials require both amorphous and crystalline phases to function properly, OTS materials exist exclusively in the amorphous state. To meet stringent thermal budget of back-end-of-line (BEOL) process, OTS materials are designed to remain stable in the amorphous state at elevated annealing temperatures of 673–723 K.

*3.2.3. Chalcogenide materials for OTS.* OTS selectors used in memory devices are primarily based on chalcogenide materials, with Se-, Te-, and S-based systems being the most common (Figure 9(d)). Each material system offers distinct electrical properties, making them suitable for specific applications in controlling currents in high-density memory arrays. The material composition of these OTS selectors directly influences key device parameters such as $V_{th}$, thermal stability, switching speed, and endurance. Se-based materials, primarily consisting of Ge-Se alloys, are known for their high crystallization temperatures and large bandgaps, both of which contribute to reduced leakage current during the off state[105] (Figures 9(e) and (f)). A notable composition is Se rich $Ge_xSe_{1-x}$, exhibiting a crystallization temperature exceeding 873 K, providing excellent thermal stability[193]. This makes Se-based materials ideal for applications requiring high-temperature operation and/or long-term reliability. However, a common drawback of Se-based materials is their high $V_{th}$, which increases with selenium content, resulting in higher energy consumption during switching. This limits their suitability for low-power applications where energy efficiency is critical. Te-based materials, such as Ge-Te alloys, are known for their low $V_{th}$, making them suitable for low-power applications[194]. A common composition, $GeTe_6$, offers low switching energy and fast switching speeds. Other Te-based compositions, including Si-Te[195], Zn-Te[196], C-Te[197], and B-Te[198], are tailored to optimize switching speeds and threshold voltage levels. While Te-based materials are excellent for applications requiring rapid switching and low-power operation, they suffer from relatively low thermal stability,

which can lead to shorter device lifetimes under high thermal loads or extended cycling conditions. Te-based materials have a strong tendency to crystallize, even when the Ge content is increased, as in $GeTe_2$, and thus, the material still exhibits a relatively low crystallization temperature of around 533 K. Such lower thermal stability can limit the use of Te-based materials in high-temperature environments or applications requiring extended endurance. S-based materials, such as Ge-S alloys, offer high thermal stability and wide bandgaps similar to Se-based materials (Figures 9(e) and (f)). Compositions including GeS, $Ge_2S_3$, and $GeS_2$ have crystallization temperatures exceeding 873 K, making them well-suited for applications demanding high endurance and long-term stability[199]. Other S-based compositions, such as Ge-As-S, have demonstrated exceptional durability, withstanding over $10^{10}$ switching cycles. This makes them promising for applications such as 3D memory architectures where long-term endurance and reliability are essential[189]. However, S-based materials also tend to exhibit relatively high $V_{th}$, making them less ideal for low-power applications.

Beyond binary alloys, multi-chalcogenide OTS materials have been developed to achieve more balanced performance. Compositions such as Si-Ge-As-Se-Te incorporate both Se- and Te-based constituents to strike a balance between low threshold voltage and high thermal stability[200]. These materials are being explored extensively for use in advanced memory applications, where endurance, power efficiency, and thermal stability are critical.

### 3.3. Selector-only memory (SOM)

*3.3.1. Device characteristics.* SOM integrates the selector and memory functions into a single chalcogenide layer, eliminating the need for a separate memory element. This simplifies the device structure, reduces device complexity, reduces power consumption, and makes SOM scalable for future technology nodes. SOM is particularly well-suited for high-density memory arrays, offering advantages in simplifying design and reducing costs. Additionally, SOM devices exhibit high endurance and reliability, as their switching mechanism involves significantly lower current densities compared to conventional PCM[201,202]. The concept of SOM originates from the previously observed instability in OTS devices, specifically the $V_{th}$ relaxation effect or drift effect occurring after the extended delay time between measurement pulses. An early observation of this behavior was a polarity-induced $V_{th}$ shift in SiGeAsTe OTS, where the magnitude of $V_{th}$ increases upon reversal of pulse polarity (Figure 10(a)). This effect was also observed in a later work on Se-based SiGeAsSe OTS[95]. This polarity-induced shift $\Delta V_{th}$ is both stable and reversible, allowing the $V_{th}$ to be electrically tuned. In SiGeAsTe devices, the $\Delta V_{th}$ is about 0.3 V when switching from positive to negative polarity under low-current conditions. In SiGeAsSe devices, the shift is more pronounced, with a $\Delta V_{th}$ of around 1.3 V in the negative branch and 0.6 V in the positive branch. Even larger polarity-induced shifts have been reported in GeSe-based OTS devices, with $\Delta V_{th}$ reaching up to 3.5 V in the positive polarity branch and about 1 V in the negative branch at high current levels of approximately 4 mA (Figure 10(b)). At lower current levels, such as 300 μA, the shift is still present but with a smaller magnitude. This ability to modulate the $V_{th}$ by reversing the pulse polarity provides a useful mechanism for fine-tuning the performance of these memory devices.

*3.3.2. Device structure and integration.* SOM devices typically feature a single chalcogenide layer that serves as both the selector and the memory element, sandwiched between two metal electrodes made of TiN or W. The chalcogenide material is engineered to exhibit both threshold switching characteristics and memory retention properties. The fabrication process for SOM devices is similar to that of OTS devices, involving the precise deposition and integration of the chalcogenide layer. Consequently, manufacturers of OTS-based resistance-variable memory have introduced fully integrated devices that consolidate selector and memory functionalities within a unified structure (Figures 10(c) and (d)). Sputtering remains the primary method used for chalcogenide film deposition in SOM devices, typically employed to deposit both the chalcogenide layer and the metal electrodes during the initial stages of fabrication.

*3.3.3. Chalcogenide materials for SOM.* SOM technology utilizes specialized chalcogenide materials that combine both memory and selector functionalities, eliminating the need for separate phase-change materials. These materials are crucial for achieving reliable threshold switching and resistive switching performance in high-density memory arrays. Extensive research has been conducted on optimizing chalcogenide compositions to achieve desirable properties for SOM, such as switching speed, endurance, and power consumption. Among a wide range of compositions, GeSe-based alloys are commonly used in SOM devices[203–207], with $Ge_{50}Se_{50}$ being the standard owing to its balance between low $V_{th}$ and high endurance[95,208]. The material also exhibits a stable switching behavior, making it suitable for low-power applications where efficiency is critical. Another variant, $Ge_{60}Se_{40}$, has been studied for its enhanced switching stability[95,206]. However, as the germanium content increases (e.g., Ge-rich compositions), performance variability tends to rise, making these materials less appealing for long-term operations. Therefore, careful control over composition is required to maintain consistent switching behavior over repeated cycles. Despite these limitations, GeSe alloys are attractive candidates for use in high-density memory arrays. In addition to binary alloys, multi-component chalcogenides, such as SiGeAsTe and SiGeAsSe, have also been investigated for SOM. These materials exhibit a more complex nonlinear *I-V* behavior, which is important for preventing sneak currents in crosspoint array memory architectures. SiGeAsTe alloys are known for their excellent thermal stability and robust switching performance, though they may suffer from $V_{th}$ drift over time, impacting their reliability in long-term applications. In contrast,

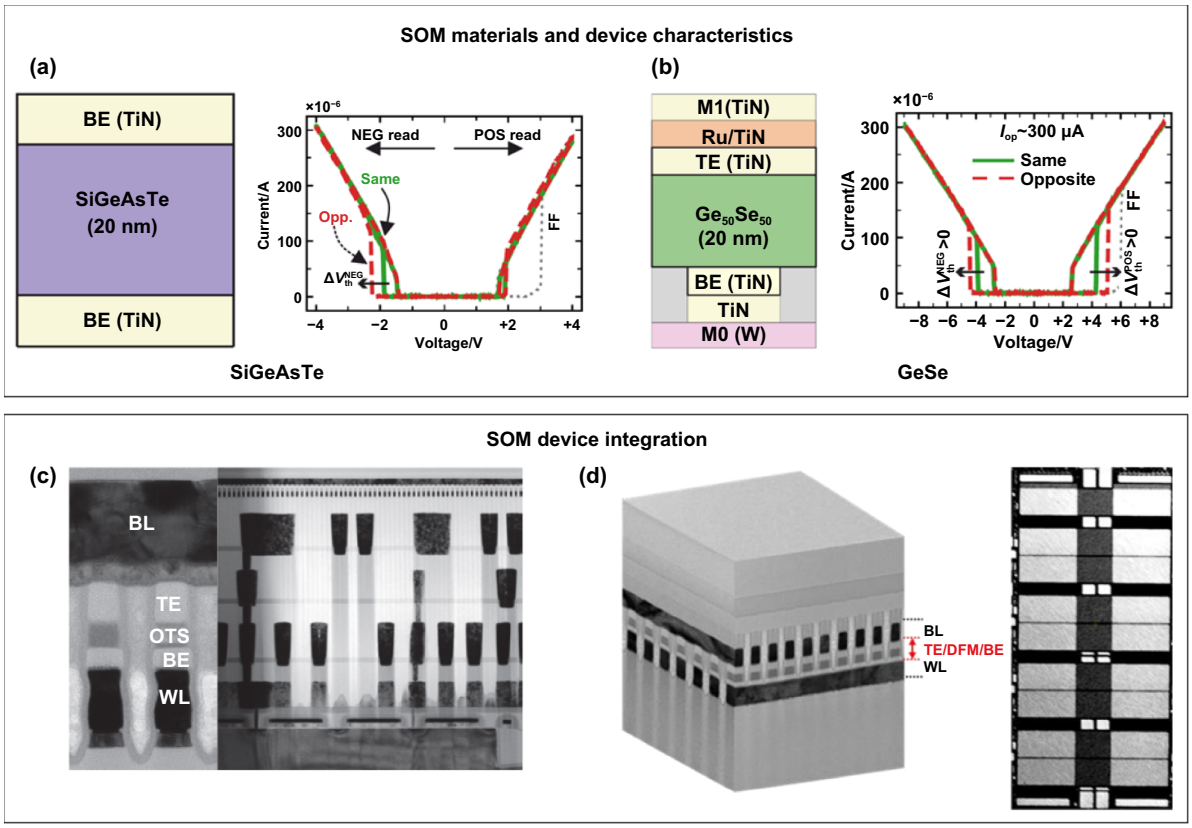


**Figure 10.** Key material systems, characteristics, and architectures of chalcogenide-based selector-only memory (SOM) devices. (a) and (b) Polarity-induced $V_{th}$ shift results of SOM devices (a) SiGeAsTe, (b) GeSe materials. (a) and (b)[95] John Wiley & Sons. © 2023 Wiley-VCH GmbH. (c) and (d) Integrated SOM devices presented by memory companies. (c) © (2023) IEEE. Reprinted, with permission, from[201]. (d) © (2022) IEEE. Reprinted, with permission, from[202].

SiGeAsSe compositions have demonstrated improved stability and reduced polarity-induced shifts in $V_{th}$, making them better suited for memory devices requiring consistent performance under fluctuating operational conditions. A primary advantage of these chalcogenide materials in SOM technology is their ability to operate at low threshold voltages, making them highly efficient for low-power applications. In particular, materials such as GeSe and SiGeAsSe have shown significant promise for minimizing power consumption while maintaining high endurance, with some compositions capable of withstanding over $10^8$ switching cycles. This makes them strong candidates for long-term memory storage applications where reliability and power efficiency are essential. Nevertheless, there are also challenges associated with using these materials. For example, SiGeAsTe compositions are prone to threshold voltage drift, which can cause variability in performance over time. Additionally, Ge-rich GeSe compositions may exhibit lower thermal stability, which can result in inconsistent threshold voltages under high-temperature conditions. Furthermore, the use of multi-component systems (e.g., SiGeAsSe) introduces added complexity in materials synthesis and integration, requiring stringent control over deposition parameters and integration processes to ensure reproducibility across large-scale device fabrication.

### *3.4. Sensors*

*3.4.1. Device characteristics.* TMDs-based sensors offer superior performance compared to conventional sensor technologies owing to the inherent properties of the material. TMDs possess an atomically thin structure, providing a high surface-to-volume ratio, which enhances interactions with the external environment. Despite their atomic thickness, TMDs exhibit excellent electrical properties, enabling high sensitivity to trace amounts of gases or chemicals. This remarkable sensitivity is further supported by their high electron mobility, which facilitates fast response times. For instance, TMDs-based sensors enable rapid detection through quick interactions between electrons and analytes, making them highly advantageous for real-time monitoring applications. Additionally, the intrinsic physical and chemical properties of TMDs can be further enhanced by incorporating functional materials, thereby improving selectivity toward specific analytes. This capability allows for the differentiation of various chemical species as well as selective reactions to specific gases or chemicals. The ultra-thin structure of TMDs, coupled with their high surface area, also contributes to low power consumption during sensor operation[209–211]. Furthermore, these materials exhibit high electrical conductivity, which enables low-voltage oper-

ation and significantly reduces power consumption. TMDs also exhibit excellent chemical and thermal stability, ensuring long-term reliability of the sensor. Materials such as $MoS_2$ and $WSe_2$, in particular, demonstrate high thermal stability, allowing for stable operation even under extreme environments. Moreover, TMDs possess tunable electronic properties that can be easily modulated by external stimuli, such as electric fields, mechanical strain, or doping[212–214]. This tunability plays a key role in optimizing sensor performance, allowing the device to function effectively under various operating conditions. The atomically thin nature of TMDs-based sensors also facilitates effortless miniaturization, and their compatibility with existing CMOS technology allows for seamless integration into integrated circuits (ICs). This makes TMDs suitable for high-density sensor arrays as well as incorporation into wearable and portable electronic devices. Additionally, TMDs are also mechanically flexible, making them ideal candidates for flexible electronics. This mechanical flexibility supports the development of next-generation sensors for emerging applications, such as wearable sensors, flexible displays, and smart patches. Overall, the device characteristics of TMDs-based sensors, combining high performance, low power consumption, and mechanical flexibility, allow them to overcome the limitations of conventional sensor technologies. As a result, they are considered as key components in the development of next-generation sensing platforms.

*3.4.2. Device structure and integration.* The unique properties of TMD materials define both the device structure and integration approaches for TMD-based sensors, with their atomic-scale thickness and the ability to form heterostructures playing central roles. Single-layer TMD structures, composed of a single atomic sheet, allow highly efficient interactions with analytes owing to their vast surface-to-volume ratio. This makes them particularly suitable for high-sensitivity applications[215]. In contrast, multi-layer TMD structures provide greater mechanical stability and can be stacked to achieve specific functional enhancements[216,217]. For example, stacking $MoS_2$ with $WSe_2$ in heterostructures enhances both sensitivity and selectivity by combining the complementary properties of constituent materials, enabling more precise and targeted sensing performance[218,219]. The structural integration of TMD-based sensors with nanoelectrodes is another critical factor in further optimizing device performance. Nanoelectrodes ensure uniform current distribution across the ultra-thin TMD layer, enhancing sensitivity and response time[220]. These electrodes can be precisely tailored in terms of shape and composition, allowing fine-tuning of the sensor's electrical properties to meet specific design requirements. Heterostructure formation is also a key structural strategy in the design of TMD sensors. By combining different 2D materials, heterostructures such as graphene/$WSe_2$ or $MoS_2$/$WSe_2$ are possible to achieve synergistic effects that go beyond the capabilities of individual materials[221,222]. Controlled stacking within these heterostructures enables precise modulation of physicochemical properties, such as charge transfer, interlayer bonding interactions, and bandgap energy, which are essential for achieving high-performance sensor characteristics. Defect engineering and surface functionalization also contribute to the structural optimization of TMD-based sensors[223,224]. Defects in the TMD layer provide active sites for analytes, increasing the material's chemical reactivity, while surface functionalization introduces specific chemical groups that further enhance selectivity. These structural modifications, at the atomic and molecular levels, enable the development of highly selective and sensitive sensors tailored for specific detection tasks. The compatibility of TMD materials with CMOS processes is another significant advantage for large-scale sensor integration. This compatibility allows TMD layers to be incorporated directly into existing semiconductor manufacturing workflows, supporting the development of CMOS-integrated sensor arrays with on-chip data processing capabilities. Additionally, the mechanical flexibility of TMDs enables integration not only with rigid CMOS systems but also with flexible electronics, expanding the scope of potential applications. Scalable fabrication methods such as chemical vapor deposition (CVD) and physical vapor deposition (PVD) play essential roles in the structural development of TMD-based sensors, offering the ability to synthesize large-area high-quality TMD layers[91,225]. Techniques such as roll-to-roll processing further support cost-effective production of flexible TMD-based sensors, facilitating their use in emerging technologies such as wearables and smart textiles. These fabrication methods also support wafer-scale synthesis, enhancing the integration of TMD-based sensors into existing silicon-based devices.

*3.4.3. Chalcogenide materials for optical sensor.* TMDs are emerging as promising materials for optical sensors due to their unique electronic and optical properties[212,226–228]. TMDs typically consist of transition metals (e.g., Mo, W, Ti) sandwiched between layers of chalcogen atoms (e.g., S, Se, Te), forming atomically thin layers. These materials possess exceptional optical properties, such as direct bandgaps in monolayers, high absorption coefficients, and strong light-matter interactions, making them suitable for various optical sensing applications. Early research on optical sensors using TMDs primarily focused on leveraging the intrinsic properties of the material and exploring new TMD compounds. However, optical sensors relying solely on the intrinsic properties of TMDs faced limitations in performance improvement. To address this issue, various strategies have been developed to modify the surface of TMDs and improve the performance of optical sensors. To this end, the use of organic dye molecules was explored to improve the performance of $MoS_2$-based photodetectors[213]. In this work, three organic dyes—methyl orange (MO), rhodamine 6G (R6G), and methylene blue (MB), with different molecular structures and optical absorption bandwidths—were drop-cast onto $MoS_2$ photodetectors to examine their impact. Among them, MB showed the highest performance improvement, increasing the photocurrent by approximately 20-fold. The device's photoresponsivity

(9.09 $A \cdot W^{-1}$), detectivity ($2.2 \times 10^{11}$ Jones), and external quantum efficiency (1 729% at 610 nm) were significantly enhanced. The performance enhancement was attributed to a photoinduced charge transfer mechanism and an n-doping effect caused by the dye molecules. MB's flat molecular structure and high absorption coefficient were cited as reasons for its superior performance. These findings suggest that dye-sensitized $MoS_2$ photodetectors have potential for applications in touch panels, environmental sensors, and biosensing devices. High-sensitivity optical sensors have also been developed using TMDs synthesized using CVD[229]. A notable example involves the use of monolayer $MoS_2$ FETs with a buried-gate structure. These devices achieved a photoresponsivity of 6.86 $A \cdot W^{-1}$ at 395 nm with zero gate bias voltage and a light intensity of 2.57 $mW \cdot cm^{-2}$. When a buried-gate voltage of 8 V was applied, the photoresponsivity increased by nearly 10-fold. The response time of these devices was approximately 350 ms, demonstrating an improvement over other $MoS_2$ photodetectors using back-gate FET structures that require high gate voltages (up to 70 V). The lower operating voltages of the buried-gate structure enhanced the feasibility of energy-efficient optical sensors for practical applications such as imaging arrays and low-power photodetection systems.

Recognizing that the sensitivity of optical sensors cannot be significantly improved through engineering of TMD materials alone, researchers have also investigated approaches to enhance sensitivity by improving the metal-TMD interface. One such approach involves the use of femtosecond laser irradiation to reduce the contact resistance between $MoS_2$ and metal contacts[117]. Femtosecond laser irradiation reduced the contact resistance by more than three orders of magnitude without causing structural damage or phase changes in $MoS_2$. A $MoS_2$-based photodetector treated with femtosecond laser irradiation exhibited a photoresponsivity of 68.8 $A \cdot W^{-1}$ at a low bias voltage of 0.5 V, which was ~80 times higher than untreated devices. The improvement was attributed to the removal of organic contaminants, enhanced interlayer coupling, and reduction in Schottky barrier at the metal-$MoS_2$ interface. This localized laser treatment represents a universal method for improving the performance of TMD-based devices, making it suitable for advanced nanoscale electronic applications such as sensors and optoelectronic devices. An alternative method involves the formation of van der Waals (vdW) contacts using buffer layers, such as selenium (Se), to mitigate Fermi level pinning (FLP)[230]. Traditional metal-semiconductor junctions suffer from high Schottky barrier heights (SBHs) owing to interfacial defects and orbital overlap between metal atoms and the semiconductor. By inserting a Se buffer layer between metals (e.g., Au) and TMDs (e.g., $WSe_2$), physical and chemical interactions are reduced, preserving the theoretically predicted Schottky-Mott limit and enabling low-resistance stable contacts. As a result, the fabricated devices demonstrated significant performance improvements, such as low contact resistance (1.25 $k\Omega \cdot \mu m$), a high on/off ratio ($>10^6$), and stable p-type operation. In contrast to direct metal contacts, which showed higher SHBs and performance degradation owing to FLP, vdW contacts followed the Schottky-Mott rule. This method is suitable for large-scale device fabrication and can be extended to various metals and 2D semiconductors, making it useful for advanced electronic and optoelectronic devices. Another way to achieve highly responsive photodetectors is to control carrier trapping at the $MoS_2$ interface[214]. Sahoo and co-workers demonstrated that pulsed gate biasing, as opposed to static direct current (DC) biasing, effectively reduces interfacial carrier trapping, resulting in significant increases in photoresponsivity and photogain. Under positive gate bias ($V_{gs} = 5$ V), the device achieved a photoresponsivity of $\sim 4.2 \times 10^3$ $A \cdot W^{-1}$ with a photogain of $\sim 11.3 \times 10^3$. A negative gate bias ($V_{gs} = -5$ V) yielded a photoresponsivity of $\sim 0.7 \times 10^3$ $A \cdot W^{-1}$ with a photogain of $\sim 1.92 \times 10^3$. The pulsed gate bias enhanced photocurrent and photoresponsivity by reducing hysteresis and improving mobility. Additionally, the pulsed method also achieved a better balance between photoresponsivity and response time, offering a low-power, highly responsive photodetector solution for next-generation optoelectronic devices such as sensors and imaging systems.

Recently, not only have engineering techniques been utilized to enhance the optical properties of TMDs, but the introduction of heterostructures has also enabled performance beyond that of single-layer TMDs. One strategy to improve the performance of $MoS_2$-based photodetectors is interfacial engineering, as illustrated in Figures 11(f)–(k)[97]. Here, a high-performance, broadband photodetector was developed using an n-type $MoS_2$ and p-type silicon heterojunction. The silicon substrate was pretreated with soft plasma process to modify the $SiO_2$ layer, thereby improving the interface between $MoS_2$ and the underlying silicon. This treatment led to a marked increase in responsivity and an extended detectable spectral range of the device. Specifically, the photodetector achieved a maximum responsivity of $4.05 \times 10^4$ $A \cdot W^{-1}$ at 637 nm with a power density of 2 $\mu W \cdot mm^{-2}$. Furthermore, its spectral detection window extended from 447 nm to 1 600 nm, covering a broad spectrum range from visible to the mid-infrared. The performance improvement was attributed to activated oxygen bonds on the $SiO_2$ surface bonding with sulfur atoms in the $MoS_2$ channel, reducing the optical bandgap and enabling infrared detection. Additionally, the plasma treatment induced a gating effect by accumulating electrons at the $MoS_2$ interface, enhancing the photodetector's photogain. The interfacial engineering method demonstrated its versatility, as it was also applicable to other 2D materials such as $MoTe_2$ and $ReS_2$. This approach presents a promising route for developing high-performance next-generation photodetectors with potential applications in optical communication, environmental monitoring, and biomedicine.

Electrically tunable vdW heterojunctions have also been explored to realize ultraminiaturized near-infrared spectrometers (Figures 11(i)–(o))[231]. In this approach, a $ReS_2/WSe_2$ vdW heterostructure intercalated with Au atoms was employed to enhance interlayer exciton coupling, thereby significantly boosting the transition dipole moment and photoresponsivity in the near-infrared regime. The device

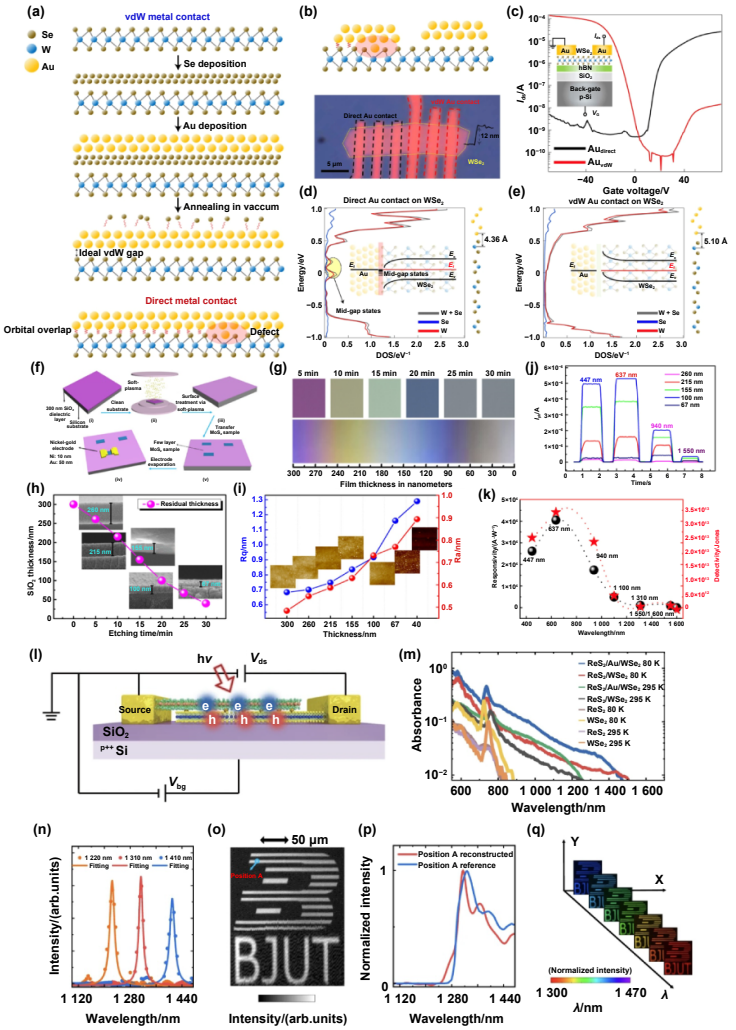


**Figure 11.** Contact engineering, interfacial modification, and heterojunction design for enhanced electrical and optoelectronic performance in 2D chalcogenide optical sensors. Field-effect transistor performance of $WSe_2$ devices fabricated with van der Waals (vdW) Au contacts versus those with directly deposited Au contacts. (a) Schematic of the vdW metal contact formation structure on the $WSe_2$ sample. (b) Schematic and optical images of $WSe_2$ (yellow dotted line) FETs fabricated with direct Au contact (black dashed line) and vdW Au contact (red dashed line). (c) Transfer curve of $WSe_2$ FET with direct Au contact (Audirect) and vdW Au contact (AuvdW). For both contacts, channel length $L = 1.6$ μm, channel width $W = 5.0$ μm, and drain voltage $V_{ds} = 1$ V. (d) Density of W and Se states in $WSe_2$ with direct Au contact and band diagram of $WSe_2$-Au interface. (e) Density of W and Se states in $WSe_2$ with vdW Au contact and band diagram of $WSe_2$-Au interface. Stable point of Au, optimized by adjusting the vdW gap between $WSe_2$ surface and Au, is larger (5.10 Å) than in the direct contact case (4.36 Å); this is consistent with the observed STEM data. DOS is the density of states of the total orbitals combined with those of the s, p, and d orbitals. $E_c$ is the energy of conduction band edge, $E_v$ is the energy of valence band edge, and $E_f$ is the energy of Fermi level. (a)–(e) Adapted from[230], with permission from Springer Nature. Interfacial engineering process and characterizing the thicknesses of a series of samples treated with $SF_6/N_2$ plasma over different treatment times. (f) Schematic diagram of the interfacial engineering process. (g) Optical contrast images of the treated $SiO_2/Si$ substrates over different treatment time. (h) Dependence of the treated oxide layer thickness on plasma treatment time. Insets are the corresponding SEM cross-sectional images of the treated $SiO_2/Si$ samples under different treatment time. (i) Evolution of $R_a$ and $R_q$ of the treated oxide layer with thickness. The insets depict the surface topography of the treated $SiO_2/Si$ samples at different thicknesses. (j) Time-dependent photocurrent curves of the photodetectors under laser illumination with different wavelengths of 447, 637, 940, and 1 550 nm. (k) Photoresponsivity and detectivity of the $MoS_2$ phototransistor with a 100 nm $SiO_2$ layer under different laser wavelengths. (f)–(k) Reprinted (adapted) with permission from[97]. Copyright (2023) American Chemical Society. (l) Schematic drawing of the 2D-vdWH spectrometer. The heterojunction is intercalated by heavy metal Au atoms to construct $ReS_2$/Au/$WSe_2$, where the junction would promote the separation of photo-excited electrons and holes. $V_{ds}$ and $V_{bg}$ are bias voltage and back gate voltage, respectively. '$h\nu$' and the red arrow represent the incident light. (m) The absorption spectra of $ReS_2$/Au/$WSe_2$, $ReS_2$/$WSe_2$, $ReS_2$, and $WSe_2$ at room temperature and 80 K in the visible and near-infrared range. (n) Reconstructed spectra from three narrow band spectra of which the peak locations are 1 220 nm, 1 310 nm, and 1 410 nm, respectively. (o) Single-pixel scanning image. The scale bar is 50 μm. Broadband white light modulated by an optical filter was applied for illumination to make sure that spectra of incident light are in the operational range of this designed spectrometer. (p) Spectral information of position A in (o), which is matched well with a result from conventional equipment (blue-line). (q) Images of the logo at some selected wavelengths from 1 300 nm to 1 470 nm are schematically shown. To clearly show the spatial information, false colors are defined for the above spectral range, and the intensities are normalized. (l)–(q) Reproduced from[231]. CC BY 4.0.

exhibited gate-tunable spectral responses across a wide range (1 150–1 470 nm), with the absorption enhanced by nearly two-fold compared to pristine junctions. By integrating regression algorithms with the gate-dependent photocurrent profiles, the spectrometer achieved effective spectral reconstruction and spectral imaging within an ultracompact footprint of ∼6 μm, which is orders of magnitude smaller than conventional designs. This strategy eliminates the need for bulky optical components or large detector arrays, offering a scalable and designable pathway toward on-chip spectroscopy. Demonstrations of wavelength-resolved detection and imaging further underscored the potential of electrically tunable vdW junctions for applications in integrated photonics, portable sensing, and biomedical diagnostics. The study highlights how interfacial engineering with heavy metal atoms can overcome the intrinsic limitation of weak interlayer exciton transitions, paving the way for programmable, nanoscale spectroscopic devices.

Despite various advantages of chalcogenide materials, long-term stability and susceptibility to oxidation remain critical challenges. Additionally, improvements in the quality and scalability of chalcogenide-based devices are needed, particularly through advanced manufacturing techniques such as CVD or MBE. The development of hybrid optical systems that combine chalcogenides with other materials such as TMDs or perovskites is actively being sought, offering proposals for enhanced sensitivity and multifunctional sensing capabilities. Chalcogenide materials are highly promising for the future of optical sensor technology, especially in applications that require high sensitivity across a wide wavelength range and stability in extreme environments. Continuous research on material optimization, integration with photonic platforms, and solutions to stability issues will further expand their potential applications in various fields, including healthcare, environmental monitoring, and industrial automation.

*3.4.4. Chalcogenide materials for gas sensors.* Gas sensors play a critical role in detecting hazardous gases in a wide range of fields, including industrial safety, environmental monitoring, and medical diagnostics. Traditional metal oxide-based gas sensors typically require high operating temperatures, which result in high energy consumption, poor stability, and elevated safety risks, especially in potentially explosive environments. TMDs with their atomically thin layered structures offer high surface-to-volume ratios, excellent adsorption properties, and tunable electronic characteristics. These features allow TMD-based gas sensors to operate effectively at room temperature, making them ideal for low-power applications and wearable electronic devices. As a result, extensive research is being conducted on TMD-based gas sensors.

Among various TMDs, $MoS_2$, a representative TMD, has emerged as a widely studied material for gas sensing that utilizes light sources to achieve high sensitivity. As illustrated in Figures 12(a) and (b), Pham and co-workers developed a highly sensitive $MoS_2$-based gas sensor capable of detecting $NO_2$ at sub-part per billion (ppb) levels[115]. The sensor employs Au electrodes and utilizes red light, which corresponds to the (direct) bandgap of single-layer $MoS_2$, to generate a photocurrent used for $NO_2$ detection instead of the dark current. This photo-activated design significantly improved the sensitivity of the sensor, achieving 4.9% per ppb (or 4 900% per part per million; ppm). Replacing Au electrodes with graphene, which has a lower work function, further increased the photocurrent and improved the signal-to-noise ratio. The sensor achieved a limit of detection (LOD) as low as 0.1 ppb for $NO_2$, far exceeding the U.S. EPA's requirement of 53 ppb for $NO_2$ detection. The enhancement in performance was attributed to the photocurrent's role in reducing channel resistance and facilitating charge transfer interactions between $NO_2$ molecules and conduction electrons in $MoS_2$. As electron acceptors, $NO_2$ molecules decrease the photocurrent upon adsorption in the sensor channel, enabling detection at sub-ppb levels. The device demonstrated fast response and recovery time, good stability, and high selectivity for $NO_2$, with minimal interference from other gases. These characteristics make it highly suitable for real-time, high-sensitivity environmental monitoring applications. Further advances in $NO_2$ detection using single-layer $MoS_2$-based gas sensors have also been achieved through a synergistic approach[232]. A flexible $NO_2$ sensor based on single-layer $MoS_2$ incorporating both photogating and piezo-phototronic effects was developed, which modulated the SBHs at the metal-semiconductor junction. A red light emitting diode (LED) illumination (625 nm) was used to generate photocurrent, while mechanical strain was applied to generate piezoelectric polarization, which aided in detecting $NO_2$ gas concentrations. Under 0.67% tensile strain and 4 $mW{\cdot}cm^{-2}$ illumination intensity, the sensor achieved a 671% increase in sensitivity for 400 ppb $NO_2$. Moreover, the response and recovery time were significantly improved −16 s and 65 s, respectively—outperforming conventional $MoS_2$ sensors. The enhanced sensitivity and speed were attributed to the interplay of piezoelectric and photoelectric effects, which modulate charge transfer at the Schottky junction. Strain-induced polarization charges reduced the Schottky barrier, allowing more $NO_2$ molecules to adsorb, thereby improving sensitivity. This approach demonstrates the potential of integrating optoelectronic and piezoelectric effects for next generation gas sensors. The development of such flexible low-power, and high-sensitivity devices offers promising prospects for wearable environmental monitoring systems and portable gas detection technologies.

Additionally, research is actively being conducted to scale up gas sensors while maintaining high sensitivity. One such advance is the development of a scalable and monolithically integrated gas sensor array based on $MoS_2$ thin-film transistors (TFTs)[234]. In this study, bilayer $MoS_2$ films were fabricated through a two-step process: radio-frequency magnetron sputtering followed by thermal sulfurization. The resulting sensor array was designed for $NO_2$ detection at room temperature, demonstrating ultra-high sensitivity across a wide detection range, from 1 ppm to 256 ppm of $NO_2$. The polycrystalline structure of the $MoS_2$ film, featuring abundant grain boundaries, facilitated $NO_2$ molecule adsorption, enhancing gas

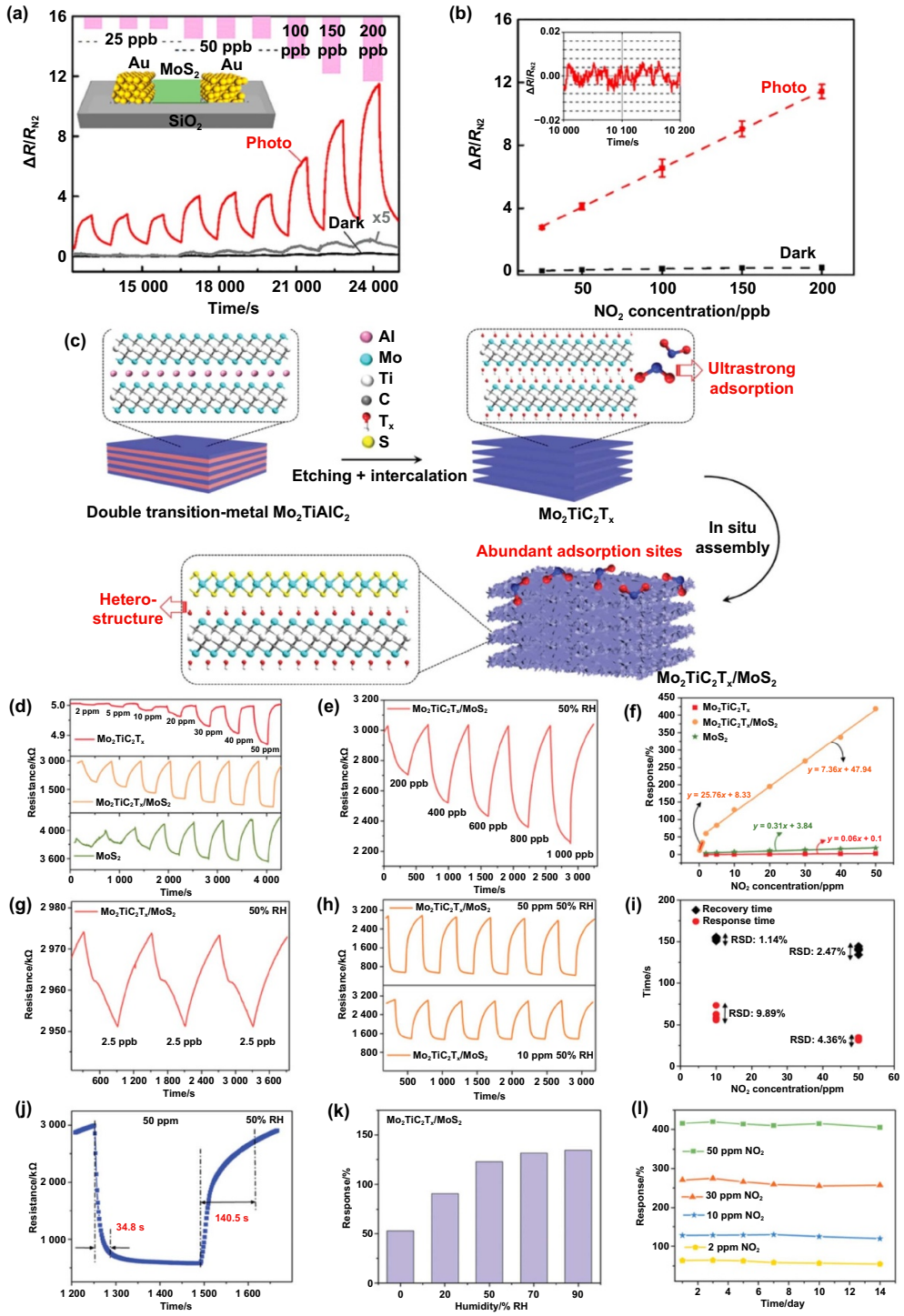


**Figure 12.** Gas sensing performance of chalcogenide based device via material engineering and design. (a) Effect of $NO_2$ gas exposure at concentrations from 25 ppb to 200 ppb on normalized resistance of the Au-$MoS_2$-Au device in the dark (black line; gray line shows 5-fold magnified data) and under red LED illumination (red curve). (b) Dependence of the normalized amplitude of resistance change $\Delta R/R_{N2}$ on the concentration of $NO_2$ gas. Inset shows a temporal trace of experimentally recorded noise of $\Delta R/R_{N2}$ under LED illumination. All data were collected under DC bias of 5 V. (a) and (b) Reprinted (adapted) with permission from[115]. Copyright (2019) American Chemical Society. (c) Schematic illustration of the synthesis of the $Mo_2TiC_2T_x/MoS_2$ composite. (d) Real-time resistance variation curves of the gas sensors based on $Mo_2TiC_2T_x$, $MoS_2$, $Mo_2TiC_2T_x/MoS_2$ to 2–50 ppm $NO_2$ at 50% RH. (e) Resistance response curve of the $Mo_2TiC_2T_x/MoS_2$ sensor to 200–1 000 ppb $NO_2$. (f) Linear fitting curves of the three gas sensors. (g) Resistance response curve of the $Mo_2TiC_2T_x/MoS_2$ sensor to 2.5 ppb $NO_2$. (h) Repeatability curves of the $Mo_2TiC_2T_x/MoS_2$ gas sensor for 6 cycles to 10 and 50 ppm $NO_2$. (i) Response/recovery time of the $Mo_2TiC_2T_x/MoS_2$ gas sensor at 10 and 50 ppm $NO_2$. (j) Amplified response curve. (k) Responses of the $Mo_2TiC_2T_x/MoS_2$ gas sensor to 10 ppm $NO_2$ at different RHs. (l) Responses of the $Mo_2TiC_2T_x/MoS_2$ gas sensor to 2/10/30/50 ppm $NO_2$ in two weeks. (c)–(l)[233] John Wiley & Sons. © 2022 Wiley-VCH GmbH.

sensing performance. The $MoS_2$ TFT-based sensors showed consistent electrical performance over large areas, maintaining excellent n-type semiconducting properties with a high on/off current ratio exceeding $2 \times 10^6$. The sensors were capable of detecting $NO_2$ concentrations as low as 1 ppm, with significant shifts in $V_{th}$ and a decrease in mobility ($\mu_{FE}$) corresponding to increased $NO_2$ concentration. Importantly, this study demonstrated the feasibility of monolithic integration in large-area active matrix arrays by constructing a $7 \times 6$ pixel active-matrix array, in which each pixel comprised both a sensing TFT and a switching TFT. The array successfully detected $NO_2$ gas while maintaining reliable switching behavior, underscoring the scalability and practicality of $MoS_2$-based gas sensors for applications in air quality monitoring, environmental sensing, and IoT systems.

To address sensitivity limitations in single-component TMD-based gas sensors, recent research has explored the use of heterostructures and p-n junctions. Figures 12(c)–(l) summarize a study on a novel heterostructure combining $Mo_2TiC_2T_x$ MXene and $MoS_2$ for $NO_2$ gas detection[233]. This approach addresses common challenges in conventional MXene-based sensors, such as limited sensitivity, selectivity, and a lack of active surface sites. The edge-enriched heterostructure provides abundant adsorption sites and enhances charge transfer efficiency, resulting in a detection limit as low as 2.5 ppb at room temperature and excellent selectivity against interfering gases such as $NH_3$ and $CO_2$. This composite platform offers a promising solution for environmental monitoring and safety applications. In another study, planar $MoS_2$ p-n junctions were formed by stacking CVD-grown n-type and p-type atomically thin $MoS_2$ films to create highly selective and sensitive $NO_2$ gas sensors[235]. These p-n junctions exhibited significantly improved sensitivity and selectivity compared to individual p-type or n-type $MoS_2$ sensors. Specifically, the p-n junction sensor demonstrated 60 times higher sensitivity to 20 ppm $NO_2$ compared to p-type $MoS_2$ alone. The LOD for $NO_2$ was as low as 8 ppb, and the sensor demonstrated recovery within 30 seconds under ultraviolet (UV) irradiation. The enhanced sensing performance was attributed to modulation of the barrier height at the p-n junction interface upon molecular adsorption. UV irradiation effectively reduced the energy barrier for $NO_2$ desorption, enabling rapid and complete sensor recovery. Moreover, the p-n junction sensor exhibited high selectivity toward $NO_2$, with negligible response to other gases such as ammonia, formaldehyde, ethanol, and acetone. This sensor's ability to operate at room temperature while providing high sensitivity, fast recovery, and strong selectivity makes it a promising technology for real-time environmental monitoring and industrial applications.

Chalcogenide materials are also gaining traction in gas sensing due to their unique electrical and optical properties. Recent trends focus on improving sensitivity, selectivity, and operational stability by leveraging tunable bandgaps and high surface reactivity. Notable advances include the use of phase-change materials (PCMs) for dynamic sensing, hybrid structures combining chalcogenides with TMDs, and the integration with photonics for optical sensing applications. Future research directions emphasize miniaturization, integration with flexible electronics, and real-time environmental monitoring applications.

*3.4.5. Chalcogenide materials for artificial neuromorphic sensors.* Neuromorphic sensing technology based on TMDs harnesses the unique electronic and optical properties of these materials to develop systems that mimic the human nervous system. This area of research plays a crucial role in AI and machine learning applications, particularly in enabling low-power, high-speed, and miniaturized sensor systems. Due to their atomically thin structures and exceptional electronic and optical characteristics, TMDs are regarded as ideal materials for constructing neuromorphic systems. Their intrinsic properties allow for the creation of neuromorphic systems that can operate at very low power levels, which is essential for the design of next-generation autonomous learning systems and neural networks. Furthermore, TMD-based neuromorphic devices are highly compatible with complementary metal-oxide-semiconductor (CMOS) processes, allowing seamless integration with existing semiconductor technologies and enabling the development of high-density ICs. TMD-based neuromorphic sensing technology thus offers the potential to replicate the complex functions of the nervous system with high energy efficiency, making them key components in future autonomous learning and AI-based sensor systems.

Various attempts are being made to develop chalcogenide neuromorphic devices, particularly those leveraging OTS characteristics. As shown in Figures 13(f)–(n), a recent study reported the development of a highly efficient selector device based on germanium sulfide (GeS) for applications in non-volatile memory and neuromorphic systems[236]. This GeS-based selector achieves an impressive drive current density of 34 $MA \cdot cm^{-2}$ and high selectivity of $\sim 10^6$, making it particularly suitable for future memory technologies such as 3D-stacked architectures and PCM cells. Notably, GeS is simple and environmentally friendly alloy, avoiding the use of toxic dopants commonly used in other selectors. The T-shaped structure of the Al/TiN/GeS/W layered device exhibits excellent characteristics in both experimental and first-principles calculations, with low OFF currents ($\sim$10 nA), high ON currents (up to 10 mA), and reliable performance under high-temperature annealing and DC stress conditions. Additionally, it supports bidirectional switching, making it compatible with various memory technologies such as ReRAM. The switching mechanism is driven by trap states in the GeS band structure, coupled with electronic transitions and local structural changes, particularly Ge-Ge chain growth under high electric fields, resulting in high ON currents and strong nonlinearity. Moreover, the GeS selector can mimic biological neurons by operating as an artificial neuron with stochastic dynamics. It exhibits a 'leaky integrate-and-fire' behavior, showing great potential for use in neuromorphic computing systems. This study highlights the advantages of the simple material system and demonstrates the potential for high-density,

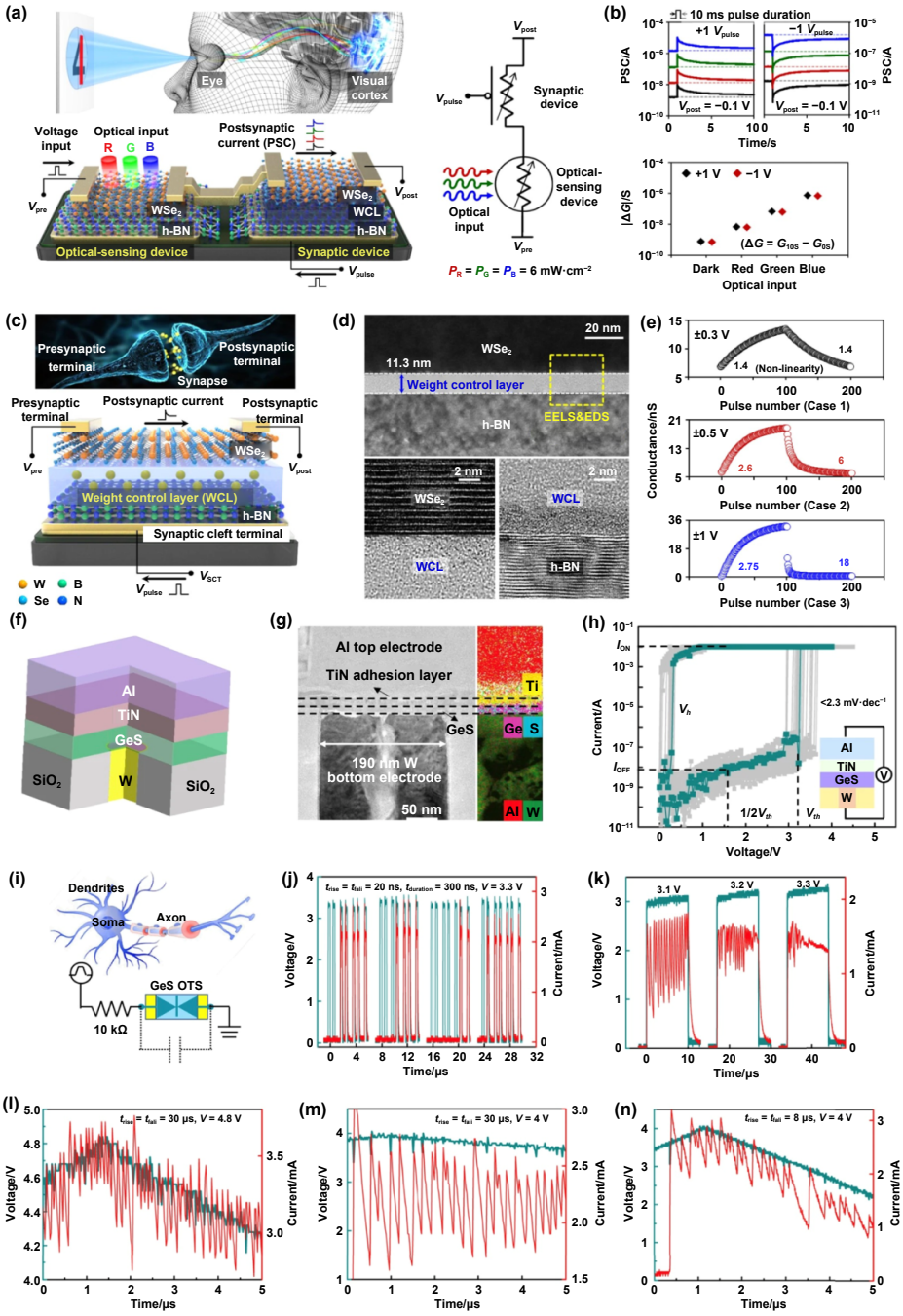


**Figure 13.** Optoelectronic synaptic and spiking neuron devices based on chalcogenide materials for neuromorphic applications. (a) Schematic of the human optic nerve system, the h-BN/$WSe_2$ synaptic device integrated with h-BN/$WSe_2$ photodetector, and the simplified electrical circuit for the ONS device. Here, the light sources were dot lasers with wavelengths of 655 nm (red), 532 nm (green), and 405 nm (blue) with a fixed power density ($P$) of 6 mW·cm$^{-2}$ for all wavelengths. (b) Excitatory and inhibitory postsynaptic current characteristics and extracted conductance changes of the h-BN/$WSe_2$ ONS device under different light conditions (no light and RGB). (c) A functional/structural/architectural comparison of a biological synapse with synthetic $WSe_2$/WCL/h-BN synaptic device. (d) X-TEM image of the $WSe_2$/WCL/h-BN structure, and the high-resolution images corresponding to the $WSe_2$/WCL and WCL/h-BN interfaces. (e) Long-term potentiation and depression characteristics by different input pulses with an amplitude of 0.3 V, 0.5 V, or 1 V. (a)–(e) Reproduced from[96]. CC BY 4.0. (f) Schematic structure of an individual cell. (g) Cross-section TEM image of device displaying the thickness of each layer and corresponding EDS elemental mapping of W, Ge, S, Ti, and Al. The scale bar is 50 nm. (h) Repeatable DC $I$-$V$ sweeps with uniform compliance current (10 mA) and low leakage current (10 nA). (i) Schematic of a biological neuron and the artificial spiking neuron. A resistor (10 kΩ) is in series with the GeS device, and the current response across the device is served as the response spiking signal. (j) Stochastic behavior of the stimulated neuron applied multiple near-threshold voltage pulses with amplitude ($V$) of 3.3 V, rising/falling time (trise/tfall) of 20 ns, and the duration time ($t_{duration}$), of 300 ns. (k) The response under square pulses with different near-threshold voltages. (l)–(n) Frequency response of the artificial neuron to which are applied different triangular stimuli pulses, 4.8 V amplitude/30 μs rising/falling time, 4 V amplitude/30 μs rising/falling time, and 4 V amplitude/8 μs rising/falling time, respectively. (f)–(n) Reproduced from[236]. CC BY 4.0.

low-power applications in both memory and neuromorphic technologies.

In addition to OTS device structures, researchers have reported heterostructure devices constructed from 2D materials to enhance neuromorphic characteristics. One notable example involves a novel floating-gate-like transistor incorporating an indium selenide (InSe) and hexagonal boron nitride (hBN) vdW heterostructure[237]. The transistor consists of an InSe/hBN/$O_2$-hBN heterostructure, where $O_2$-hBN (oxygen plasma-treated hBN) acts as a charge-trapping layer, hBN serves as the tunneling layer, and InSe functions as the conducting channel. This structure mimics conventional floating-gate transistors while providing improved performance and flexibility. The device demonstrates excellent synaptic behaviors, such as short-term plasticity, long-term plasticity, paired-pulse facilitation, and long-term potentiation/depression (LTP/LTD), all of which are crucial for emulating biological neural networks. The excitatory postsynaptic current (EPSC) reaches a synaptic weight of 104% and remains above 300% after 200 seconds, effectively mimicking biological synaptic behavior. The device demonstrated stable LTP and LTD curves with high symmetry and linearity, with a $G_{max}/G_{min}$ (maximum-to-minimum conductance ratio) exceeding 10, all crucial for neuromorphic computing. The charge-trapping mechanism driven by the $O_2$-hBN layer offers more flexibility compared to conventional floating-gate materials such as graphene, allowing for better charge capture and memory performance. The device's response is influenced by gate voltage pulses, where larger pulse widths and amplitudes improve synaptic weight and plasticity. Under UV laser irradiation (365 nm), the InSe device also exhibited a large memory window and high operational stability, confirming its suitability as a synaptic device in neuromorphic systems.

More recently, the development of an artificial synaptic transistor based on a 2D $SnS_2$/T-layer (plasma-treated h-BN) heterostructure, aimed at mimicking essential biological synaptic behaviors for neuromorphic computing, has been reported[238]. The $SnS_2$ channel was paired with a T-layer of oxygen plasma-treated h-BN, which facilitated surface-level charge-trapping to emulate synaptic functions such as EPSC, short-term plasticity, and LTP. The synaptic transistor's transfer characteristics revealed a clear hysteresis behavior, indicating charge storage in the T-layer. This charge-trapping mechanism enabled effective synaptic operations, successfully reproducing synaptic responses such as EPSC and STP. The device exhibited typical synaptic behavior, where EPSC increases with greater pulse width and amplitude, controlled by gate voltage pulses. LTP and LTD characteristics were also observed, demonstrating the device's ability to mimic more complex synaptic functions. Under 820 nm light irradiation, the synaptic performance was significantly enhanced. Specifically, the nonlinearity of LTP was reduced to −0.19, and its symmetry improved to 39.4, making it one of the best-performing 2D artificial synaptic devices reported to date. The LTP/LTD dynamic range ($G_{max}/G_{min}$) of 9.32 was measured under dark conditions, while light exposure reduced the dynamic range, it also improved stability across multiple cycles. This work highlights the potential of 2D materials for developing high-performance light-modulated artificial synapses, contributing to advancements in neuromorphic systems.

Moreover, recent research has explored the development of an artificial vdW (van der Waals) hybrid synapse that integrate neuromorphic devices utilizing plasma-treated h-BN with sound recognition devices[239]. These artificial synapses mimic biological synapses by utilizing a hybrid structure composed of $WSe_2$ and $MoS_2$, enabling bidirectional control over synaptic conductance. The hybrid synapse uses two channels: $WSe_2$ for increasing conductance (potentiation) and $MoS_2$ for decreasing conductance (depression). This dual-channel approach provides linear and symmetric modulation of conductance, which is essential for hardware neural networks (HW-NNs). The hybrid device demonstrated excellent synaptic behaviors such as LTP and LTD, with minimized nonlinearity (1.9 for both potentiation and depression) and improved symmetry compared to conventional devices. When applied to an HW-NN for acoustic pattern recognition, the hybrid synapse achieved a recognition rate of 94.2%, which is comparable to the 95.3% recognition rate of software-based neural networks (SW-NNs). This study indicates the potential of vdW hybrid synapses for real-world neuromorphic applications such as acoustic pattern recognition and brain-inspired computing systems. In another study illustrated in Figures 13(a)–(e)[96], researchers developed an artificial optic-neural synapse (ONS) for recognizing color and mixed-color patterns. The ONS device integrates optical sensing and synaptic functions into a single platform using a h-BN/$WSe_2$ heterostructure. The device adjusts synaptic behavior based on different wavelengths of light (red, green, blue), similar to how the human visual system processes color patterns. The ONS device operates at a low voltage spike (0.3 V) and consumes only 66 fJ per spike, highlighting its potential for energy-efficient neuromorphic systems. It achieved over 90% recognition rates for color and mixed-color patterns and outperformed traditional neural networks (NNs) in recognizing complex mixed-color patterns when applied to an optic-neural network (ONN). This research represents a significant advancement in the integration of synaptic and sensory functions for complex pattern recognition tasks, with promising implications for developing neuromorphic systems that mimic human sensory processing.

The development of artificial neuromorphic sensors using chalcogenide materials is a rapidly growing field. Owing to their inherent phase-change properties, chalcogenides are well-suited to emulate the dynamic functions of biological neurons and synapses. Current research efforts focus on developing memory and learning capable devices using phase-change chalcogenides (such as GST), enhancing neuromorphic characteristics through heterostructures with 2D materials, and engineering scalable, low-power systems optimized for next-generation artificial intelligence (AI) and autonomous computing applications. The overarching goal is

to replicate brain-like information processing with high energy efficiency.

## 4. Challenges and future directions

Chalcogenide materials have advanced memory and sensing technologies by leveraging their unique properties, such as phase-change behavior, high sensitivity to external stimuli, and multi-level resistance states. These features enable a wide range of applications, including non-volatile memory, neuromorphic computing, wearable electronics, and emerging quantum technologies. However, key challenges remain, including material stability[240,241], scalability[242], dimensional control[243], and integration into modern architectures. Addressing these issues is essential for seamless incorporation into platforms such as artificial intelligence, neuromorphic systems, and quantum devices, as summarized in Figure 14. Overcoming these hurdles requires the development of innovative synthesis techniques, hybrid systems, and multifunctional device designs.

### 4.1. Materials challenges

Stability remains as one of the critical material challenges limiting the performance and broader application of chalcogenides[164]. For instance, phase separation, resistance drift, and unintended crystallization—particularly in materials like GST-225—compromise device reliability. Additionally, repeated phase transitions introduce mechanical stress, leading to fatigue and reduced lifespan. Addressing these challenges is essential for ensuring long-term stability and the continued advancement of chalcogenide-based technologies.

Scalability presents another significant challenge. As devices continue to shrink, the crystallization temperature and switching energy of phase-change materials become critical factors that affect device efficiency and reliability. This is particularly true at the nanoscale, where surface energy effects disrupt phase-change dynamics, introducing variability and complicating device performance. Furthermore, advanced structural designs that aim to retain bulk-like properties in nanostructures often rely on intricate fabrication techniques, which are susceptible to defects and reproducibility issues. To address these challenges, enhanced fabrication techniques, improved material synthesis methods, and a deeper understanding of nanoscale behavior are crucial[155].

Similarly, dimensional control presents synthetic challenges, particularly for applications that require specific structural configurations, such as nanophotonic materials or inverse opal structures[87,88]. Maintaining consistent dimensionality is critical for achieving desired optical and/or electronic properties. For instance, the synthesis of 3D chalcogenide structures often relies on complex template-based methods, which can introduce defects during template removal, compromising material's quality. Additionally, ensuring pore size control and uniformity in porous chalcogenides remains a challenge, limiting the reproducibility of these structures. Addressing these issues necessitates advances in synthetic precision and the development of defect mitigation techniques.

### 4.2. Integration with next-generation technologies

Chalcogenides offer immense potential for integration into next-generation technologies, including quantum computing, AI, and the IoT. Additionally, these materials are pivotal in advancing human-like electronic artificial sensory systems—cutting-edge innovations designed to replicate the human ability to sense, process, and respond to environmental stimuli.

A key area of focus is the use of chalcogenide PCMs in neuromorphic computing, which seeks to emulate the synaptic behavior of the human brain. In artificial sensory systems designed to process information like human senses, memory plays an essential role in learning, adapting, and responding to environmental inputs. To enable human-like perception, chalcogenide materials must reliably demonstrate multi-level resistance states that can mimic the analog behavior of neurons. These multi-level states allow artificial sensory systems to process and store multiple layers of information, much like the human brain, enabling complex, dynamic responses to environmental changes. Furthermore, ensuring the energy efficiency of chalcogenides in neuromorphic architectures is essential for large-scale integration. Energy-efficient, chalcogenide-based synaptic devices could pave the way for low-power, real-time artificial sensory systems capable of continuous learning and adaptation, all of which are critical functions in autonomous robots, wearable health monitors, and other AI-driven devices that interact with their surroundings. In the realm of quantum computing, 2D TMDs like $MoS_2$ are promising candidates due to their unique electronic and optical properties. These materials exhibit strong spin-orbit coupling, which could be harnessed in quantum bits (qubits) for quantum information storage. However, chalcogenides' role in human-like sensory systems could also extend to quantum computing applications by providing ultrasensitive quantum sensors capable of detecting subtle environmental changes. The challenge of integrating chalcogenides into quantum architectures will require advances in material deposition techniques, such as ALD or ALE, to achieve the ultra-thin, defect-free films needed for quantum coherence, which is crucial for precision and accuracy in quantum sensing.

Sensing is another critical function that bridges chalcogenide materials with human-like electronic systems. Chalcogenides are well-suited for integration into IoT devices due to their versatility in sensing applications, which are crucial for artificial sensory systems that aim to mimic human perception. 2D chalcogenides, with their large surface area and high sensitivity to environmental changes, are ideal candidates for low-power, flexible sensors that can monitor temperature, gas concentrations, or light intensity in real-time, just as human senses continuously gather information from the environment. These materials have also garnered significant interest owing to quantum confinement effects merging from their atomic-scale thickness. These materials possess a

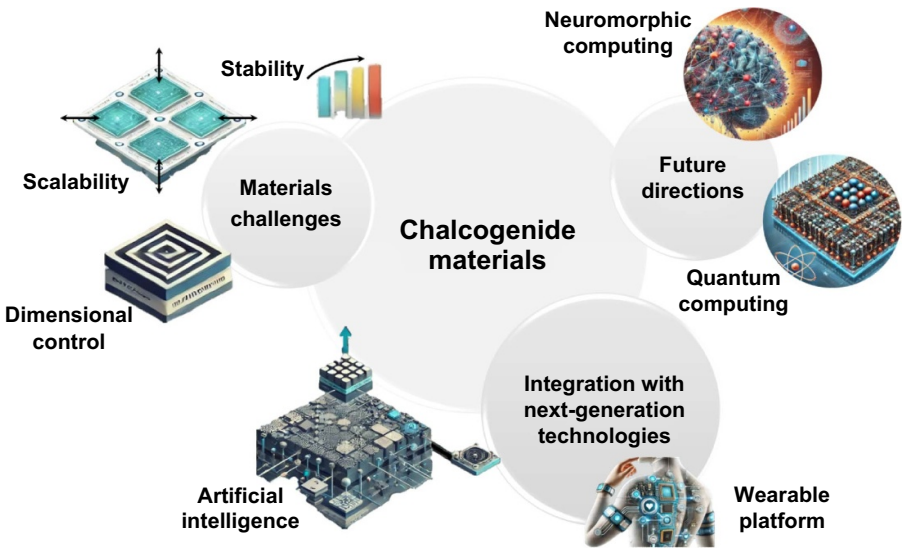


**Figure 14.** A schematic summary of challenges and future direction for chalcogenide materials. Parts of the elements in this figure were generated using OpenAI's generative AI tool (DALL·E) based on author-provided descriptions.

layered structure, where individual layers are held together by weak van der Waals forces, allowing them to be exfoliated into monolayer or few-layer forms. In such configurations, charge carriers are confined within a two-dimensional plane, leading to discrete energy states and significant modifications in their band structure, optical absorption, and electrical behavior. These quantum confinement effects enhance optical absorption and photocurrent generation, enabling high-performance photodetectors with improved sensitivity. Additionally, the large surface-to-volume ratio of atomically thin TMDs amplifies their response to external chemical or biological stimuli, facilitating the detection of trace-level analytes. These properties are crucial not only for environmental and biochemical sensing but also for neuromorphic applications, where quantum confinement contributes to nonlinearity, hysteresis, and conductance switching, which are essential for mimicking synaptic plasticity in neuromorphic architectures. The synergy between quantum effects and surface reactivity makes TMDs promising materials for a broad range of sensing and intelligent electronic applications. These sensors, integrated into human-like systems, could perform in autonomous vehicles, smart homes, and wearable devices, providing real-time feedback similar to how the human body responds to external stimuli.

Moreover, the development of neuromorphic sensory systems, in which sensing and memory are strongly coupled, relies heavily on the ability of materials like chalcogenides to process and store sensory information simultaneously. For example, chalcogenide-based gas sensors could detect environmental toxins and store historical data on toxin levels, allowing the system to 'learn' and improve its response over time. This integration of sensing and memory in artificial systems mirrors the way human sensory systems use past experiences to refine responses to new stimuli. However, the challenge remains to develop robust and scalable manufacturing processes that can maintain the material performance of chalcogenides while reducing cost and complexity for large-scale integration. Future human-like electronic sensory systems will demand both the precision and reliability of these materials to function effectively in real-world environments, from healthcare monitoring systems to autonomous robots.

Clearly, the integration of memory and sensing functions through chalcogenide materials is not only a path toward enhancing AI, IoT, and quantum technologies, but also a critical enabler of human-like electronic artificial sensory systems. These materials hold the key to unlocking the potential of systems that can perceive, learn, adapt, and respond to their environment, much like human sensory organs, positioning them at the forefront of next-generation technological advances.

### *4.3. Emerging memory architectures*

As traditional memory technologies like flash and DRAM encounter scaling limitations, chalcogenide materials are being explored as key components in emerging memory architectures beyond phase-change memory. One such architecture is ReRAM, which leverages the reversible switching between high and low resistance states in chalcogenides. OTS, a switching mechanism inherent to some chalcogenide materials, is particularly promising for developing selector-only memory devices that can reduce power consumption and improve data storage density.

Vertical structured SOM (VSOM) is an emerging configuration that increases storage density by stacking multiple layers of memory cells vertically, akin to 3D NAND technology. This structure is advantageous for applications requiring large storage capacities in a compact area, such as data centers

and high-performance computing environments. The deposition of chalcogenide films in VSOM requires methods that provide excellent conformal coverage and precise thickness control to ensure uniform performance across all layers. ALD is particularly important for VSOM because it offers atomic-level precision in film deposition, ensuring that each layer of chalcogenide material is uniformly coated, even on the sidewalls of deep trenches and other complex 3D structures. To achieve node separation between layers when forming the chalcogenide material on the sidewalls of deep trenches in 3D structures, area-selective ALD (AS-ALD) technology, which selectively deposits material only on the electrode, is proving to be highly promising. The AS-ALD process leverages differences in adsorption properties of the precursor between the surfaces where growth is undesired and those where it is intended (inherent AS-ALD). Alternatively, an inhibitor material, acting as a surface modifier, can be selectively adsorbed onto the undesired growth surface to reduce its adsorption properties with the precursor. Subsequently, a thin film is selectively deposited only on the desired growth area through the selective reaction of the precursor and the active sites during the ALD process, creating a nanostructure pattern. By utilizing AS-ALD, it is possible to selectively form chalcogenide materials only on the electrode surface by exploiting the differences in adsorption properties between the interlayer dielectric and the electrode. This approach not only enhances the device's characteristics but also simplifies the manufacturing process.

Moreover, neuromorphic computing, which aims to mimic the behavior of biological synapses and neurons, is another area where chalcogenides are gaining attention. Chalcogenide materials, with their ability to exhibit multi-level resistance states and adaptive behaviors, are ideal candidates for artificial synapses in brain-inspired computing systems. However, for these materials to reach their full potential in neuromorphic systems, there must be further breakthroughs in material stability, energy efficiency, and scalability.

Finally, optoelectronic memory is another frontier where chalcogenides are expected to play a significant role. Some chalcogenide materials exhibit properties that are highly responsive to optical stimuli, enabling light-driven memory devices. By controlling the optical reflectivity or refractive index of chalcogenide materials, multi-level optical memory can be developed, offering the potential for higher storage capacity and faster access time compared to traditional electronic memory. However, integrating chalcogenide-based optoelectronic memory into existing architectures will require innovations in fabrication and interface design to ensure compatibility and performance.

### *4.4. Future research directions and outlook*

Moving forward, there are several areas where breakthroughs in chalcogenide materials research are expected. One critical avenue is the development of hybrid material systems that combine chalcogenides with other advanced materials such as 2D graphene, metal oxides, or organic semiconductors. These hybrid systems could enhance the performance and functionality of chalcogenide-based devices by offering new pathways for charge transport, light-matter interaction, and thermal management. Additionally, improving the synthesis methods for chalcogenide materials is a key priority. While techniques such as ALD and CVD have made significant progress, there is a need for scalable, low-cost methods that maintain the high structural precision required for next-generation applications. Developing solution-based or additive manufacturing techniques for chalcogenide nanomaterials could unlock new horizons for low-cost, high-performance devices.

As discussed earlier, material stability under varying environmental conditions is another important area of focus. In particular, research on doping or alloying chalcogenides to improve their thermal and chemical stability, while maintaining their phase-change properties, will be vital for applications such as non-volatile memory and sensors. And, exploring alternative phase-change mechanisms beyond the traditional heat-induced changes in chalcogenides will likely yield new applications. For example, investigating electric field-induced or pressure-induced phase changes could lead to the development of memory devices with lower power consumption or faster switching time. Additionally, research into multifunctional materials, which can perform both memory storage and sensing functions, will be crucial for developing more integrated and versatile devices in the future.

In summary, chalcogenide materials offer a unique combination of properties that make them indispensable in memory and sensing technologies. However, there remain significant challenges related to material stability, scalability, and dimensional control, particularly in advanced applications such as phase-change memory, neuromorphic computing, and optoelectronic devices. While current synthesis methods, such as CVD, ALD, and template-based approaches, provide promising pathways for material fabrication, further improvements in these techniques are needed to ensure the scalability and performance required for next-generation devices. In emerging fields such as quantum computing, AI, and the IoT, chalcogenides are poised to play an increasingly critical role, though successful integration will depend on addressing the technical challenges associated with device miniaturization and energy efficiency. The future of chalcogenide materials looks promising, as we continue to push the boundaries of their applications in electronics, sensing, and quantum technologies. With advances in hybrid material systems, multifunctional devices, and new phase-change mechanisms, chalcogenides are expected to remain at the forefront of materials research. As the demand for high-performance, scalable, and energy-efficient devices continues to grow, addressing these challenges will unlock chalcogenides' further potential, driving innovation in memory architectures, smart sensors, and beyond across fields from consumer electronics to next-generation computing.

## Acknowledgments

This work was supported by the National Research Foundation of Korea (NRF) grant funded by the Korean government (MSIT) (RS-2024-00358623), the Technology Innovation Program (or Industrial Strategic Technology Development Program-Development of Next Generation Intelligent Semiconductors) (20025643, Development of intelligent physical vapor deposition equipment for hard mask applications with high selectivity) funded By the Ministry of Trade, Industry & Energy (MOTIE, Korea), and KIST intramural Grants (2V10250 and 2E33221). T.E. acknowledges support from the faculty research fund of Sejong University in 2024. W.-K. L. was supported by 2024 Hongik University Research Fund. Parts of elements in Figures 1 and 14 were generated using OpenAI's generative AI tool (DALL·E) based on author-provided descriptions.

## Conflicts of interest

The authors declare that they have no conflict of interest.

## ORCID iDs

Pengfei Liu 0000-0003-2032-0979
Won-Kyu Lee 0000-0002-7878-1981
Myung-Gil Kim 0000-0002-8607-5972
Donghee Son 0000-0002-3772-8009
Joohoon Kang 0000-0002-6578-2547
Taeyong Eom 0000-0002-9646-9553
Sungjin Park 0000-0002-8803-6176
In Soo Kim 0000-0003-1615-3119

## References

[1] Manivannan R and Victoria S N. 2018. Preparation of chalcogenide thin films using electrodeposition method for solar cell applications—a review. *Sol. Energy* **173**, 1144–1157.
[2] Woods-Robinson R, Han Y B, Zhang H Y, Ablekim T, Khan I, Persson K A and Zakutayev A. 2020. Wide band gap chalcogenide semiconductors. *Chem. Rev.* **120**, 4007–4055.
[3] Sanghera J S and Aggarwal I D. 1999. Active and passive chalcogenide glass optical fibers for IR applications: a review. *J. Non-Cryst. Solids* **256–257**, 6–16.
[4] Singh P K and Dwivedi D K. 2017. Chalcogenide glass: fabrication techniques, properties and applications. *Ferroelectrics* **520**, 256–273.
[5] Guo P F, Sarangan A M and Agha I. 2019. A review of germanium-antimony-telluride phase change materials for non-volatile memories and optical modulators. *Appl. Sci.* **9**, 530.
[6] Harmgarth N, Zörner F, Liebing P, Burte E P, Silinskas M, Engelhardt F and Edelmann F T. 2017. Molecular precursors for the phase-change material germanium-antimony-telluride, $Ge_2Sb_2Te_5$ (GST). *Z. Anorg. Allg. Chem.* **643**, 1150–1166.
[7] Lee S-Y, Kim Y-H, Cho S-M, Kim G H, Kim T-Y, Ryu H, Kim H N, Kang H B, Hwang C-Y and Hwang C-S. 2017. Holographic image generation with a thin-film resonance caused by chalcogenide phase-change material. *Sci. Rep.* **7**, 41152.
[8] Baillieul M et al. 2021. Toward chalcogenide platform infrared sensor dedicated to the in situ detection of aromatic hydrocarbons in natural waters via an attenuated total reflection spectroscopy study. *Sensors* **21**, 2449.
[9] Zhang Y et al. 2022. Two-dimensional $Ta_2NiSe_5$/GaSe van der Waals heterojunction for ultrasensitive visible and near-infrared dual-band photodetector. *Appl. Phys. Lett.* **120**, 261101.
[10] Bureau B et al. 2004. Recent advances in chalcogenide glasses. *J. Non-Cryst. Solids* **345–346**, 276–283.
[11] Zhang H et al. 2021. Solution-synthesized $SnSe_{1-x}S_x$: dual-functional materials with enhanced electrochemical storage and thermoelectric performance. *ACS Appl. Mater. Interfaces* **13**, 37201–37211.
[12] Feng X W, Liu X K and Ang K-W. 2020. 2D photonic memristor beyond graphene: progress and prospects. *Nanophotonics* **9**, 1579–1599.
[13] Jana R, Ghosh S, Bhunia R and Chowdhury A. 2024. Recent developments in the state-of-the-art optoelectronic synaptic devices based on 2D materials: a review. *J. Mater. Chem. C* **12**, 5299–5338.
[14] Liu X R, Sun C, Ye X Y, Zhu X J, Hu C, Tan H W, He S, Shao M J and Li R-W. 2024. Neuromorphic nanoionics for human–machine interaction: from materials to applications. *Adv. Mater.* **36**, 2311472.
[15] Schöning M J and Kloock J P. 2007. About 20 years of silicon-based thin-film sensors with chalcogenide glass materials for heavy metal analysis: technological aspects of fabrication and miniaturization. *Electroanalysis* **19**, 2029–2038.
[16] Chen L et al. 2024. Bioinspired iontronic synapse fibers for ultralow-power multiplexing neuromorphic sensorimotor textiles. *Proc. Natl Acad. Sci. USA* **121**, e2407971121.
[17] Li Y, Qiu Z C, Kan H, Yang Y X, Liu J, Liu Z R, Yue W J, Du G Q, Wang C and Kim N-Y. 2024. A human-computer interaction strategy for an FPGA platform boosted integrated 'perception-memory' system based on electronic tattoos and memristors. *Adv. Sci.* **11**, 2402582.
[18] Li Y, Lin Q H, Sun T, Qin M Z, Yue W J and Gao S. 2024. A perceptual and interactive integration strategy toward telemedicine healthcare based on electroluminescent display and triboelectric sensing 3D stacked device. *Adv. Funct. Mater.* **34**, 2402356.
[19] Zhang K N, Zhang T Y, You J W, Zheng X D, Zhao M, Zhang L J, Kong J, Luo Z T and Huang S M. 2024. Low-temperature vapor-phase growth of 2D metal chalcogenides. *Small* **20**, 2307587.
[20] Lee Y K, Yoo C, Kim W, Jeon J W and Hwang C S. 2021. Atomic layer deposition of chalcogenides for next-generation phase change memory. *J. Mater. Chem. C* **9**, 3708–3725.
[21] Kwon K C, Baek J H, Hong K, Kim S Y and Jang H W. 2022. Memristive devices based on two-dimensional transition metal chalcogenides for neuromorphic computing. *Nano-Micro Lett.* **14**, 58.
[22] Bauers S R, Tellekamp M B, Roberts D M, Hammett B, Lany S, Ferguson A J, Zakutayev A and Nanayakkara S U. 2021. Metal chalcogenides for neuromorphic computing: emerging materials and mechanisms. *Nanotechnology* **32**, 372001.
[23] Ovshinsky S R. 1968. Reversible electrical switching phenomena in disordered structures. *Phys. Rev. Lett.* **21**, 1450–1453.
[24] Nelson D L. 1970. Ovonic device applications. *J. Non-Cryst. Solids* **2**, 528–539.
[25] Yamada N, Ohno E, Akahira N, Nishiuchi K, Nagata K and Takao M. 1987. High speed overwritable phase change optical disk material. *Jpn. J. Appl. Phys.* **26**, 61–66.
[26] Novoselov K S, Jiang D, Schedin F, Booth T J, Khotkevich V V, Morozov S V and Geim A K. 2005.

Two-dimensional atomic crystals. *Proc. Natl Acad. Sci. USA* **102**, 10451–10453.
[27] Wuttig M and Yamada N. 2007. Phase-change materials for rewriteable data storage. *Nat. Mater.* **6**, 824–832.
[28] Kuzum D, Jeyasingh R G D, Lee B and Philip Wong H-S P. 2012. Nanoelectronic programmable synapses based on phase change materials for brain-inspired computing. *Nano Lett.* **12**, 2179–2186.
[29] Zhu M, Ren K and Song Z T. 2019. Ovonic threshold switching selectors for three-dimensional stackable phase-change memory. *MRS Bull.* **44**, 715–720.
[30] Yoo C, Kim W, Jeon J W, Park E-S, Ha M, Lee Y K and Hwang C S. 2020. Atomic layer deposition of $Ge_xSe_{1-x}$ thin films for endurable ovonic threshold selectors with a low threshold voltage. *ACS Appl. Mater. Interfaces* **12**, 23110–23118.
[31] Sarwat S G, Moraitis T, Wright C D and Bhaskaran H. 2022. Chalcogenide optomemristors for multi-factor neuromorphic computation. *Nat. Commun.* **13**, 2247.
[32] Shuang Y, Chen Q, Kim M, Wang Y L, Saito Y, Hatayama S, Fons P, Ando D, Kubo M and Sutou Y. 2023. $NbTe_4$ phase-change material: breaking the phase-change temperature balance in 2D Van der Waals transition-metal binary chalcogenide. *Adv. Mater.* **35**, 2303646.
[33] Vlasov Y G, Bychkov E A and Medvedev A M. 1986. Copper ion-selective chalcogenide glass electrodes: analytical characteristics and sensing mechanism. *Anal. Chim. Acta* **185**, 137–158.
[34] Buffiere M, Dhawale D S and El-Mellouhi F. 2019. Chalcogenide materials and derivatives for photovoltaic applications. *Energy Technol.* **7**, 1900819.
[35] Eggleton B J, Luther-Davies B and Richardson K. 2011. Chalcogenide photonics. *Nat. Photon.* **5**, 141–148.
[36] Chung I and Kanatzidis M G. 2014. Metal chalcogenides: a rich source of nonlinear optical materials. *Chem. Mater.* **26**, 849–869.
[37] Chen H, Ran M-Y, Wei W-B, Wu X-T, Lin H and Zhu Q-L. 2022. A comprehensive review on metal chalcogenides with three-dimensional frameworks for infrared nonlinear optical applications. *Coord. Chem. Rev.* **470**, 214706.
[38] Zakery A and Elliott S R. 2003. Optical properties and applications of chalcogenide glasses: a review. *J. Non-Cryst. Solids* **330**, 1–12.
[39] Simon U, Goldberg L and Tittel F K. 1993. Difference-frequency mixing in $AgGaS_2$ by use of a high-power GaAlAs tapered semiconductor amplifier at 860 nm. *Opt. Lett.* **18**, 1931–1933.
[40] Shi Y X, Sturm C and Kleinke H. 2019. Chalcogenides as thermoelectric materials. *J. Solid State Chem.* **270**, 273–279.
[41] Liu B, Li K Q, Zhou J and Sun Z M. 2024. Reversible crystalline-crystalline transitions in chalcogenide phase-change materials. *Adv. Funct. Mater.* **34**, 2407239.
[42] Jiang -T-T, Wang X-D, Wang -J-J, Zhang H-Y, Lu L, Jia C L, Wuttig M, Mazzarello R, Zhang W and Ma E. 2024. In situ characterization of vacancy ordering in Ge-Sb-Te phase-change memory alloys. *Fundam. Res.* **4**, 1235–1242.
[43] Sa B S and Sun Z M. 2014. Electron interactions and Dirac fermions in graphene-$Ge_2Sb_2Te_5$ superlattices. *J. Appl. Phys.* **115**, 233714.
[44] Maeda T, Gong W Y and Wada T. 2016. Crystallographic and optical properties and band structures of $CuInSe_2$, $CuIn_3Se_5$, and $CuIn_5Se_8$ phases in Cu-poor $Cu_2Se$–In2$Se_3$ pseudo-binary system. *Jpn. J. Appl. Phys.* **55**, 04ES15.
[45] Jin Z L, Liao Q W, Fang H S, Liu Z C, Liu W, Ding Z D, Luo T F and Yang N. 2015. A revisit to high thermoelectric performance of single-layer $MoS_2$. *Sci. Rep.* **5**, 18342.
[46] Gajić N, Kamberović Ž, Anđić Z, Trpčevská J, Plešingerova B and Korać M. 2019. Synthesis of tribological $WS_2$ powder from $WO_3$ prepared by ultrasonic spray pyrolysis (USP). *Metals* **9**, 277.
[47] Wu Y B, Xia W Y, Gao W W, Ren W and Zhang P H. 2017. Engineering the near-edge electronic structure of snse through strains. *Phys. Rev. Appl.* **8**, 034007.
[48] Bouzid A, Gabardi S, Massobrio C, Boero M and Bernasconi M. 2015. First-principles study of amorphous $Ga_4Sb_6Te_3$ phase-change alloys. *Phys. Rev. B* **91**, 184201.
[49] Grüning M and Attaccalite C. 2016. Performance of polarisation functionals for linear and nonlinear optical properties of bulk zinc chalcogenides ZnX (X = S, Se, and Te). *Phys. Chem. Chem. Phys.* **18**, 21179–21189.
[50] Kobayashi H, Kanbara H, Koga M and Kubodera K. 1993. Third-order nonlinear optical properties of $As_2S_3$ chalcogenide glass. *J. Appl. Phys.* **74**, 3683–3687.
[51] Li C X, Sang D D, Ge S H, Zou L R and Wang Q L. 2024. Recent excellent optoelectronic applications based on two-dimensional $WS_2$ nanomaterials: a review. *Molecules* **29**, 3341.
[52] Fathi S, Sheikhi M H and Zerafat M M. 2022. Fast photodetection in eco-friendly wurtzite $CuInS_2$ nanocrystals based photodiode with a planar geometry. *Mater. Sci. Semicond. Process.* **148**, 106823.
[53] Liu P F et al. 2023. Functional radiative cooling: basic concepts, materials, and best practices in measurements. *ACS Appl. Electron. Mater.* **5**, 5755–5776.
[54] Clima S, Ravsher T, Garbin D, Degraeve R, Fantini A, Delhougne R, Kar G S and Pourtois G. 2023. Ovonic threshold switch chalcogenides: connecting the first-principles electronic structure to selector device parameters. *ACS Appl. Electron. Mater.* **5**, 461–469.
[55] Kato K, Badikov V V, Wang L, Panyutin V L, Mitin K V, Miyata K and Petrov V. 2020. Effective nonlinearity of the new quaternary chalcogenide crystal $BaGa_2GeSe_6$. *Opt. Lett.* **45**, 2136–2139.
[56] Lei H W, Chen J J, Tan Z J and Fang G J. 2019. Review of recent progress in antimony chalcogenide-based solar cells: materials and devices. *Sol. RRL* **3**, 1900026.
[57] Singh N B, Su C-H, Arnold B and Choa F-S. 2016. Optical and morphological characteristics of zinc selenide-zinc sulfide solid solution crystals. *Opt. Mater.* **60**, 474–480.
[58] Park B-I, Hwang Y, Lee S Y, Lee J-S, Park J-K, Jeong J, Kim J Y, Kim B, Cho S-H and Lee D-K. 2014. Solvent-free synthesis of $Cu_2ZnSnS_4$ nanocrystals: a facile, green, up-scalable route for low cost photovoltaic cells. *Nanoscale* **6**, 11703–11711.
[59] Nefzi C, Yahmadi B, Guesmi N E, García J M, Kamoun-Turki N and Ahmed S A. 2022. A successful exploitation of gamma-radiation on chalcogenide $Cu_2InSnS_4$ towards clean water under photocatalysis approach. *J. Mol. Struct.* **1251**, 131943.
[60] Xiao J-R, Yang S-H, Feng F, Xue H-G and Guo S-P. 2017. A review of the structural chemistry and physical properties of metal chalcogenide halides. *Coord. Chem. Rev.* **347**, 23–47.
[61] Hoye R L Z, Hidalgo J, Jagt R A, Correa-Baena J-P, Fix T and MacManus-Driscoll J L. 2022. The role of dimensionality on the optoelectronic properties of oxide and halide perovskites, and their halide derivatives. *Adv. Energy Mater.* **12**, 2100499.
[62] Zhu S-C and Xiao F-X. 2023. Transition metal chalcogenides quantum dots: emerging building blocks toward solar-to-hydrogen conversion. *ACS Catal.* **13**, 7269–7309.
[63] Yang J, Xue C, Yu S-H, Zeng J-H and Qian Y-T. 2002. General synthesis of semiconductor chalcogenide nanorods by using the monodentate ligand n-butylamine as a shape controller. *Angew. Chem., Int. Ed.* **41**, 4697–4700.
[64] Jia Z L et al. 2023. Charge-carrier dynamics of solution-processed antimony- and bismuth-based chalcogenide thin films. *ACS Energy Lett.* **8**, 1485–1492.

[65] Kohoutek T, Orava J, Strizik L, Wagner T, Greer A L, Bardosova M and Fudouzi H. 2013. Large-area inverse opal structures in a bulk chalcogenide glass by spin-coating and thin-film transfer. *Opt. Mater.* **36**, 390–395.
[66] Zhang T Y, Wang J T, Wu P, Lu A-Y and Kong J. 2023. Vapour-phase deposition of two-dimensional layered chalcogenides. *Nat. Rev. Mater.* **8**, 799–821.
[67] Mihai C, Sava F, Simandan I D, Galca A C, Burducea I, Becherescu N and Velea A. 2021. Structural and optical properties of amorphous Si–Ge–Te thin films prepared by combinatorial sputtering. *Sci. Rep.* **11**, 11755.
[68] Sun L Z, Yuan G W, Gao L B, Yang J, Chhowalla M, Gharahcheshmeh M H, Gleason K K, Choi Y S, Hong B H and Liu Z F. 2021. Chemical vapour deposition. *Nat. Rev. Methods Primers* **1**, 5.
[69] He Y, Zhao R L, He Y, Chen X Y, Tao G M and Hou C. 2023. Chalcogenide glass nanospheres with tunable morphology by liquid-phase template approach. *iScience* **26**, 106111.
[70] Ponomarenko V P, Popov V S and Popov S V. 2022. Photoelectronics based on 0D materials. *J. Commun. Technol. Electron.* **67**, S1–S36.
[71] Liu H, Cai P, McHugh K J, Perkinson C F, Li L S, Wang S N, Wang W, Jiao M X, Luo X L and Jing L H. 2022. Aqueous synthesis of bright near-infrared-emitting Zn-Cu-In-Se quantum dots for multiplexed detection of tumor markers. *Nano Res.* **15**, 8351–8359.
[72] Jha R K and Bhat N. 2020. Recent progress in chemiresistive gas sensing technology based on molybdenum and tungsten chalcogenide nanostructures. *Adv. Mater. Interfaces* **7**, 1901992.
[73] Gao M-R, Jiang J and Yu S-H. 2012. Solution-based synthesis and design of late transition metal chalcogenide materials for oxygen reduction reaction (ORR). *Small* **8**, 13–27.
[74] Yadav S, Yashas S R and Shivaraju H P. 2021. Transitional metal chalcogenide nanostructures for remediation and energy: a review. *Environ. Chem. Lett.* **19**, 3683–3700.
[75] Zhang H and Hock A S. 2017. Crystalline $WS_2$ via room temperature, solution-phase synthesis. *Inorg. Chem.* **56**, 106–109.
[76] Baláž P, Baláž M, Achimovičová M, Bujňáková Z and Dutková E. 2017. Chalcogenide mechanochemistry in materials science: insight into synthesis and applications (a review). *J. Mater. Sci.* **52**, 11851–11890.
[77] Wu J B, Cong X, Niu S Y, Liu F X, Zhao H, Du Z H, Ravichandran J, Tan P-H and Wang H. 2019. Linear dichroism conversion in quasi-1D perovskite chalcogenide. *Adv. Mater.* **31**, 1902118.
[78] Kohoutek T, Orava J, Wagner T, Hrdlicka M, Vlcek M and Frumar M. 2009. 1D-photonic crystals prepared from the amorphous chalcogenide films. *J. Mater. Sci., Mater. Electron.* **20**, 346–350.
[79] Haque F, Daeneke T, Kalantar-Zadeh K and Ou J Z. 2018. Two-dimensional transition metal oxide and chalcogenide-based photocatalysts. *Nano-Micro. Lett.* **10**, 23.
[80] Eng A Y S, Ambrosi A, Sofer Z, Šimek P and Pumera M. 2014. Electrochemistry of transition metal dichalcogenides: strong dependence on the metal-to-chalcogen composition and exfoliation method. *ACS Nano* **8**, 12185–12198.
[81] Bochmann M. 1996. Metal chalcogenide materials: chalcogenolato complexes as 'single-source' precursors. *J. Chem. Vapor Depos.* **2**, 85–96.
[82] Crowell J E. 2003. Chemical methods of thin film deposition: chemical vapor deposition, atomic layer deposition, and related technologies. *J Vac. Sci. Technol. A* **21**, S88–S95.
[83] Nipane A et al. 2021. Damage-free atomic layer etch of $WSe_2$: a platform for fabricating clean two-dimensional devices. *ACS Appl. Mater. Interfaces* **13**, 1930–1942.
[84] Tan C L et al. 2015. High-yield exfoliation of ultrathin two-dimensional ternary chalcogenide nanosheets for highly sensitive and selective fluorescence DNA sensors. *J. Am. Chem. Soc.* **137**, 10430–10436.
[85] Song O and Kang J. 2023. Solution-processed 2d materials for electronic applications. *ACS Appl. Electron. Mater.* **5**, 1335–1346.
[86] Beydoun N, Farhat R and Halaoui L I. 2020. Enhanced solar light harvesting with Q-CdTe/Se sensitized inverse opal $TiO_2$. *ACS Appl. Energy Mater.* **3**, 3104–3119.
[87] Landon P B, Gilleland C L and Glosser R. 2007. Properties of metallo-dielectric opals and metallic inverse opal photonic crystals. *J. Mater. Sci., Mater. Electron.* **18**, 469–472.
[88] Chia X Y and Pumera M. 2018. Inverse opal-like porous $MoSe_x$ films for hydrogen evolution catalysis: overpotential-pore size dependence. *ACS Appl. Mater. Interfaces* **10**, 4937–4945.
[89] Lalova A and Todorov R. 2012. Optical properties of porous chalcogenide films for sensor application. *J. Phys.: Conf. Ser.* **398**, 012023.
[90] Kwon D-H et al. 2010. Atomic structure of conducting nanofilaments in $TiO_2$ resistive switching memory. *Nat. Nanotechnol.* **5**, 148–153.
[91] Lee Y-H et al. 2012. Synthesis of large-area $MoS_2$ atomic layers with chemical vapor deposition. *Adv. Mater.* **24**, 2320–2325.
[92] Chen X, Denninger P, Stimpel-lindner T, Spiecker E, Duesberg G S, Backes C, Knirsch K C and Hirsch A. 2020. Defect engineering of two-dimensional molybdenum disulfide. *Chemistry* **26**, 6535–6544.
[93] Chhowalla M, Shin H S, Eda G, Li L-J, Loh K P and Zhang H. 2013. The chemistry of two-dimensional layered transition metal dichalcogenide nanosheets. *Nat. Chem.* **5**, 263–275.
[94] Raeis-Hosseini N and Rho J. 2019. Dual-functional nanoscale devices using phase-change materials: a reconfigurable perfect absorber with nonvolatile resistance-change memory characteristics. *Appl. Sci.* **9**, 564.
[95] Ravsher T et al. 2023. Polarity-induced threshold voltage shift in ovonic threshold switching chalcogenides and the impact of material composition. *Phys. Status Solidi RRL* **17**, 2200417.
[96] Seo S et al. 2018. Artificial optic-neural synapse for colored and color-mixed pattern recognition. *Nat. Commun.* **9**, 5106.
[97] Wang C L et al. 2023. High-responsivity and broadband $MoS_2$ photodetector using interfacial engineering. *ACS Appl. Mater. Interfaces* **15**, 46236–46246.
[98] Giuffredi G, Asset T, Liu Y C, Atanassov P and Di Fonzo F. 2021. Transition metal chalcogenides as a versatile and tunable platform for catalytic $CO_2$ and $N_2$ electroreduction. *ACS Mater. Au* **1**, 6–36.
[99] Zhang L, Li Z J, Liu J, Peng Z C, Zhou J, Zhang H and Li Y C. 2020. Optoelectronic gas sensor based on few-layered InSe nanosheets for $NO_2$ detection with ultrahigh antihumidity ability. *Anal. Chem.* **92**, 11277–11287.
[100] Lee M L, Miao X S and Shi L P. 2008. Blu-ray type super-resolution near-field phase change disk with $In_2Ge_8Sb_{85}Te_5$ mask layer. *Jpn. J. Appl. Phys.* **47**, 6025–6028.
[101] Shi L P, Chong T C, Tan P K, Li J M, Hu X, Miao X S and Wang Q F. 2005. Investigation on super-resolution near-field blu-ray-type phase-change optical disk with $Sb_2Te_3$ mask layer. *Jpn. J. Appl. Phys.* **44**, 3615–3619.
[102] Choi B J, Choi S, Shin Y C, Hwang C S, Lee J W, Jeong J, Kim Y J, Hwang S-Y and Hong S K. 2007. Cyclic PECVD of $Ge_2Sb_2Te_5$ films using metallorganic sources. *J. Electrochem. Soc.* **154**, H318–H324.
[103] Pore V, Hatanpää T, Ritala M and Leskelä M. 2009. Atomic layer deposition of metal tellurides and selenides using

alkylsilyl compounds of tellurium and selenium. *J. Am. Chem. Soc.* **131**, 3478–3480.
[104] Pavlov V V. 2019. Linear and nonlinear magneto-optical phenomena in epitaxial films of europium chalcogenides EuX (X = O, Se, Te). *Phys. Solid State* **61**, 408–413.
[105] Govoreanu B et al. 2017. Thermally stable integrated Se-based OTS selectors with >20 MA/cm$^2$ current drive, >3.10$^3$ half-bias nonlinearity, tunable threshold voltage and excellent endurance. *In Proceeding 2017 Symposium on VLSI Technology* (IEEE, Kyoto, Japan) pp T92–T93.
[106] Li Y, Zhong Y P, Xu L, Zhang J J, Xu X H, Sun H J and Miao X S. 2013. Ultrafast synaptic events in a chalcogenide memristor. *Sci. Rep.* **3**, 1619.
[107] Kim J, Jung M, Lim D U, Rhee D, Jung S H, Cho H K, Kim H-K, Cho J H and Kang J. 2022. Area-selective chemical doping on solution-processed $MoS_2$ thin-film for multi-valued logic gates. *Nano Lett.* **22**, 570–577.
[108] Cai M H et al. 2024. Topological magneto-optical effect from skyrmions in two-dimensional ferromagnets. *ACS Nano* **18**, 20055–20064.
[109] Mi M J, Xiao H, Yu L X, Zhang Y X, Wang Y S, Cao Q and Wang Y L. 2023. Two-dimensional magnetic materials for spintronic devices. *Mater. Today Nano* **24**, 100408.
[110] Sanghera J S, Shaw L B and Aggarwal I D. 2002. Applications of chalcogenide glass optical fibers. *C. R. Chim.* **5**, 873–883.
[111] Tao S P, Li Q, Wang J F, Wang X Y, Cai J Z, Li S B, Xu W, Zhang K and Hu C Q. 2020. Phase change materials for nonvolatile, solid-state reflective displays: from new structural design rules to enhanced color-changing performance. *Adv. Opt. Mater.* **8**, 2000062.
[112] Tan Q S, Chang Y H, He Q, Tong H and Miao X S. 2023. Enhanced stretchability towards a flexible and wearable reflective display coating using chalcogenide phase change materials. *Opt. Express* **31**, 75–85.
[113] El-Bana M S, Bohdan R and Fouad S S. 2016. Optical characteristics and holographic gratings recording on $As_{30}Se_{70}$ thin films. *J. Alloys Compd.* **686**, 115–121.
[114] Sun Y F et al. 2012. Fabrication of flexible and freestanding zinc chalcogenide single layers. *Nat. Commun.* **3**, 1057.
[115] Pham T, Li G H, Bekyarova E, Itkis M E and Mulchandani A. 2019. $MoS_2$-based optoelectronic gas sensor with sub-parts-per-billion limit of $NO_2$ gas detection. *ACS Nano* **13**, 3196–3205.
[116] Lin C-Y, Ulaganathan R K, Sankar R, Murugesan R C, Subramanian A, Rozhin A and Firdoz S. 2021. Silicon-based two-dimensional chalcogenide of p-type semiconducting silicon telluride nanosheets for ultrahigh sensitive photodetector applications. *J. Mater. Chem. C* **9**, 10478–10486.
[117] Huo J P, Xiao Y, Sun T M, Zou G S, Shen D Z, Feng B, Lin L C, Wang W G, Zhao G L and Liu L. 2021. Femtosecond laser irradiation-mediated $MoS_2$–metal contact engineering for high-performance field-effect transistors and photodetectors. *ACS Appl. Mater. Interfaces* **13**, 54246–54257.
[118] Kim J, Kim S, Cho Y S, Choi M, Jung S-H, Cho J H, Whang D and Kang J. 2021. Solution-processed $MoS_2$ film with functional interfaces via precursor-assisted chemical welding. *ACS Appl. Mater. Interfaces* **13**, 12221–12229.
[119] Spelthahn H, Kirsanov D, Legin A, Osterrath T, Schubert J, Zander W and Schöning M J. 2012. Development of a thin-film sensor array for analytical monitoring of heavy metals in aqueous solutions. *Phys. Status Solidi a* **209**, 885–891.
[120] Iwasaki R, Hori S, Kanno R, Yajima T, Hirai D, Kato Y and Hiroi Z. 2019. Weak anisotropic lithium-ion conductivity in single crystals of $Li_{10}GeP_2S_{12}$. *Chem. Mater.* **31**, 3694–3699.
[121] Lamiel C, Hussain I, Rabiee H, Ogunsakin O R and Zhang K L. 2023. Metal-organic framework-derived transition metal chalcogenides (S, Se, and Te): challenges, recent progress, and future directions in electrochemical energy storage and conversion systems. *Coord. Chem. Rev.* **480**, 215030.
[122] Romanyuk Y E et al. 2015. All solution-processed chalcogenide solar cells—from single functional layers towards a 13.8% efficient CIGS device. *Adv. Funct. Mater.* **25**, 12–27.
[123] Jiang B B et al. 2021. High-entropy-stabilized chalcogenides with high thermoelectric performance. *Science* **371**, 830–834.
[124] Feng D, Ge Z-H, Chen Y-X, Li J and He J Q. 2017. Hydrothermal synthesis of SnQ ($Q$ = Te, Se, S) and their thermoelectric properties. *Nanotechnology* **28**, 455707.
[125] Yang D et al. 2023. High thermoelectric performance of aluminum-doped cuprous selenide thin films with exceptional flexibility for wearable applications. *Nano Energy* **117**, 108930.
[126] Wang Y F, Lin P J, Lou Q, Zhang Z C, Huang S, Lu Y and He J Q. 2021. Design guidelines for chalcogenide-based flexible thermoelectric materials. *Mater. Adv.* **2**, 2584–2593.
[127] Abir S S H, Sharma S, Sharma P, Karla S, Balasubramanian G, Samuel J and Koratkar N. 2024. Piezoelectricity in chalcogenide perovskites. *Nat. Commun.* **15**, 5768.
[128] Talib M et al. 2023. Development of high-performance broadband optical detector for cryogenic to elevated operating temperature. *Mater. Sci. Semicond. Process.* **158**, 107364.
[129] Sidik R A and Anderson A B. 2006. $Co_9S_8$ as a catalyst for electroreduction of $O_2$: quantum chemistry predictions. *J. Phys. Chem. B* **110**, 936–941.
[130] Park J et al. 2024. Conversion of layered $WS_2$ crystals into mixed-domain electrochemical catalysts by plasma-assisted surface reconstruction. *Adv. Mater.* **36**, 2314031.
[131] Olawale F, Oladimeji O, Ariatti M, Singh M and Vijayakumar S. 2022. Emerging roles of green-synthesized chalcogen and chalcogenide nanoparticles in cancer theranostics. *J. Nanotechnol.* **2022**, 6176610.
[132] Nieves L M, Mossburg K, Hsu J C, Maidment A D A and Cormode D P. 2021. Silver chalcogenide nanoparticles: a review of their biomedical applications. *Nanoscale* **13**, 19306–19323.
[133] Pal S, Verma A, Prajapati Y K and Saini J P. 2020. Sensitive detection using heterostructure of black phosphorus, transition metal di-chalcogenides and MXene in SPR sensor. *Appl. Phys. A* **126**, 809.
[134] Llorente V B, Dzhagan V M, Gaponik N, Iglesias R A, Zahn D R T and Lesnyak V. 2017. Electrochemical tuning of localized surface plasmon resonance in copper chalcogenide nanocrystals. *J. Phys. Chem. C* **121**, 18244–18253.
[135] Wong S, Deubel M, Pérez-willard F, John S, Ozin G A, Wegener M and Von freymann G. 2006. Direct laser writing of three- dimensional photonic crystals with a complete photonic bandgap in chalcogenide glasses. *Adv. Mater.* **18**, 265–269.
[136] Petit G, Malherbe C, Bianchi P and Monbaliu J-C M. 2024. An innovative chalcogenide transfer agent for improved aqueous quantum dot synthesis. *Chem. Sci.* **15**, 13148–13159.
[137] Alfieri A, Anantharaman S B, Zhang H Q and Jariwala D. 2023. Nanomaterials for quantum information science and engineering. *Adv. Mater.* **35**, 2109621.
[138] Lai S. 2003. Current status of the phase change memory and its future. *In Proceeding IEEE International Electron Devices Meeting 2003* (IEEE, Washington, DC, USA) pp 10.1.1–10.1.4.

[139] Kim W et al. 2016. ALD-based confined PCM with a metallic liner toward unlimited endurance. *In Proceeding 2016 IEEE International Electron Devices Meeting* (IEEE, San Francisco, CA, USA) pp 4.2.1–4.2.4.
[140] Pellizzer F et al. 2004. Novel $\mu$-trench phase-change memory cell for embedded and stand-alone non-volatile memory applications. *In Proceeding Digest of Technical Papers. 2004 Symposium on VLSI Technology, 2004* (IEEE, Honolulu, HI, USA) pp 18–19.
[141] Shukla K D, Saxena N, Durai S and Manivannan A. 2016. Redefining the speed limit of phase change memory revealed by time-resolved steep threshold-switching dynamics of AgInSbTe devices. *Sci. Rep.* **6**, 37868.
[142] Lee J I et al. 2007. Highly scalable phase change memory with CVD GeSbTe for sub 50nm generation. *In Proceeding 2007 IEEE Symposium on* VLSI Technology (IEEE, Kyoto, Japan) pp 102–103.
[143] Tolkach N M, Vishnyakov N V, Lazarenko P I, Sherchenkov A A, Sudakova A U and Nazimov D R. 2020. Optical switching in multilayer structures based on $Ge_2Sb_2Te_5$. *J. Phys.: Conf. Ser.* **1695**, 012075.
[144] Gericke F, Flissikowski T, Lähnemann J, Katmis F, Braun W, Riechert H and Grahn H T. 2012. Optical switching and related structural properties of epitaxial $Ge_2Sb_2Te_5$ films. *J. Appl. Phys.* **111**, 113524.
[145] Pirovano A, Lacaita A L, Benvenuti A, Pellizzer F, Hudgens S and Bez R. 2003. Scaling analysis of phase-change memory technology. *In Proceeding IEEE International Electron Devices Meeting 2003* (IEEE, Washington, DC, USA) pp 29.6.1–29.6.4.
[146] Sadeghipour S M, Pileggi L and Asheghi M. 2006. Phase change random access memory, thermal analysis. *In Proceeding Thermal and Thermomechanical Proceedings 10th Intersociety Conference on Phenomena in Electronics Systems* (IEEE, San Diego, CA, USA) pp 660–665.
[147] Jeong C-W et al. 2006. Highly reliable ring-type contact for high-density phase change memory. *Jpn. J. Appl. Phys.* **45**, 3233–3237.
[148] Pellizzer F, Benvenuti A, Gleixner B, Kim Y, Johnson B, Magistretti M, Marangon T, Pirovano A, Bez R and Atwood G. 2006. A 90nm phase change memory technology for stand-alone non-volatile memory applications. *In Proceeding 2006 Symposium on VLSI Technology, 2006. Digest of Technical Papers* (IEEE, Honolulu, HI, USA) pp 122–123.
[149] Kim Y-T et al. 2005. Programming characteristics of phase change random access memory using phase change simulations. *Jpn. J. Appl. Phys.* **44**, 2701–2705.
[150] Kim T et al. 2018. High-performance, cost-effective 2z nm two-deck cross-point memory integrated by self-align scheme for 128 Gb SCM. *In Proceeding 2018 IEEE International Electron Devices Meeting* (IEEE, San Francisco, CA, USA) pp 37.1.1–37.1.4.
[151] Ahn S J et al. 2005. Highly reliable 50nm contact cell technology for 256Mb PRAM. *In Proceeding Digest of Technical Papers. 2005 Symposium on VLSI Technology, 2005* (IEEE, Kyoto, Japan) pp 98–99.
[152] Oh J H et al. 2006. Full integration of highly manufacturable 512Mb PRAM based on 90nm technology. *In Proceeding 2006 International Electron Devices Meeting* (IEEE, San Francisco, CA, USA) pp 1–4.
[153] Hwang Y N et al. 2003. Writing current reduction for high-density phase-change RAM. *In IEEE International Electron Devices Meeting 2003* (IEEE, Washington, DC, USA) pp 37.1.1–37.1.4.
[154] Li Y M, Hwang C-H, Li T-Y and Cheng H-W. 2009. The geometric effect and programming current reduction in cylindrical-shaped phase change memory. *Nanotechnology* **20**, 285701.
[155] DerChang K et al. 2009. A stackable cross point phase change memory. *In Proceeding 2009 IEEE International Electron Devices Meeting* (IEEE, Baltimore, MD, USA) pp 1–4.
[156] Lencer D, Salinga M, Grabowski B, Hickel T, Neugebauer J and Wuttig M. 2008. A map for phase-change materials. *Nat. Mater.* **7**, 972–977.
[157] Kohara S et al. 2006. Structural basis for the fast phase change of $Ge_2Sb_2Te_5$: ring statistics analogy between the crystal and amorphous states. *Appl. Phys. Lett.* **89**, 201910.
[158] Kellner J et al. 2018. Mapping the band structure of GeSbTe phase change alloys around the Fermi level. *Commun. Phys.* **1**, 5.
[159] Matsunaga T, Akola J, Kohara S, Honma T, Kobayashi K, Ikenaga E, Jones R O, Yamada N, Takata M and Kojima R. 2011. From local structure to nanosecond recrystallization dynamics in AgInSbTe phase-change materials. *Nat. Mater.* **10**, 129–134.
[160] Cho E, Han S, Kim D, Horii H and Nam H-S. 2011. *Ab initio* study on influence of dopants on crystalline and amorphous $Ge_2Sb_2Te_5$. *J. Appl. Phys.* **109**, 043705.
[161] Shelby R M and Raoux S. 2009. Crystallization dynamics of nitrogen-doped $Ge_2Sb_2Te_5$. *J. Appl. Phys.* **105**, 104902.
[162] Chen Y C et al. 2006. Ultra-thin phase-change bridge memory device using GeSb. *In Proceeding 2006 International Electron Devices Meeting* (IEEE, San Francisco, CA, USA) pp 1–4.
[163] Bruns G, Merkelbach P, Schlockermann C, Salinga M, Wuttig M, Happ T D, Philipp J B and Kund M. 2009. Nanosecond switching in GeTe phase change memory cells. *Appl. Phys. Lett.* **95**, 043108.
[164] Zhou X L, Wu L C, Song Z T, Rao F, Zhu M, Peng C, Yao D N, Song S N, Liu B and Feng S L. 2012. Carbon-doped $Ge_2Sb_2Te_5$ phase change material: a candidate for high-density phase change memory application. *Appl. Phys. Lett.* **101**, 142104.
[165] Park T-J, Choi S-Y and Kang M-J. 2007. Phase transition characteristics of Bi/Sn doped $Ge_2Sb_2Te_5$thin film for PRAM application. *Thin Solid Films* **515**, 5049–5053.
[166] Choi B J, Choi S, Shin Y C, Kim K M, Hwang C S, Kim Y J, Son Y J and Hong S K. 2007. Combined atomic layer and chemical vapor deposition, and selective growth of $Ge_2Sb_2Te_5$ films on TiN/W contact plug. *Chem. Mater.* **19**, 4387–4389.
[167] Lee J, Choi S, Lee C, Kang Y and Kim D. 2007. GeSbTe deposition for the PRAM application. *Appl. Surf. Sci.* **253**, 3969–3976.
[168] Eom T et al. 2012. Conformal formation of $(GeTe_2)_{(1-x)}(Sb_2Te_3)_x$ layers by atomic layer deposition for nanoscale phase change memories. *Chem. Mater.* **24**, 2099–2110.
[169] Eom T, Gwon T, Yoo S, Choi B J, Kim M-S, Buchanan I, Ivanov S, Xiao M C and Hwang C S. 2015. Combined ligand exchange and substitution reactions in atomic layer deposition of conformal $Ge_2Sb_2Te_5$ film for phase change memory application. *Chem. Mater.* **27**, 3707–3713.
[170] Sarnet T, Pore V, Hatanpää T, Ritala M, Leskelä M, Schrott A, Zhu Y, Raoux S and Cheng H-Y. 2011. Atomic layer deposition and characterization of GeTe thin films. *J. Electrochem. Soc.* **158**, D694–D697.
[171] Ritala M, Pore V, Hatanpää T, Heikkilä M, Leskelä M, Mizohata K, Schrott A, Raoux S and Rossnagel S M. 2009. Atomic layer deposition of $Ge_2Sb_2Te_5$ thin films. *Microelectron. Eng.* **86**, 1946–1949.
[172] Knapas K, Hatanpää T, Ritala M and Leskelä M. 2010. In situ reaction mechanism studies on atomic layer deposition of $Sb_2Te_3$ and GeTe from $(Et_3Si)_2Te$ and chlorides. *Chem. Mater.* **22**, 1386–1391.
[173] Sundaram S, Johnson B R, Schweiger M J, Martinez J E, Riley B J, Saraf L V, Anheier J N C, Allen P J and

Schultz J F. 2004. Chalcogenide glasses and structures for quantum sensing. *Proc. SPIE* **5359**, 234–245.
[174] Sanghera J S et al. 2000. Development and infrared applications of chalcogenide glass optical fibers. *Fiber Integr. Opt.* **19**, 251–274.
[175] Faraon A, Englund D, Bulla D, Luther-Davies B, Eggleton B J, Stoltz N, Petroff P and Vučković J. 2008. Local tuning of photonic crystal cavities using chalcogenide glasses. *Appl. Phys. Lett.* **92**, 043123.
[176] Lee J S, Farmakidis N, Aggarwal S, Dong B W, Zhou W, Pernice W H P and Bhaskaran H. 2024. Spatio-spectral control of coherent nanophotonics. *Nanophotonics* **13**, 2117–2125.
[177] Zhao M Y, Yang Z, Zhang R Z, Zheng J J, Xu P P, Zhang W, DaiS S, Wang R P and Majumdar A. 2021. High Q chalcogenide photonic crystal nanobeam cavities. *IEEE Photonics Technol. Lett.* **33**, 525–528.
[178] Gholipour B, Zhang J F, MacDonald K F, Hewak D W and Zheludev N I. 2013. An all-optical, non-volatile, bidirectional, phase-change meta-switch. *Adv. Mater.* **25**, 3050–3054.
[179] Zhang S J et al. 2022. Terahertz multi-level nonvolatile optically rewritable encryption memory based on chalcogenide phase-change materials. *Iscience* **25**, 104866.
[180] Kim J, Jeong K, Park H, Hong S, Kim D, Nam G, Rho S, Shin H J, Kang C and Cho M-H. 2023. Exchange interaction-driven surface state hybridization in $Bi_2Se_3$ topological insulator. *Adv. Quantum Technol.* **6**, 2300014.
[181] Hu Z, Li Y R, Li Y, Yao S Y, Chen H F, Zhang T, Ao Z H and Li Z H. 2024. Lithography-free patterning of chalcogenide materials for integrated photonic devices. (arXiv:2408.05099)
[182] Park H, Rho S, Kim J, Kim H, Kim D, Kang C and Cho M-H. 2022. Topological surface-dominated spintronic THz emission in topologically nontrivial $Bi_{1-x}Sb_x$ films. *Adv. Sci.* **9**, 2200948.
[183] Jia Y Y et al. 2024. Superconductivity from on-chip metallization on 2D topological chalcogenides. *Phys. Rev. X* **14**, 021051.
[184] Seok J Y, Song S J, Yoon J H, Yoon K J, Park T H, Kwon D E, Lim H, Kim G H, Jeong D S and Hwang C S. 2014. A review of three-dimensional resistive switching cross-bar array memories from the integration and materials property points of view. *Adv. Funct. Mater.* **24**, 5316–5339.
[185] Zhao Z H, Clima S, Garbin D, Degraeve R, Pourtois G, Song Z T and Zhu M. 2024. Chalcogenide ovonic threshold switching selector. *Nano-Micro Lett.* **16**, 81.
[186] Wu R J, Jia S J, Gotoh T, Luo Q, Song Z T and Zhu M. 2022. Screening switching materials with low leakage current and high thermal stability for neuromorphic computing. *Adv. Electron. Mater.* **8**, 2200150.
[187] Owen A E and Robertson J M. 1970. Electronic properties of some simple chalcogenide glasses. *J. Non-Cryst. Solids* **2**, 40–51.
[188] Yuan S J et al. 2025. Unveiling the nature of Ga-based chalcogenides for electrical switching selectors. *J. Alloys Compd.* **1024**, 180241.
[189] Wu R J et al. 2023. The role of arsenic in the operation of sulfur-based electrical threshold switches. *Nat. Commun.* **14**, 6095.
[190] Slassi A et al. 2023. Device-to-materials pathway for electron traps detection in amorphous GeSe-based selectors. *Adv. Electron. Mater.* **9**, 2201224.
[191] Bilovol V and Arcondo B. 2016. Exploring the applicability of amorphous films of system In-Sb-Te as phase change materials. *J. Non-Cryst. Solids* **447**, 315–321.
[192] Matsubayashi D, Clima S, Ravsher T, Garbin D, Delhougne R, Kar G S and Pourtois G. 2022. OTS physics-based screening for environment-friendly selector materials. *In Proceeding 2022 International Electron Devices Meeting* (IEEE, San Francisco, CA, USA) pp 8.6.1–8.6.4.
[193] Avasarala N S et al. 2018. Half-threshold bias Ioff reduction down to nA range of thermally and electrically stable high-performance integrated OTS selector, obtained by Se enrichment and N-doping of thin GeSe layers. *In Proceeding 2018 IEEE Symposium on VLSI Technology* (IEEE, Honolulu, HI, USA) pp 209–210.
[194] Anbarasu M, Wimmer M, Bruns G, Salinga M and Wuttig M. 2012. Nanosecond threshold switching of $GeTe_6$ cells and their potential as selector devices. *Appl. Phys. Lett.* **100**, 143505.
[195] Koo Y, Baek K and Hwang H. 2016. Te-based amorphous binary OTS device with excellent selector characteristics for x-point memory applications. *In Proceeding 2016 IEEE Symposium on VLSI Technology* (IEEE, Honolulu, HI, USA) pp 1–2.
[196] Koo Y and Hwang H. 2018. $Zn_{1-x}Te_x$ ovonic threshold switching device performance and its correlation to material parameters. *Sci. Rep.* **8**, 11822.
[197] Chekol S A, Yoo J, Park J, Song J, Sung C and Hwang H. 2018. A C–Te-based binary OTS device exhibiting excellent performance and high thermal stability for selector application. *Nanotechnology* **29**, 345202.
[198] Yoo J, Lee D, Park J, Song J and Hwang H. 2018. Steep slope field-effect transistors with B–Te-based ovonic threshold switch device. *IEEE J. Electron Devices Soc.* **6**, 821–824.
[199] Lee M et al. 2023. $Ge_{1-x}S_x$ chalcogenide alloys for OTS applications using magnetron sputtering. *J. Alloys Compd.* **930**, 167409.
[200] Cheng H Y et al. 2017. An ultra high endurance and thermally stable selector based on TeAsGeSiSe chalcogenides compatible with BEOL IC Integration for cross-point PCM. *In Proceeding 2017 IEEE International Electron Devices Meeting* (IEEE, San Francisco, CA, USA) pp 2.2.1–2.2.4.
[201] Park I M et al. 2023. Enhanced endurance characteristics in high performance 16nm selector only memory (SOM). *In Proceeding 2023 International Electron Devices Meeting* (IEEE, San Francisco, CA, USA) pp 1–4.
[202] Hong S et al. 2022. Extremely high performance, high density 20nm self-selecting cross-point memory for Compute Express Link. *In Proceeding 2022 International Electron Devices Meeting* (IEEE, San Francisco, CA, USA) pp 18.6.1–18.6.4.
[203] Ban S, Choi H, Lee W, Hong S, Zang H, Lee B, Kim M, Lee S, Lee H and Kim T. 2020. Pulse dependent threshold voltage variation of the ovonic threshold switch in cross-point memory. *IEEE Electron Device Lett.* **41**, 373–376.
[204] Wen J Y, Yi C Q, Chen J X, Wang L, Liu Z X, Chen Z, Tong H and Miao X. 2025. Write endurance enhanced and large memory window of gese-based selector-only memory with indium doping scheme. *IEEE Electron Device Lett.* **46**, 115–118.
[205] Sung H-J et al. 2024. Microscopic origin of polarity-dependent $V_{TH}$ shift in amorphous chalcogenides for 3D self-selecting memory. *Adv. Sci.* **11**, 2408028.
[206] Liu Z-L et al. 2024. A $Ge_xSe_{1-x}$ switch-only-memory technology through polarized atomic distribution. *Sci. Rep.* **14**, 22115.
[207] Jeong W H, Jung J, Jeong J-S, Yang M K and Kim G H. 2025. In-doped GeSbSeTe thin films for increased memory window of selector-only-memory devices. *J. Alloys Compd.* **1031**, 181079.
[208] Ravsher T et al. 2024. Evidence of heat-assisted atomic migration in GeSe self-selecting memory at high operating current density. *Phys. Status Solidi RRL* **18**, 2300415.
[209] Wang Y, Kim J C, Wu R J, Martinez J, Song X J, Yang J, Zhao F, Mkhoyan A, Jeong H Y and Chhowalla M. 2019.

Van der Waals contacts between three-dimensional metals and two-dimensional semiconductors. *Nature* **568**, 70–74.
[210] Marschall R. 2014. Semiconductor composites: strategies for enhancing charge carrier separation to improve photocatalytic activity. *Adv. Funct. Mater.* **24**, 2421–2440.
[211] Zhang W S, Zhang P P, Su Z Q and Wei G. 2015. Synthesis and sensor applications of $MoS_2$-based nanocomposites. *Nanoscale* **7**, 18364–18378.
[212] Xiao Y et al. 2022. Van der Waals epitaxial growth and optoelectronics of a vertical $MoS_2/WSe_2$ p–n junction. *Front. Optoelectron.* **15**, 41.
[213] Huang Y M, Zheng W, Qiu Y F and Hu P G. 2016. Effects of organic molecules with different structures and absorption bandwidth on modulating photoresponse of $MoS_2$ photodetector. *ACS Appl. Mater. Interfaces* **8**, 23362–23370.
[214] Sahoo S, Sahu M C, Mallik S K, Jena A K, Pradhan G K and Sahoo S. 2023. High responsivity in monolayer $MoS_2$ photodetector via controlled interfacial carrier trapping. *ACS Appl. Electron. Mater.* **5**, 1077–1087.
[215] Radisavljevic B, Radenovic A, Brivio J, Giacometti V and Kis A. 2011. Single-layer $MoS_2$ transistors. *Nat. Nanotechnol.* **6**, 147–150.
[216] Imani Yengejeh S, Wen W and Wang Y. 2021. Mechanical properties of lateral transition metal dichalcogenide heterostructures. *Front. Phys.* **16**, 13502.
[217] Wang T, Tan X X, Wei Y D and Jin H. 2022. Unveiling the layer-dependent electronic properties in transition-metal dichalcogenide heterostructures assisted by machine learning. *Nanoscale* **14**, 2511–2520.
[218] Dhara S, Jawa H, Ghosh S, Varghese A and Lodha S. 2020. Enhanced gas sensing performance and all-electrical room temperature operation enabled by a $WSe_2/MoS_2$ heterojunction. (arXiv:2009.11350)
[219] Xiao H D, Lin L, Zhu J, Guo J X, Ke Y Z, Mao L N, Gong T X, Cheng H Y, Huang W and Zhang X S. 2022. Highly sensitive and broadband photodetectors based on $WSe_2/MoS_2$ heterostructures with van der Waals contact electrodes. *Appl. Phys. Lett.* **121**, 023504.
[220] Ying Y-L, Ding Z F, Zhan D P and Long Y-T. 2017. Advanced electroanalytical chemistry at nanoelectrodes. *Chem. Sci.* **8**, 3338–3348.
[221] Xing X, Zhang Z Y, Quan C J, Zhao L T, Wang C W, Jia T Y, Ren J F, Du J and Leng Y X. 2022. Tunable ultrafast electron transfer in $WSe_2$–graphene heterostructures enabled by atomic stacking order. *Nanoscale* **14**, 7418–7425.
[222] Xiao J W, Zhang Y, Chen H J, Xu N S and Deng S Z. 2018. Enhanced performance of a monolayer $MoS_2/WSe_2$ heterojunction as a photoelectrochemical cathode. *Nano-Micro Lett.* **10**, 60.
[223] Hajlaoui R, Baachaoui S, Ben Aoun S, Ridene S and Raouafi N. 2024. Surface tailoring of $MoS_2$ nanosheets with substituted aromatic diazonium salts for gas sensing: a DFT study. *ACS Omega* **9**, 37953–37964.
[224] Liu G, Liu J F, Yan J, Chen Y L, Zhu Y B and Tian Y H. 2022. Effect of defect types in monolayer $MoS_2$ on $SO_2$ adsorption. *J. Korean Phys. Soc.* **81**, 409–418.
[225] Wang G M et al. 2015. Wafer-scale growth of large arrays of perovskite microplate crystals for functional electronics and optoelectronics. *Sci. Adv.* **1**, e1500613.
[226] Wang H M, Li C H, Fang P F, Zhang Z L and Zhang J Z. 2018. Synthesis, properties, and optoelectronic applications of two-dimensional $MoS_2$ and $MoS_2$-based heterostructures. *Chem. Soc. Rev.* **47**, 6101–6127.
[227] Huang Y X, Guo J H, Kang Y J, Ai Y and Li C M. 2015. Two dimensional atomically thin $MoS_2$ nanosheets and their sensing applications. *Nanoscale* **7**, 19358–19376.
[228] Li F et al. 2020. High-performance optoelectronic devices based on van der Waals vertical $MoS_2/MoSe_2$ heterostructures. *Nano Res.* **13**, 1053–1059.
[229] Li Y N, Li L N, Li S S, Sun J Y, Fang Y and Deng T. 2022. Highly sensitive photodetectors based on monolayer $MoS_2$ field-effect transistors. *ACS Omega* **7**, 13615–13621.
[230] Kwon G et al. 2022. Interaction- and defect-free van der Waals contacts between metals and two-dimensional semiconductors. *Nat. Electron.* **5**, 241–247.
[231] Deng W J et al. 2022. Electrically tunable two-dimensional heterojunctions for miniaturized near-infrared spectrometers. *Nat. Commun.* **13**, 4627.
[232] Guo J M, Wen R M, Zhai J Y and Wang Z L. 2019. Enhanced $NO_2$ gas sensing of a single-layer $MoS_2$ by photogating and piezo-phototronic effects. *Sci. Bull.* **64**, 128–135.
[233] Zhao Q N et al. 2022. Edge-enriched $Mo_2TiC_2T_x/MoS_2$ heterostructure with coupling interface for selective $NO_2$ monitoring. *Adv. Funct. Mater.* **32**, 2203528.
[234] Kim S, Park H, Choo S, Baek S, Kwon Y, Liu N, Yang J Y, Yang C-W, Yoo G and Kim S. 2020. Active-matrix monolithic gas sensor array based on $MoS_2$ thin-film transistors. *Commun. Mater.* **1**, 86.
[235] Zheng W, Xu Y S, Zheng L L, Yang C, Pinna N, Liu X H and Zhang J. 2020. $MoS_2$ Van der Waals p–n junctions enabling highly selective room-temperature $NO_2$ sensor. *Adv. Funct. Mater.* **30**, 2000435.
[236] Jia S J et al. 2020. Ultrahigh drive current and large selectivity in GeS selector. *Nat. Commun.* **11**, 4636.
[237] Wang J C, Wang Q L T, Chen Q, Lei T, Lv W M, Tu H Y, Hu R, Wang Y P, Zeng Z M and Ma T Y. 2022. A floating-gate-like transistor based on InSe vdW heterostructure with high-performance synaptic characteristics. *Phys. Status Solidi a* **219**, 2200156.
[238] Fang P J, Wang Q L T, Lei T, Wang Y P, Wang B H, Luo Y, Wu H, Lv W X and Zeng Z M. 2023. Synaptic properties of plasma-treated $SnS_2$/h-BN van der Waals heterostructure. *Appl. Phys. Lett.* **122**, 223101.
[239] Seo S et al. 2020. Artificial van der Waals hybrid synapse and its application to acoustic pattern recognition. *Nat. Commun.* **11**, 3936.
[240] Pitchappa P, Kumar A, Prakash S, Jani H, Venkatesan T and Singh R. 2019. Chalcogenide phase change material for active terahertz photonics. *Adv. Mater.* **31**, 1808157.
[241] Liang M Y, Ali A, Belaidi A, Hossain M I, Ronan O, Downing C, Tabet N, Sanvito S, EI-Mellouhi F and Nicolosi V. 2020. Improving stability of organometallic-halide perovskite solar cells using exfoliation two-dimensional molybdenum chalcogenides. *npj 2D Mater. Appl.* **4**, 40.
[242] Kwon S M et al. 2018. High-performance and scalable metal-chalcogenide semiconductors and devices via chalco-gel routes. *Sci. Adv.* **4**, eaap9104.
[243] Zheng J, Zhang H, Dong S H, Liu Y P, Tai Nai C, Suk Shin H, Young Jeong H, Liu B and Ping Loh K. 2014. High yield exfoliation of two-dimensional chalcogenides using sodium naphthalenide. *Nat. Commun.* **5**, 2995.